

DART T690/E550

Hitting the Bullseye in Air Racing Technology



Alfred Gessow Rotorcraft Center
Department of Aerospace Engineering
University of Maryland, College Park
Maryland, 20742



University of Maryland
Alfred Gessow Rotorcraft Center
Department of Aerospace Engineering
College Park, Maryland 20742



DART T690/E550

Hitting the Bullseye in Air Racing Technology

In Response to the 2012 American Helicopter Society Student Design Competition
Graduate Student Category
PYLON RACING ROTORCRAFT

June 1, 2012

Handwritten signature of Anish Sydney.

Anish Sydney, Graduate Student (Team Leader)

Handwritten signature of William Staruk.

William Staruk, Graduate Student

Handwritten signature of Mathieu Amiraux.

Mathieu Amiraux, Graduate Student

Handwritten signature of Nitin Sydney.

Nitin Sydney, Graduate Student

Handwritten signature of Jonathan Elliott.

Jonathan Elliott, Graduate Student

Handwritten signature of Dr. Inderjit Chopra.

Dr. Inderjit Chopra, Faculty Adviser

Handwritten signature of Joseph Schmaus.

Joseph Schmaus, Graduate Student

Handwritten signature of Dr. J. Gordon Leishman.

Dr. J. Gordon Leishman, Faculty Adviser

Handwritten signature of Conor Stahlhut.

Conor Stahlhut, Graduate Student

Handwritten signature of Dr. V.T. Nagaraj.

Dr. V.T. Nagaraj, Faculty Adviser

Permission to release

AHS Design Team

Alfred Gessow Rotorcraft Center

University of Maryland

College Park, MD 20740, USA

To the American Helicopter Society,

We hereby give AHS permission to distribute this report as they see fit.

Thank you,

UMD Design Team

Acknowledgements

The *Dart T690/E550* design team wishes to acknowledge the following people for their assistance and guidance.

Dr. Vengalattore T. Nagaraj — Senior Research Scientist, Dept. of Aerospace Engineering, University of Maryland, College Park.

Dr. Inderjit Chopra – Gessow Professor, Director of Gessow Rotorcraft Center (AGRC), Dept. of Aerospace Engineering, University of Maryland, College Park.

Dr. J. Gordon Leishman – Minta Martin Professor of Engineering, Dept. of Aerospace Engineering, University of Maryland, College Park.

Dr. James Baeder – Associate Professor, Dept. of Aerospace Engineering, University of Maryland, College Park.

Dr. Derek A. Paley – Assistant Professor, Dept. of Aerospace Engineering, University of Maryland, College Park.

Dr. Omri Rand – Shirley and Burt Harris Academic Chair, Technion Israel Institute of Technology, Technion City, Haifa, Israel.

Dr. Sudarshan N. Koushik – Assistant Research Scientist, Dept. of Aerospace Engineering, University of Maryland, College Park.

Charley Kilmain – Director, Rotor and Drive System Design, Bell Helicopter Textron, Inc.

Rob Ransone – President, Ransone Associates, Inc.

Dr. Nicholas Wilson – Rotorcraft Dynamics Engineer, The Boeing Company

Advanced Helicopter Concepts, Frederick, MD

Maryland State Police Aviation Command, Frederick Section

Fellow graduate students at the Dept. of Aerospace Engineering, University of Maryland, College Park:

Tarandeep Kalra

France Vigouroux

Elizabeth Weiner

Special thanks to Ananth Sridharan for his assistance with stability analysis

Special thanks to Shane Boyer for his expertise in X-Plane test piloting

Contents

Acknowledgements	i
List of Figures	vi
List of Tables	ix
1 Introduction	1
2 Mission Requirements	1
2.1 Summary of the Mission	1
2.1.1 Course Rules and Regulations	1
2.1.2 Qualitative Assessment of Design Requirements	2
2.2 Flight Path Planning	3
2.2.1 Slalom	3
2.2.2 Short Stop	5
2.2.3 Quad Pylon	6
2.2.4 Quantitative Assessment of Design Requirements	8
3 Vehicle Configuration Selection	9
3.1 Analytical Hierarchical Process	9
3.2 Possible Configurations	11
3.2.1 Conventional Helicopter	11
3.2.2 Tiltrotor	11
3.2.3 Tailsitter	12
3.2.4 Compound Helicopters	12
3.3 Pugh Decision Matrix	13
3.4 Selection of a Configuration	14
3.5 House of Quality	15
4 Preliminary Sizing	17
4.1 Description of the Sizing Algorithm	17
4.2 Sizing Considerations	18
4.3 Trade Studies	19
4.3.1 Rotor Diameter and Number of Blades	19
4.3.2 Rotor/Wing Load Sharing during Maneuver	21
4.4 Tail Selection and Sizing	22
4.4.1 Empennage Configuration	22

4.4.2	Empennage Sizing	22
4.4.3	Control Surfaces Sizing	23
4.5	Initial Aircraft	24
5	Performance Overview	25
6	Rotor Design	25
6.1	Aerodynamics	26
6.1.1	Blade Twist	26
6.1.2	Blade Tip Shape	26
6.1.3	Blade Airfoils	28
6.2	Blade Structural Design	28
6.2.1	Material Selection for the Rotor Blade	28
6.2.2	Manufacturing the Rotor Blade	29
6.2.3	Sectional Properties of the Rotor Blade	30
6.3	Rotor Hub Design	31
6.4	Rotor Dynamics	32
6.4.1	Rotor Flap-Lag and Pitch-Flap	32
6.4.2	Ground Resonance and Air Resonance	33
7	Propeller Design	33
7.1	Aerodynamics	34
7.1.1	Propeller Diameter	34
7.1.2	Number of Blades and Rotational Speed	34
7.1.3	Anti-torque Requirements	35
7.1.4	Blade Twist	36
7.1.5	Blade Tip Shape	37
7.1.6	Propeller Airfoils	37
7.2	Propeller Blade Structure	37
7.3	Propeller Hub	38
7.4	Compatibility with the <i>Dart E550</i>	39
7.5	Propeller Dynamics	39
8	Power System and Transmission	39
8.1	Turboshaft Engine	40
8.2	Alternative Propulsion System: The <i>Dart E550</i>	41
8.2.1	Propulsion System Selection	42
8.2.2	Power Requirements	42
8.2.3	Power Plant Trade Study	43
8.2.4	Fully-Electric Hybrid Power Plant Design	45
8.2.5	Motor Selection and Design	48
8.3	Transmission	50
8.3.1	Transmission Selection	50
8.3.2	Main Gearbox	51
8.3.3	Nose Gearbox and Overrunning Clutch	52
8.3.4	Propeller Gearboxes	52
8.3.5	Main Rotor Shaft	52
8.3.6	Propeller Driveshafts	52

8.3.7	Electrical Power Distribution System	53
8.4	Power-By-Wire	54
8.4.1	Transmission for the <i>Dart E550</i>	54
9	Airframe Design	54
9.1	Material Selection for the Airframe	55
9.2	Primary Load Paths	56
9.3	Wing to Fuselage Attachments	57
9.4	Tail Boom Structure	57
9.5	Cockpit Structure	58
9.6	Landing Gear	58
9.7	Transportability	58
9.8	Slung Load Capability	59
9.9	Wing Design	59
9.9.1	Wing Geometry	59
9.9.2	Airfoil Selection	60
9.9.3	Wing Structural Design	60
9.9.4	Wing Finite Element Analysis	60
9.9.5	Whirl Flutter Analysis	62
10	Weight Analysis	62
10.1	Center of Gravity Location	63
10.2	Center of Gravity Excursions During Flight	63
11	Avionics	63
11.1	Instrument Panel Layout	64
11.1.1	Glass versus Dial Cockpit Displays	64
11.1.2	Baseline Equipment	64
11.1.3	Payload Camera and Caution-and-Advisory Display	66
11.1.4	Communications	66
11.1.5	Force Feel Stick Feedback System	66
11.2	Health and Usage Monitoring (HUMS)	67
11.2.1	Health Monitoring	67
11.2.2	Usage Monitoring	67
11.2.3	Maintenance Interface	68
12	Stability and Control	68
12.1	Flight Control System	68
12.1.1	Cockpit Flight Controls	68
12.1.2	Control Mixing	69
12.1.2.1	Governing Propeller Pitch	69
12.1.2.2	Control Surface Management	69
12.1.3	Control Coupling	70
12.1.4	Digital Fly-by-Wire Architecture	71
12.2	Dynamics and Stability	72
13	Performance Analysis	73
13.1	Drag Estimation	74
13.2	Aerodynamic Download	74

13.3 Hover Performance	75
13.4 Rotor/Wing Load Sharing	76
13.5 Forward Flight Performance	77
13.6 Sideward Flight Performance	78
13.7 Dash Capability	78
14 Acoustics	78
14.1 Noise Requirements	78
14.2 Rotor Noise	79
14.3 Propeller Noise	79
14.4 Other Sources of Noise	79
14.5 Numerical Simulation	80
14.6 Results	80
15 Safety and Survivability	80
15.1 Electric System	82
15.2 Lightning Strike	82
15.3 Engine Failure	83
15.3.1 H-V Diagram	83
15.3.2 Autorotational Index	83
15.3.3 Zoom-Climb Performance	84
15.4 Impact Survivability	84
15.5 Water Recovery	84
16 Project Development Timeline	84
16.1 Technology Development Program	84
16.2 Project Development	85
16.3 Life-Cycle Cost Analysis	85
16.3.1 Acquisition Cost	85
16.3.2 Direct Operating Cost (DOC)	86
16.3.3 Indirect Operating Cost (IOC)	87
17 X-Plane Flight Simulator	87
17.1 X-Plane Flight Dynamics Model	88
17.2 Aircraft Development	88
17.2.1 Configuration Selection	88
17.2.2 Rolling Moment Analysis	89
17.2.3 Control Surfaces	89
17.2.4 Cockpit Design	89
17.2.5 Final Design	90
17.3 Course Development	90
17.4 Racing the Course	90
18 Summary	92

List of Figures

2.1	Air race course waypoints.	3
2.2	States of the aircraft through the slalom and the time to complete the maneuver for a sweep of design parameters.	4
2.3	States of the aircraft through the short stop.	5
2.4	Flight times for the short stop maneuver for varying accelerations and forward speeds at load factor of 5g.	6
2.5	Flight times for the short stop maneuver for varying decelerations, load factor, and forward speeds.	7
2.6	States of the aircraft through the quad pylon.	8
2.7	The final optimization results.	9
3.1	Representative images of the VTOL vehicle configurations that were considered	10
3.2	AHP1 results for vehicle configuration	11
3.3	Eurocopter X ³ and Sikorsky X2 compound helicopters.	13
3.4	Pugh matrix	16
4.1	Block diagram of sizing algorithm.	18
4.2	Historical data for blade loading coefficient versus MGTOW. MSL ISA.	19
4.3	Parametric study of the effects of rotor diameter and number of blades on vehicle characteristics.	20
4.4	Trade study of the effects of maneuver load sharing on vehicle characteristics.	21
4.5	Empennage overview.	22
4.6	Historical data for tail designs.	23
4.7	The preliminary aircraft design.	24
6.1	Trade study of blade twist and its effect on rotor power: (a) comparison of twist shapes; (b) comparison of linear twist rates. MSL 103°F.	27
6.2	Trade study of blade tip shape: (a) tip sweep reduces power required for the short stop maneuver; (b) taper coupled with tip sweep can reduce power required. MSL 103°F.	27
6.3	Lift distributions on the rotor blades at different forward speeds.	28
6.4	The three rotor blade structural sections.	29
6.5	Internal structure of the blade and flexure	29
6.6	Sectional properties along the rotor blade.	30
6.7	Fan plot showing rotor blade structural modes as a function of rotor rpm.	31
6.8	Pitch bearing arrangement	32
6.9	Results from the aeroelastic analysis of the isolated rotor.	33
6.10	Stability analysis of ground resonance.	33
7.1	The effect of propeller diameter on propulsive efficiency.	34

7.2	Performance of optimum combinations of propeller rotational speed and number of blades. MSL 103°F.	35
7.3	Effect of differential propeller shaft speed on power and roll moment. MSL 103°F.	36
7.4	Trade study on propeller blade twist. MSL 103°F.	36
7.5	Trade study on propeller taper. MSL 103°F.	37
7.6	Propeller lift coefficients at zero acceleration and maximum acceleration. MSL 103°F.	38
7.7	Propeller blade structure	38
7.8	Propeller hub and collective pitch actuation mechanism.	39
7.9	Propeller blade fan plot.	40
8.1	Engine historical data.	40
8.2	Turboshaft engine and fuel tanks.	41
8.3	The specific energies and powers of various power generation technologies.	43
8.4	Diagram of a PEM Fuel Cell.	44
8.5	Flow of power through the system. M_R is the main rotor motor and M_P is a propeller motor.	45
8.6	Preliminary system weight and volume.	46
8.7	Cell potential and power density as a function of current density.	46
8.8	The system weight, component weight, and volume as a function of current density.	47
8.9	A Halbach array motor and a cutaway of a Halbach array motor stack.	48
8.10	A sketch of a Halbach array motor and the power curve for the LP HA motor.	49
8.11	<i>Dart T690</i> transmission layout.	50
8.12	Propeller Gearbox.	52
8.13	Power distribution schematic. The generators and DC buses are isolated by the relays in the case of a short circuit.	53
8.14	The two electro-hydrostatic actuators (EHA) used in the <i>Dart</i>	53
9.1	Cut away view of the internal components of the <i>Dart T690</i>	55
9.2	Layout considerations of rollover, tail strike etc.	55
9.3	Load paths viewed from the (a) front and (b) side of the aircraft.	56
9.4	<i>Dart T690</i> wing removal process. (a) Wing in flight condition with the fairing attached. (b) Wing structure with fairing removed, 4 bolts secure each wing. (c) Wing removed from the <i>Dart T690</i> for transport.	57
9.5	Landing gear (a) extended and (b) retracted.	58
9.6	Slung load support consisting of an electric winch, a hook, and a housing with ensures the hook properly retracts into the fuselage.	59
9.7	Wing geometry and structure.	60
9.8	Wing box structure.	61
9.9	Whirl flutter analysis, damping.	61
10.1	Distribution of the weight of primary systems throughout the helicopter, the c.g. is identified in red.	63
11.1	<i>Dart T690</i> cockpit.	65
11.2	Racing cockpits.	66
12.1	<i>Dart T690</i> Flight Controls Diagram.	69
12.2	Maximum propeller pitch versus forward speed (kts).	70
12.3	Steady level flight control inputs.	71
12.4	Control mixing scheme versus airspeed.	71

12.5 Flight Control System Architecture.	72
12.6 Dynamics of the different modes.	73
13.1 Elevator deflects to reduce download on the horizontal tail surface.	75
13.2 HOGE hover performance.	76
13.3 Load sharing reduces power compared to lifting with only the wing or rotor.	76
13.4 Rotor/wing load sharing: (a) load sharing schedule; (b) power bands.	77
13.5 Power and fuel flow in forward flight. MSL 80°F.	77
13.6 Power required in sideward flight at design takeoff weight. MSL 103°F.	78
13.7 Dash capability versus airspeed. MSL 80°F.	79
14.1 Comparison in hover of thickness and loading noise.	80
14.2 Comparison at 220 kts of thickness and loading noise.	81
14.3 Total sound pressure level for different airspeeds.	81
14.4 FAR36 requirement.	82
15.1 Engine out performance for the <i>Dart</i>	83
16.1 Milestones chart for development of the <i>Dart T690</i>	86
16.2 Operating Costs.	87
16.3 Operating Costs comparison.	87
17.1 Graphical representation of the X-Plane flight dynamics model.	88
17.2 Prototype X-Plane.	89
17.3 X-Plane model of <i>Dart T690/E550</i>	90
17.4 Race course model in X-Plane	91

List of Tables

2.1	Optimal vehicle parameter values for slalom maneuver.	5
2.2	Optimal vehicle parameters for short stop maneuver.	6
2.3	Optimal vehicle parameter values for quad pylon maneuver.	7
2.4	Optimal vehicle parameters found from path planning optimization.	8
3.1	Representative prioritization matrix	10
3.2	Pugh decision matrix for the compound designs	13
3.3	Pugh matrix	14
4.1	Preliminary sizing results.	21
4.2	Sizes summary.	23
8.1	Engine characteristics.	41
8.2	Lapse rates.	41
8.3	Power values required for the different mission segments.	42
8.4	Maximum power required by the rotor and propellers.	43
8.5	Battery and fuel cell properties projected to expected values for 2017.	44
8.6	Weight and volumes for a pure battery and a pure fuel cell vehicle.	45
8.7	Design specifications for the PEM fuel cell and Li-ion batteries.	47
8.8	LaunchPoint HA motor and motor controller properties. [1]	49
8.9	HA motors used on the <i>Dart 550</i>	50
8.10	Breakdown of transmission stage sizes and ratings.	51
10.1	Dart T690 component weight estimates.	62
10.2	Mass properties of the helicopter at various points in the course.	63
13.1	Parasitic drag buildup.	74
16.1	Current TRL and projected year ready for advanced technologies on the <i>Dart T690/E550</i>	85
16.2	Cost comparison	86
17.1	<i>Dart T690</i> race segment times.	91
17.2	<i>Dart T690</i> race statistics.	91

1 Introduction

Air racing captured the eye of the public early in the twentieth century and has since grown into an international phenomenon. With the revitalization of public interest in air racing from the introduction of the Red Bull Air Races and also its increased popularity in Reno, it has come to the realization of the rotorcraft industry that there is no equivalent VTOL racing aircraft in the rotorcraft world. To spark interest in a rotorcraft racing sport to rival Reno and the Red Bull series, the 2012 AHS Student Design Competition Request For Proposal (RFP) is to design a purpose-built rotorcraft to race on a prescribed pylon course.

One of the main challenges faced in such a design is the unprecedented maneuverability of the aircraft that is required to complete such a course. For instance, Red Bull series pilots regularly pull 9g turns during a race, a load factor unheard of for a conventional rotor system. The goal is to finish the course in as fast of a time as possible, while keeping a balance between load factor, forward speed, and fuel efficiency, all while maintaining large margins of safety for the pilot and spectators.

Using advances in technology and innovative design concepts, the University of Maryland Design Team has created the *Dart T690*, a lift and thrust compounded pylon racing rotorcraft and its electric counterpart, the *Dart E550*. The *Dart* is designed to fulfill and exceed all the requirements of a pylon racing aircraft and bring VTOL into the air racing community.

2 Mission Requirements

The design of a VTOL racing aircraft is unique, and as such, there were a broad number of configurations considered before settling on a lift and thrust compounded rotorcraft design. The final compound configuration was chosen because it demonstrated the ability to meet all the requirements dictated by the RFP, including agility, hover capability, and high-speed forward flight.

2.1 Summary of the Mission

The mission stated in the RFP is to complete a pylon race over the Hudson River, in between New York and New Jersey, on a calm day at sea level. The vehicle must fly the course in the fastest time possible, while demonstrating good fuel efficiency. During the flight, the pilot must follow the designated path demarcated by the pylon gates, making sure not to exceed the boundaries of the pylons or the course, in general.

2.1.1 Course Rules and Regulations

While the course outlined by the RFP is similar to that of the Red Bull and Reno air races, there are some differences in the rules for a rotorcraft-specific race. The course regulations are:

- The crew of the rotorcraft consists of one 225 lb occupant.
- The pilot must maintain full control of the vehicle. While stability augmentation is not prohibited, the pilot must be able to fly the aircraft in the event of a stability augmentation system failure.
- Any contact with the pylons results in immediate disqualification.
- The aircraft cannot bank more than 90°.
- The aircraft must pass through the pylons at or below the top of the pylon.



Flying the Course



DART T690



Start



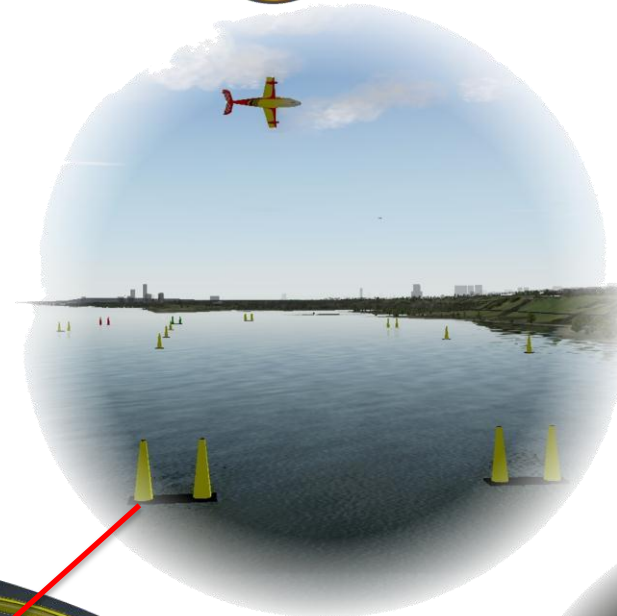
Quad Pylon



Coordinated Turn



Short Stop



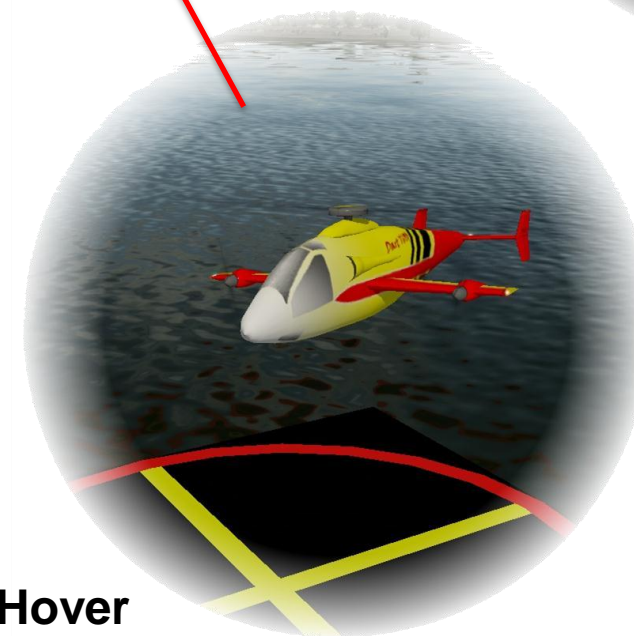
Slalom



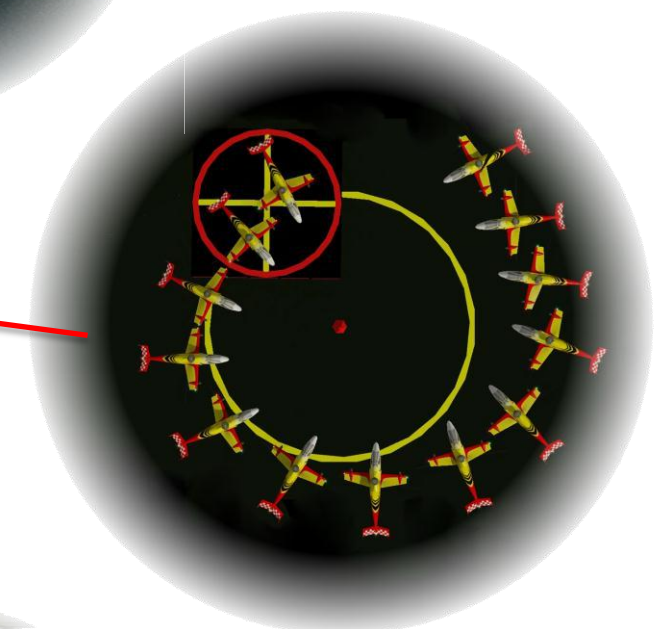
Slung Load



Hover



Pirouette



- Any deviation from the course boundaries will result in a 30 second penalty for every second outside of the boundaries. In segment 7, passing the 300 ft short stop results in only a single 30 second penalty to the overall course time.

The RFP does not provide specific range or performance characteristics of the aircraft, but does include a set of flight constraints (e.g., loiter time, takeoff time, etc.) that the aircraft must satisfy. These additional requirements include:

- A 10 minute engine warm-up period.
- Takeoff within 5 minutes of being given the rotors turning signal.
- A maximum 10 minutes of elapsed time between take-off and the passing through the start gate.
- Enough fuel for 15 minutes of sustained flight at TOGW at V_{be} .
- The aircraft must be capable of OGE hover at MSL/103 °F at TOGW.
- The aircraft must be able to cruise at 125 kts at 90% MCP.
- The aircraft must demonstrate the ability to perform a 60 kts sideward flight at MSL/103 ° at TOGW.

2.1.2 Qualitative Assessment of Design Requirements

Unlike typical rotorcraft designs, which are driven by performance requirements such as speed, payload, endurance, and range, the design of a pylon racer must focus on a vehicle that can complete a race course quickly and efficiently. The driving factors for this mission are not explicitly known a priori, however, initial insight can be drawn by examining the course and aircraft that compete in the Red Bull and Reno air races.

Slalom: During the course, the pilot must complete two slalom maneuvers by weaving in and out of three successive pylons. Aircraft that are capable of performing this maneuver fly at high speeds and perform hard, almost 90° banked turns, suggesting that the aircraft needs to have exceptional roll and pitch rates, as well as the ability to sustain high load factors.

Short Stop: In this section, the pilot flies through a gate and must immediately perform a hammerhead-type maneuver to fly through another set of gates. This maneuver requires extreme translational deceleration, as well as high yaw and pitch rates. The completion of this segment also requires the performance of a high load factor maneuver in a confined space.

Straight Away: The straight away gives the aircraft an opportunity to reach its maximum speed. This section runs almost the entire length of the course, so faster aircraft can take less time to complete this segment. This requirement suggests that a high forward acceleration and top speed is advantageous to a pylon racer.

Quad Pylon: The quad pylon is a classic segment found in many air races. The pilot is required to perform either an extremely tight banked turn or another hammerhead-type maneuver. These maneuvers require the aircraft to have good turning rates, as well as high load factor capability.

Hover, Pirouette, Pickup: After completing the second slalom and a turn, the aircraft slows to a hover, thereby requiring good deceleration characteristics. It then perform a pirouette maneuver, requiring good low speed handling qualities. The pilot then positions the aircraft to pick up a slung load.

Sideward Flight: Upon picking up the slung load, the aircraft performs a sideward flight for a distance of 500 yards. This requirement demands good low speed handling qualities as well as the ability to maintain a steady sideward flight with a slung load.



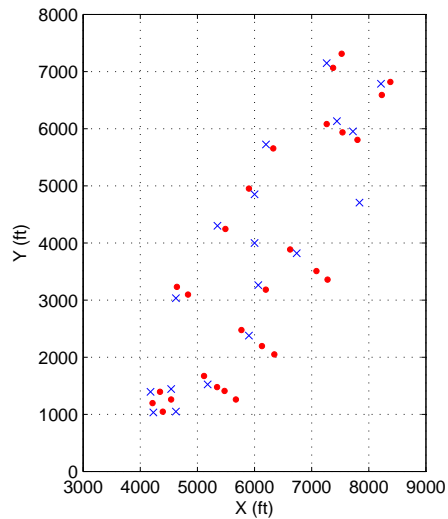


FIGURE 2.1: The air race course with dots representing the pylons and blue x's representing the waypoints.

After examining each segment of the course, several critical requirements stand out: acceleration (dash capability), deceleration, top speed, vertical load factor, and agility (e.g., high turn rates). These requirements are used as a starting point in the assessment of the aircraft design parameters that are discussed in the following section.

2.2 Flight Path Planning

A flight path planning optimization technique is used to quantify the design requirements for the vehicle (e.g., acceleration, deceleration, top speed, load factor, and agility). The flight path planning also provided the optimal course for the pilot to fly to minimize the flight time. The key results obtained from this analysis set down the operating requirements for the aircraft.

As inputs, the path planner takes the constraints on the aircraft and the required path, including vehicle dynamics, control limits, a list of waypoints the vehicle must pass through (shown in Fig. 2.1), and any trajectory limitations such as maximum altitude, etc. A Radau Pseudospectral Optimizer [2] was implemented to determine the optimal flight path and completion time given a set of vehicle parameters. By running the path planning optimizer for a range of realistic vehicle parameters, the vehicle requirements that minimize the course time were determined.

Each part of the course laid down different vehicle requirements, so the optimizer was run individually for several sections of the course. The entire course was optimized sequentially, one segment at a time, using the end conditions from the previous segment as the initial conditions for the next segment. It was found that three sections of the course drove the vehicle requirements: the slalom, short stop, and quad pylon maneuvers.

2.2.1 Slalom

Figure 2.2 shows a typical output from the path planner for a given set of vehicle parameters for the slalom maneuver. Figure 2.2(a) shows the X and Y position of the vehicle. The red dots are the pylons and the



blue x's are the chosen waypoints for this section. Figure 2.2(b) shows the speed of the vehicle as a function of time, and Fig. 2.2(c) shows the roll angle of the aircraft. The red lines represent the times at which the vehicle crosses a gate.

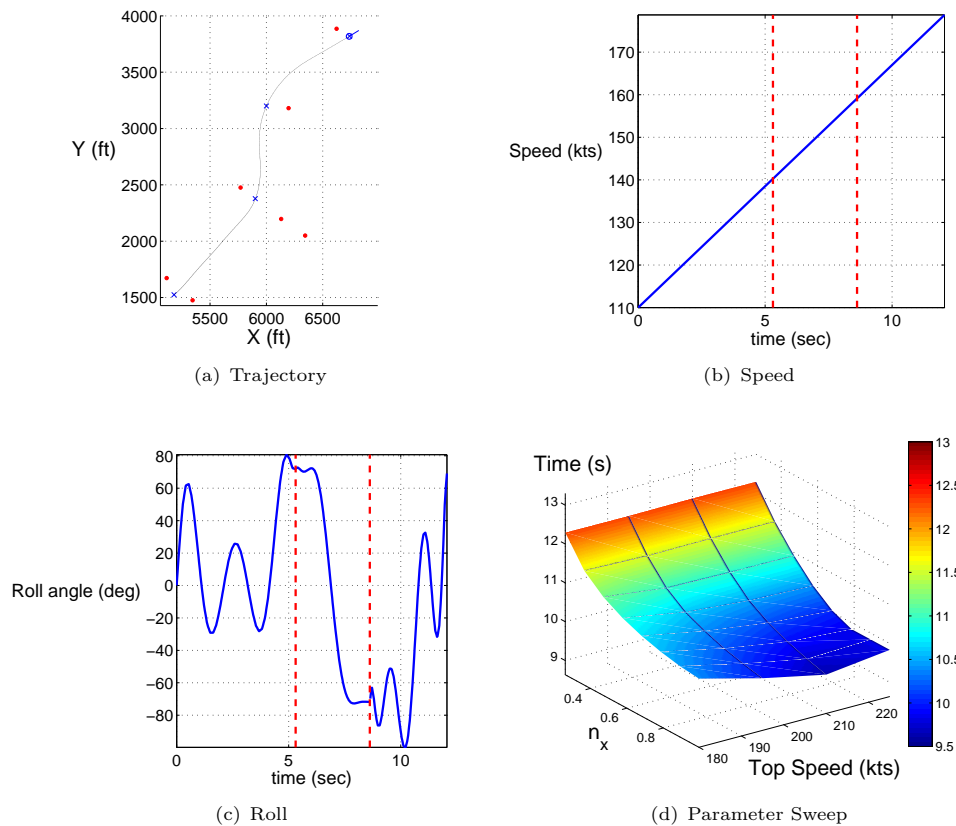


FIGURE 2.2: (a) Trajectory of the vehicle through the slalom; (b) speed of the vehicle; (c) roll angle of the vehicle as a function of time; (d) segment time as a function of top speed and forward acceleration.

This sample output shows that the vehicle accelerates the entire time through the slalom, and that there are large changes in roll angle over a short period of time, i.e., the n_x (maximum forward acceleration) and roll rate must be high to quickly complete this section of the course.

The path planner was run for a range of vehicle parameters to confirm these results, and to determine what set of vehicle parameters allow the completion of the course in the shortest time. Figure 2.2(d) shows the flight times for the slalom maneuver for varying maximum accelerations, n_x (in g's) and maximum forward speed for a n_z (maximum vertical acceleration) limit of 5g. On the x -axis is the maximum forward speed, on the y -axis is the maximum n_x and on the z -axis is the time taken to complete the maneuver in seconds. The color of the graph also shows the time to complete the maneuver, with blue being a low time and red being a high time. For example, at an n_x of 0.6g and a maximum forward speed of 200 knots, the time to complete this point of the course is 10.5 seconds. Figure 2.2(d) shows that the maximum vehicle speed does not generally affect the completion time until an n_x of about 0.6g is reached. The value of n_x , on the other hand, does improve the course time until about 0.8g. Table 2.1 summarizes the optimal vehicle parameters during this section of the course.



TABLE 2.1: Optimal vehicle parameter values for slalom maneuver.

Vehicle parameter	Optimal value
n_x	0.6g
n_z	4g
Top speed	200 kts

2.2.2 Short Stop

The optimizer for this section of the course starts at the end of the slalom, goes through the two pylons and ends about halfway through the straightaway. Figure 2.3 shows a sample output of the path planner for this maneuver, as well as the speed, yaw, pitch, and altitude of the vehicle as a function of time. The results show that the vehicle speed rapidly decreases immediately out of the slalom. As soon as the vehicle enters the first gate of the short stop, it rapidly pitches up and begins to yaw left while continuing to decelerate. Halfway through the short stop the vehicle has yawed 180° and begins to accelerate on its way down to the second gate. This maneuver is known as a “hammerhead.” The vehicle then continues to accelerate through the first leg of the straightaway.

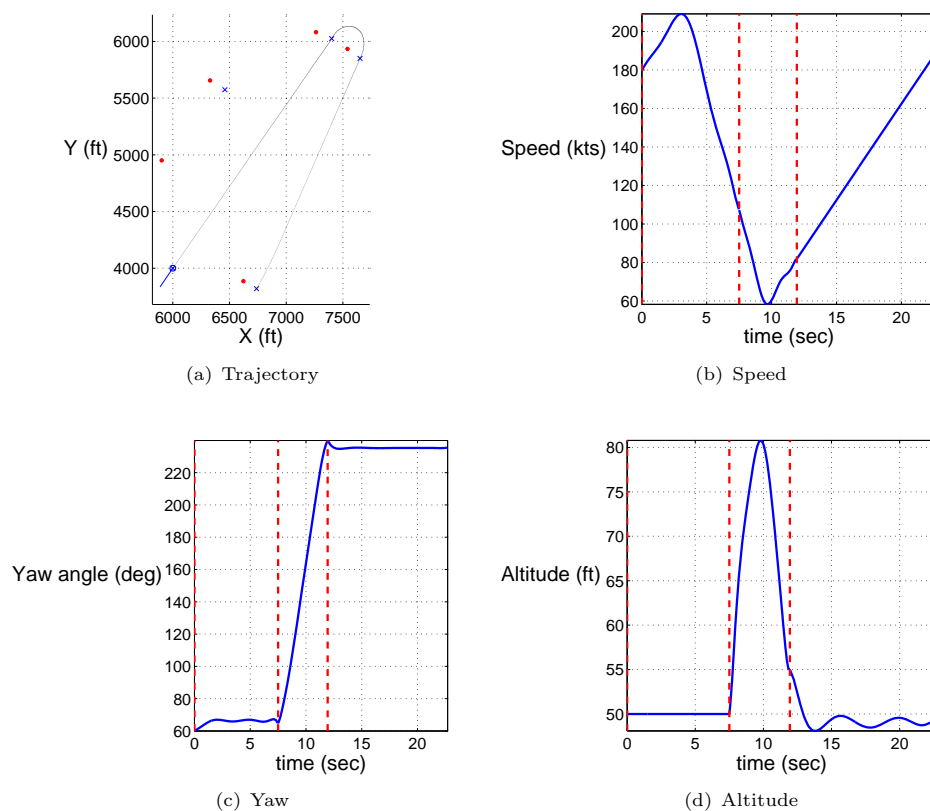


FIGURE 2.3: States of the aircraft through the short stop.

The path planning optimizer was run for a range of top speeds and values of n_x , $-n_x$, and n_z to determine



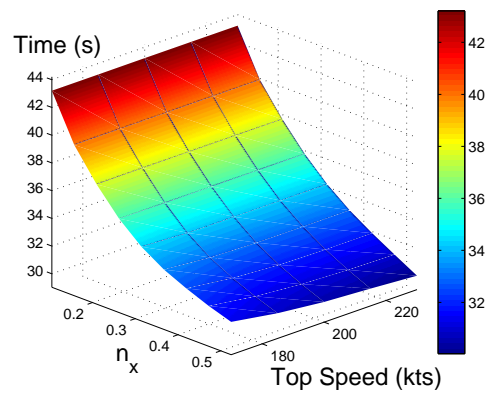


FIGURE 2.4: Flight times for the short stop maneuver for varying accelerations and forward speeds at load factor of 5g.

TABLE 2.2: Optimal vehicle parameters for short stop maneuver.

Vehicle parameter	Optimal value
n_x	0.9g
$-n_x$	0.9g
n_z	5g
Top speed	220 kts

the optimal vehicle parameters for this hammerhead maneuver. Figure 2.4 shows the time to complete the course as a function of top speed and n_x , similar to that shown in Fig. 2.2(d). Here it is seen that both n_x and top speed affect the flight time. In general, increasing n_x will always improve the flight time, but there is a fundamental limit to the effect of top speed. For a given n_x , the speed that the vehicle can attain during the straightaway portion of the maneuver is limited by the length of the straightaway. Hence, the vehicle may not reach its top speed before it has to slow down for the quad pylon. This implies that the maximum speed the vehicle is capable of reaching during the race course is limited by the available forward acceleration. For example, in Fig. 2.4, for an n_x of 0.5g, the vehicle course time barely changes when the vehicle speed is 200 kts or greater, so 200 kts could be set as the maximum speed of the vehicle.

Figure 2.5 shows how $-n_x$, n_z , and top speed change the flight time with an n_x of 0.6g. The path planner predicts that all three of these quantities will affect the flight time to varying degrees. As n_z increases, the completion time decreases, but there is a point of diminishing returns between 5g and 6g. Based on this result, an n_z of 5g was chosen as the design point for this maneuver. Using an n_z of 5g, the top speed, n_x and $-n_x$ were chosen at points of diminishing returns.

Table 2.2 shows the optimal vehicle parameters for this section of the course based on the path planning optimization. Compared to the slalom maneuver, it is seen that the optimal n_x stays the same, but the optimal top speed and n_z both increase.

2.2.3 Quad Pylon

Figure 2.6 shows the trajectory of the vehicle through the quad pylon along with a few key vehicle states as a function of time. The qualitative analysis in Section 2.1.2 suggested a possible coordinated turn to complete



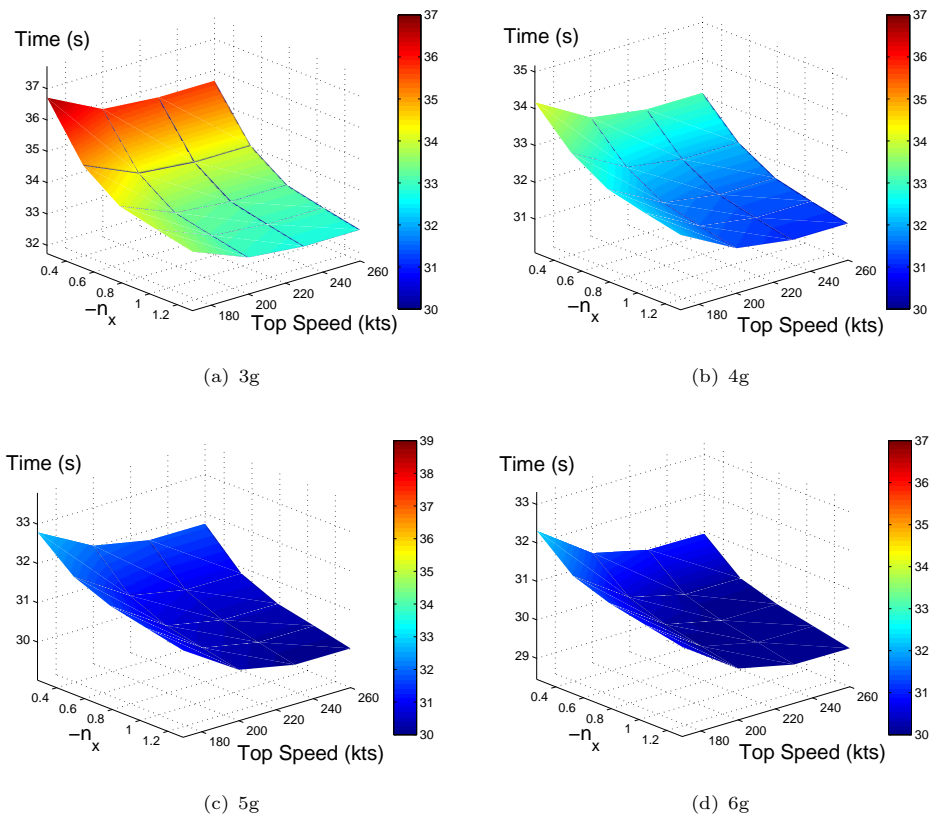


FIGURE 2.5: Flight times for the short stop maneuver for varying decelerations, load factor, and forward speeds.

TABLE 2.3: Optimal vehicle parameter values for quad pylon maneuver.

Vehicle parameter	Optimal value
$-n_x$	0.9g
n_z	5g
Top speed	220 kts

this segment, however, the flight path planning optimizer found that a hammerhead-type maneuver will be needed to minimize the segment time (similar to the short stop). This means that pitch rate, $-n_x$, and n_z are important for this portion of the course as well.

The path planner was run for a range of $-n_x$, n_z , and top speeds, as was done for the short stop. Because the vehicle decelerates for most of this maneuver, the parameter n_x was not included in the parameter sweep for this maneuver. Additionally, the optimization of the slalom maneuver showed that the vehicle must be capable of an n_z of 4g, so the 3g limit was omitted in the sweep as well. The results show that there is a benefit in increasing n_z from 4g to 5g, but not as much from 5g to 6g. Hence, an n_z of 5g was set as the design point for this maneuver. For $-n_x$, there is a point of diminishing returns around 0.9g, for which increasing the top speed is only beneficial up to 220 kts. Table 2.3 shows the optimal vehicle parameters to complete this particular maneuver.



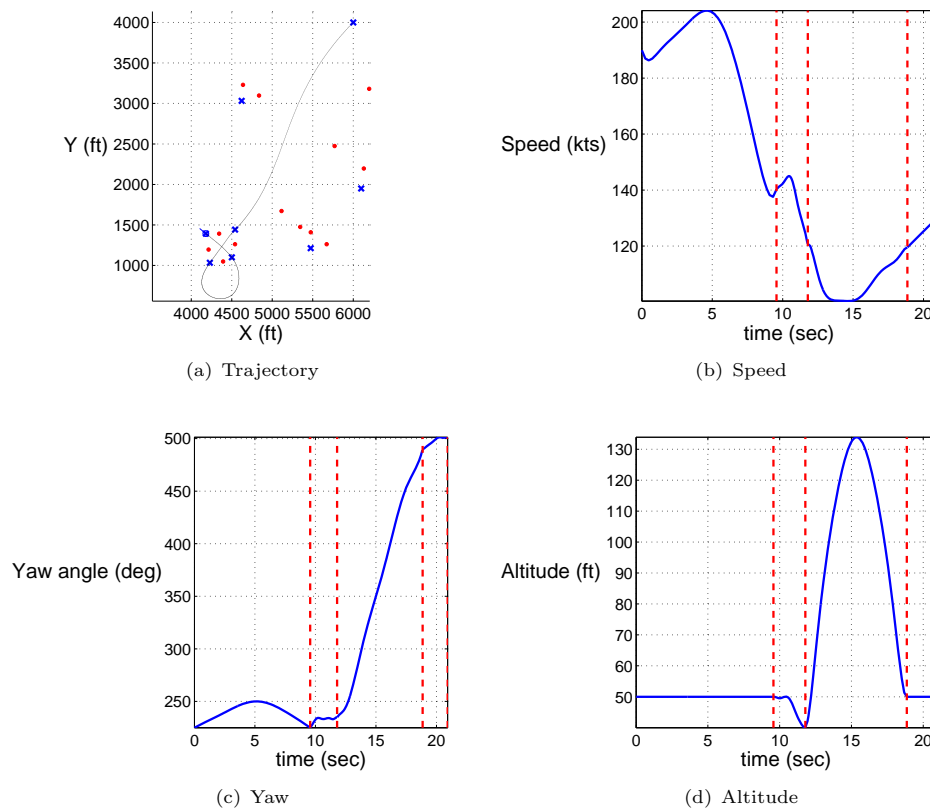


FIGURE 2.6: States of the vehicle through the quad pylon.

TABLE 2.4: Optimal vehicle parameters found from path planning optimization.

Vehicle parameter	Optimal value
n_x	0.9g
$-n_x$	0.9g
n_z	5g
Top speed	220 kts
Pitch rate	20 °/s
Roll rate	180 °/s
Yaw rate	60 °/s

2.2.4 Quantitative Assessment of Design Requirements

For each maneuver, the path planning optimization provided the optimal vehicle parameters. Table 2.4 shows the final results that minimize the flight time, as well as the necessary attitude rates. This set of parameters define the requirements for the design of the aircraft. Using the optimal vehicle parameters in Table 2.4, the course up to the helipad at waypoint 7 was optimized. Conservative estimates for side flight and slung load performance were used to predict the flight time for the remaining portion of the course. Figure 2.7(a) shows the optimal flight path, and Fig. 2.7(b) shows the corresponding $n_z - V$ diagram, which is used to determine what maneuver provides the most stringent requirement. Based on the $n_z - V$ diagram,



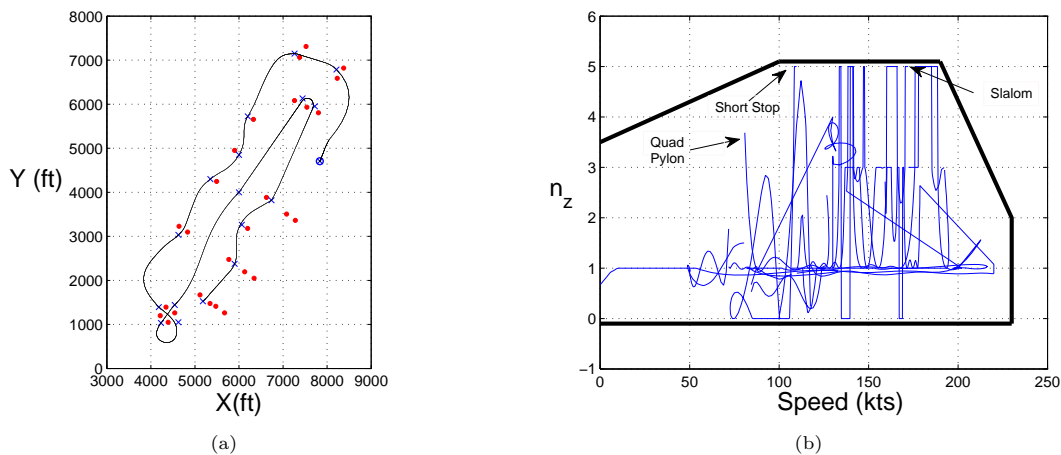


FIGURE 2.7: The final optimization results (a) The optimized path; (b) $n_z - V$ diagram for the optimal flight path.

the short stop maneuver sets the requirement for the lifting capability of the vehicle since it requires the highest load factor (5g) at the lowest speed (110 kts).

3 Vehicle Configuration Selection

The opportunity to design a rotorcraft meant purely for the sport of pylon racing is a unique challenge and, as such, the resultant vehicle configuration is not an obvious choice. The extreme capabilities (high airspeed, acceleration, agility and load factor capacity) required of this aircraft necessitated the examination of a broad set of possible VTOL configurations. The configurations studied included: single main rotor (conventional helicopter), coaxial rotor system, tiltduct, tiltrotor, quadrotor, fan-in-wing, compound, tip-jet driven autogiro, and tailsitter; these configurations are shown in Fig. 3.1.

The design process used to down-select from these configurations started with the use of an Analytical Hierarchical Process (AHP), followed by a Pugh decision matrix. The configuration that was finally selected was a lift and thrust compounding rotorcraft.

3.1 Analytical Hierarchical Process

To objectively compare the large number of configurations being considered, an Analytical Hierarchical Process (AHP) was used to rank the critical design variables. The flight path planning identified that forward airspeed, translational acceleration, and agility set the vehicle design requirements. The RFP also requires the vehicle to have the ability to hover, perform lateral flight, remain fuel efficient, have a small geometric footprint, and be relatively inexpensive. As such, these requirements were also included in the AHP.

The rankings for each design parameter were obtained by comparing their relative importance. While all the design parameters are important, this AHP provides a heavier weighting to the design parameters that are



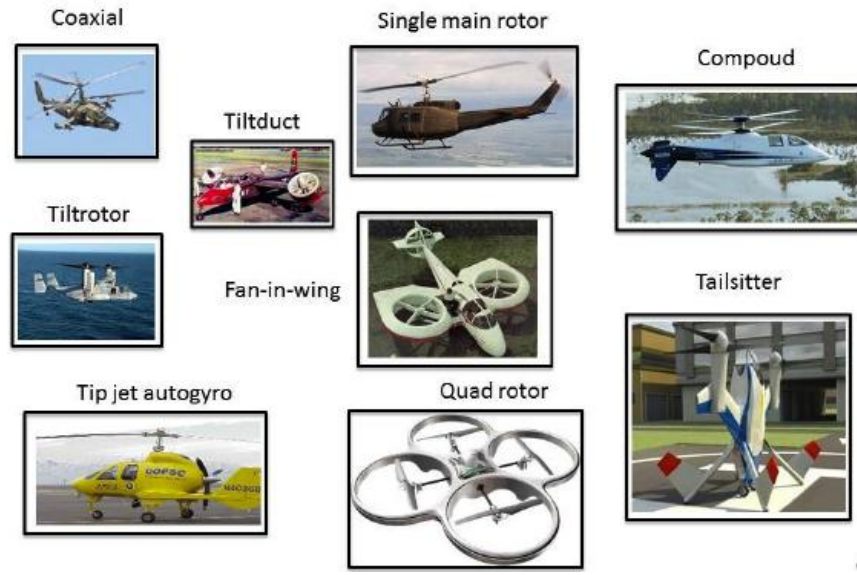


FIGURE 3.1: Representative images of the VTOL vehicle configurations that were considered.

TABLE 3.1: Representative prioritization matrix given by the AHP. The top three variables are forward speed, agility, and acceleration.

	Hover Capability	Forward Speed	Fuel Efficiency	Agility	1/Development	Acceleration	Lateral Flight	Score	Rank
Hover Capability	0.07	0.10	0.11	0.05	0.06	0.05	0.19	0.09	4
Forward Speed	0.22	0.30	0.26	0.25	0.31	0.49	0.19	0.29	1
Fuel Efficiency	0.02	0.04	0.04	0.05	0.02	0.03	0.02	0.03	7
Agility	0.37	0.30	0.19	0.25	0.18	0.16	0.19	0.23	2
1/Development	0.07	0.06	0.11	0.08	0.06	0.05	0.02	0.07	6
Acceleration	0.22	0.10	0.19	0.25	0.18	0.16	0.32	0.20	3
Lateral Flight	0.02	0.10	0.11	0.08	0.18	0.03	0.06	0.09	5

more critical to the mission outlined in the RFP and also as given by the flight path planning optimization. A sample prioritization matrix is shown in Table. 3.1.

From the results in Fig. 3.1, it is apparent that three design parameters stand out as the most important, namely forward airspeed, agility, and translational acceleration; this was expected because these design parameters were identified by the flight path optimization as the most important for a pylon racer.

All of the aircraft configurations were then compared for each of these design parameters, with each configuration being given a relative score. The score was multiplied by the weight of each individual design parameter and the resultant products were summed. The results were then normalized and the configurations were ranked, as shown in Fig. 3.2. A higher number means that the aircraft configuration scored better for the given set of design parameters.

The results in Fig. 3.2 show that the top three aircraft configurations that best met the design requirements are the tailsitter, tiltrotor, and compound. These aircraft configurations have relatively good speed, acceleration, deceleration, and agility characteristics, thereby meeting many of the RFP requirements.



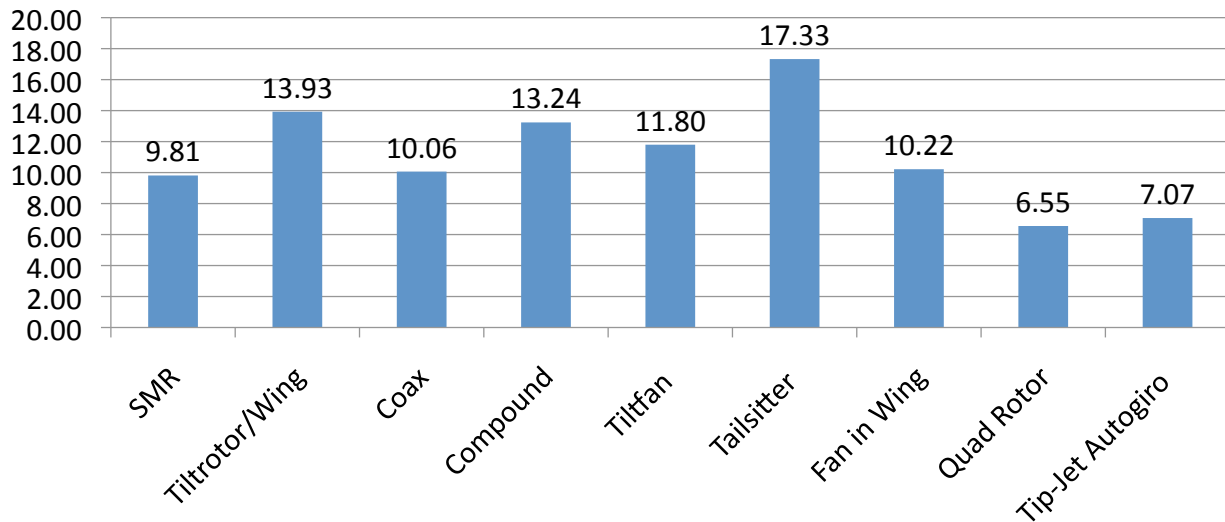


FIGURE 3.2: The relative vehicle rankings from the AHP. A higher number corresponds to a more suitable configuration.

3.2 Possible Configurations

The advantages and disadvantages of each configuration were considered both from a historical perspective and as they apply specifically to a pylon racing type of aircraft.

3.2.1 Conventional Helicopter

While a conventional, single main rotor/tail rotor helicopter was an unlikely choice for a fast, agile, high load factor capable racing aircraft, it was analyzed to provide a basis for comparison with the other configurations. Advantages of this configuration include good endurance, low empty weight fraction, and good hover efficiency. However, there are also many disadvantages, such as limited agility and low maximum forward speed, which are key design requirements for a pylon racer. As such, a conventional helicopter was deemed not to be a suitable choice.

3.2.2 Tiltrotor

The tiltrotor is a concept that swivels its rotors vertically for hovering flight and horizontally for forward flight. The advantage is that the vehicle can fly in both helicopter mode and airplane mode, allowing it to reach much higher forward flight speeds compared to a conventional helicopter. The disadvantages of this design include complexity of design, relatively high engineering risk, higher empty weight fraction, high cost of production, and a download penalty on the wings in hover. In addition, the smaller rotor diameter required for good propulsive efficiency in forward flight results in a high disk loading and a lower hovering efficiency. Consequently, this concept is not as efficient as a helicopter in hover or an airplane in forward flight. Nevertheless, the tiltrotor concept has proved its worth by demonstrating increased range, endurance, and speed. These capabilities allow the tiltrotor (and similar convertible rotorcraft concepts) to fill a niche that neither airplanes nor helicopters can occupy. In terms of a pylon racer, the tiltrotor may be a good candidate because of its high forward airspeed. However, its ability to accelerate and decelerate is limited



because there is a finite transition time between airplane and hover mode, making it less likely to meet the requirements of a pylon racer.

3.2.3 Tailsitter

The tailsitter design is a concept in which the aircraft takes off and lands on its tail. It takes off like a conventional helicopter and is capable of hover, and transitions to forward flight by tilting the rotor plane. This concept is unconventional and, as such, there are no production vehicles of this design. Historically, tailsitter designs were plagued with control issues that led to unsafe flight conditions. Only in recent years has the concept of the tail sitter been revisited as a personal flying aircraft with NASA's electric powered Puffin (currently a paper design) [3].

The major advantage with the tailsitter is that in forward flight it acts exactly like a twin propeller airplane and would presumably be as capable as a fixed-wing pylon racing aircraft. The advantage over the tiltrotor is that the transition time from hover to forward flight is considerably shorter, providing an improved acceleration capability. In comparison to a conventional helicopter, the tailsitter has smaller rotors and is, therefore, less efficient in hover but much more efficient in forward flight. The disadvantages include a higher empty weight fraction, greater mechanical complexity, the lack of historical precedent, increased design risk, and costs. Because of the numerous disadvantages, the tailsitter was deemed unsuitable as a pylon racer.

3.2.4 Compound Helicopters

While there are no compound helicopters currently in production, there are several experimental technology demonstrators and prototypes that have flown. Recently, the Eurocopter X³ design and the Sikorsky X2 have used advances in technology to push the limits of rotorcraft speed and agility, both of which are key to the success of a pylon racer. The exact use of compounding significantly impacts the potential flight envelope and the vehicle design. Helicopters can be lift compounded, thrust compounded, or dual compounded. Within these categories there are, again, a number of different possible configurations.

For thrust compounding concepts, the addition of a propeller or turbojet provides a major part of the forward thrust, allowing the main rotor to produce lift. Lift compounding requires the addition of wings on the fuselage that alleviate the lift and propulsion requirements of the main rotor. For thrust and lift compounding designs, both wings and propellers or thrusters can be used in a variety of combinations. The benefits of compounding are improved maximum speeds, endurance and range. The penalties of the design are increased empty weight fraction, complexity of design, and a higher engineering risk. Some of these factors are less important than for a conventional helicopter (e.g., empty weight fraction which is a less important consideration for a pylon racer). Additionally, compound designs have shown higher achievable forward speeds, acceleration and agility, which are major requirements for a pylon racer.

The list of compounds that were considered, with historical examples for reference, are given below:

- Adding a thruster on the tail while keeping the tail rotor. This basic concept was demonstrated by the Lockheed AH-56 Cheyenne. Adding additional propulsion as a tractor was also considered.
- A coaxial advancing blade concept (ABC) with a pusher, similar to the X2. The coaxial configuration balances torque reaction, while the pusher provides additional thrust.
- Swivelling the tail propeller so that it thrusts sideways in hover and low speed flight, but transitions to a propulsor at higher forward speeds, as used on the S-61F technology demonstrator.
- Fixing the tail rotor as a thruster and adding a duct with vanes so the thrust can be directed sideways in hover, like the Piasecki 16H Pathfinder. This vehicle configuration was also considered, but without the duct to mitigate weight issues.



FIGURE 3.3: Eurocopter X³ and Sikorsky X2 compound helicopters.

TABLE 3.2: Pugh decision matrix for compound designs. The single main rotor configuration is included for comparison.

		SMR	Pusher + TR	Tractor + TR	Pusher + Coax	Swiveling TR	Vaned Pusher	Vaned Duct	Dual Thruster
Weight	5	0	-3	-3	-2	-2	-2	-3	-3
Acceleration	10	0	2	2	2	2	2	2	3
Transition	10	0	2	2	2	0	1	1	2
Power Req	6	0	0	0	0	0	-2	-1	-1
Control Auth	5	0	2	2	2	-1	-2	-2	2
Total		0	35	35	40	5	-2	-1	39



- Adding two propellers on either side of the airframe to provide anti-torque at low speed, with the propellers also in the best position to generate thrust at high forward speed, as used on the Eurocopter X³.

These compound configurations were analyzed using a Pugh Decision Matrix (PDM) to down-select to a final configuration, as shown in Table 3.2. The results from showed that three configurations should be advanced to the next step in the selection process: Pusher+tail rotor, coax+pusher, and dual thruster.

3.3 Pugh Decision Matrix

A larger, more robust, PDM was used to examine the different compound designs (as well as the tailsitter and tiltrotor). The advantage of using a PDM was that it included the important design parameters determined from the flight path planning (acceleration, forward speed, and agility), but also other important design parameters such as cost, feasibility, maturity of technology, etc. The conventional helicopter was included for reference. The PDM is shown in Table 3.3, where higher scores indicate a more suitable design (i.e., a negative or low score is unfavorable).



TABLE 3.3: Pugh matrix rankings for several compound designs as compared to a tailsitter, conventional helicopter, and tiltrotor.

	Weightings	SMR	Tailsitter	X2	Cheyenne	X3	Tiltrotor	X2 + Wing
Top Speed	9	0	2	1	-1	1	2	1
Footprint	5	0	-1	1	0	0	-1	1
Acceleration	10	0	2	1	1	2	2	1
Deceleration	10	0	-1	1	1	1	-1	1
Conversion Time	5	0	-1	1	1	1	-2	1
Maturity of Tech	4	0	-2	-1	-1	-1	-1	-1
Agility (FF)	9	0	2	1	1	1	2	2
Agility (Hover)	5	0	-1	1	0	0	-1	1
G-Limit	7	0	2	1	1	2	2	2
Vibration	3	0	0	-2	0	-1	-1	-2
Downwash	3	0	-2	-1	0	0	-2	-1
Side Flight Performance	6	0	-1	0	-1	-1	-1	-1
Slung Load Stability	5	0	-1	0	0	0	1	0
Safety	10	0	0	0	0	0	-1	0
Feasibility of Design	4	0	-2	-1	-1	-1	-1	-2
Hover Efficiency	5	0	-1	-1	-1	-1	-2	-2
FF Efficiency	6	0	2	1	1	1	2	1
Manufacturability	2	0	-1	-2	-1	-2	-2	-2
Manufacturing Cost	3	0	-1	-2	-1	-2	-2	-2
Maintainability	2	0	-1	-1	0	-1	-2	-1
O&M Cost	3	0	-1	-1	0	-1	-2	-1
Alt. Power Source	8	0	0	0	0	0	0	0
Storage Compactness	2	0	0	1	-1	-1	-1	-1
Weighted Score		0	9	31	30	34	-8	28

The Pugh matrix revealed that while a tailsitter is, in theory, a good candidate for meeting the specific requirements of this RFP, it would not be a practically feasible design. The maturity of the technology is extremely low, and the many of the design tools required to perform a thorough analysis of this concept are not available. The tailsitter also ranks low in terms of side-flight performance, slung load operation, hover efficiency, manufacturing cost, operation and maintenance cost, and maneuverability to perform a pirouette. While none of these characteristics by themselves preclude the selection of a tailsitter, these less acceptable attributes makes the tailsitter a poor choice.

3.4 Selection of a Configuration

The top two designs from the PDM were the coaxial+thruster and the dual thruster. Both of these designs have advantages and disadvantages, but the dual thruster was ultimately deemed the better choice for a pylon racing mission. The coaxial+thruster, demonstrated most recently by the Sikorsky X2, is an elegant concept that alleviates the need for lift compounding. A rigid rotor is used to reduce the spacing between coaxial rotors, with the counterrotating rotors balancing torque. The advantage of this system is that the retreating side of each rotor is offloaded to reduce the effects of retreating blade stall. However, the



significant effort needed to reduce hub drag and rotor vibratory loads suggest that this is likely to be a heavier and more complicated system than the dual thruster configuration. Another disadvantage of this configuration is the close rotor/rotor spacing of a coaxial, which is undesirable for an agile aircraft; high load factor maneuvers may cause blade strikes. To prevent this, the blades need to have high stiffness, causing the rotor to be relatively heavy.

The Dual Thruster configuration, as demonstrated most recently by the Eurocopter X³, uses two propellers to provide forward thrust, acceleration in forward flight, and balancing of torque at low airspeeds. In a configuration where wings are already being considered, the placement of the propellers is logical and the alignment between the engine, gearboxes, propellers and rotor is configurationally simple. Furthermore, the addition of wings presents an opportunity to carry load on the wings rather than the rotor during maneuvers. Limitations of this concept include the possibility of whirl flutter when locating the propellers at the wing tips, and potentially having a large wing in the rotor downwash. However, careful design of the wing reduces any aeroelastic concerns. An advantage of this system over the coaxial+thruster configuration is that the torque from each propeller is balanced across a majority of the flight envelope, so reducing the rolling moment (see Section 7.1.3). Eurocopter has demonstrated this particular concept successfully without a fly-by-wire or stability augmentation system.

After weighing the advantages and limitations of both the coaxial+thruster design and the dual thruster design, the dual thruster configuration was selected because of its ability to off-load the vertical load factor from the rotor onto the wings. The dual thruster design also has a relatively logical center of gravity placement, no need for stability augmentation, and lower hub drag. The requirements listed in the RFP combined with the results from the flight path planning optimization called for an aircraft that is not only fast but extremely agile. If the aircraft was required to fly fast, similar to a drag racer, then a coaxial+thruster design is a more suitable candidate. However, because the design requirements are tailored more to a rally racing type of concept with an emphasis on agility and not just speed, the dual thruster design was decided to be the configuration for what was to become the *Dart T690*.

3.5 House of Quality

Once the vehicle configuration was selected, a house of quality was completed to best determine the engineering requirements that were most critical to the requirements of the path planning and RFP. This house of quality showed that parameters such as blade design, blade loading coefficient, and wing aspect ratio would prove to be the three most important aspects that would influence the design.



4 Preliminary Sizing

After the dual thruster compound configuration had been decided upon, a preliminary vehicle sizing was performed to obtain estimates of empty weight, engine size, fuel burned during the course, and other vehicle characteristics. Trade studies were conducted to examine the merits of varying the rotor diameter, the number of blades, and the lift sharing between the rotor and wing during the critical short stop maneuver. From these trade studies, a preliminary rotor design was determined. The key parameters that were taken into account when sizing the vehicle included gross weight, power required, stall margins, wing download, and cost.

4.1 Description of the Sizing Algorithm

The sizing methodology, as first developed by Tishchenko [4], takes the mission requirements and user-defined initialization data as inputs, and then provides the takeoff weight of the aircraft as an output. As intermediate steps, component weights are calculated based on historical data. To generate results for the *Dart T690*'s compound rotorcraft configuration, the methodology was modified to include the effects of adding a wing and propellers and removing the tail rotor. The equation for wing weight was taken from the V/STOL Aircraft Sizing and Performance Computer Program [5] (VASCOMP), while the propeller weight was calculated based on an equation from Roskam [6]. The “rubber” engine detailed in the RFP was included in the sizing code to determine the weight of the engine and its specific fuel consumption. All other component weights were determined using equations from Tishchenko's methodology. The methodology was validated against known component weights of helicopters in the same weight class as the *Dart T690*.

The sizing algorithm used for the *Dart T690* is shown in Fig. 4.1. After the appropriate initial data has been entered, an iterative process is used until convergence occurs for the vehicle takeoff weight. The procedure is carried out as follows:

1. All mission requirements and initial vehicle data are established before the iteration procedure begins. Mission data includes payload weight, crew weight, cruise speed, and the speed and rotor/wing load sharing during the short stop maneuver. Initial vehicle data includes the geometry and performance characteristics of the rotor, wing, and propellers.
2. An initial estimate is made for the takeoff weight of the vehicle.
3. Rotor blade chord is calculated based on the takeoff weight, rotor diameter, and maximum rotor thrust.
4. Wing surface area is calculated based on the takeoff weight, attainable wing $C_{L_{\max}}$, and the maximum load factor on the wing that is anticipated during the course.
5. The download on the wing from the action of the rotor wake is determined.
6. An estimate is made for the equivalent parasitic drag area of the fuselage and the rotor hub.
7. Vehicle drag at the design cruise and maneuver speeds are summed from the parasitic drag of the fuselage and hub, wing profile drag, and wing induced drag.
8. The power required is calculated for hover, cruise, and the short stop maneuver. Among these, the highest power requirement determines the installed power of the vehicle.
9. The estimated fuel weight is calculated.
10. The empty weight components are calculated.



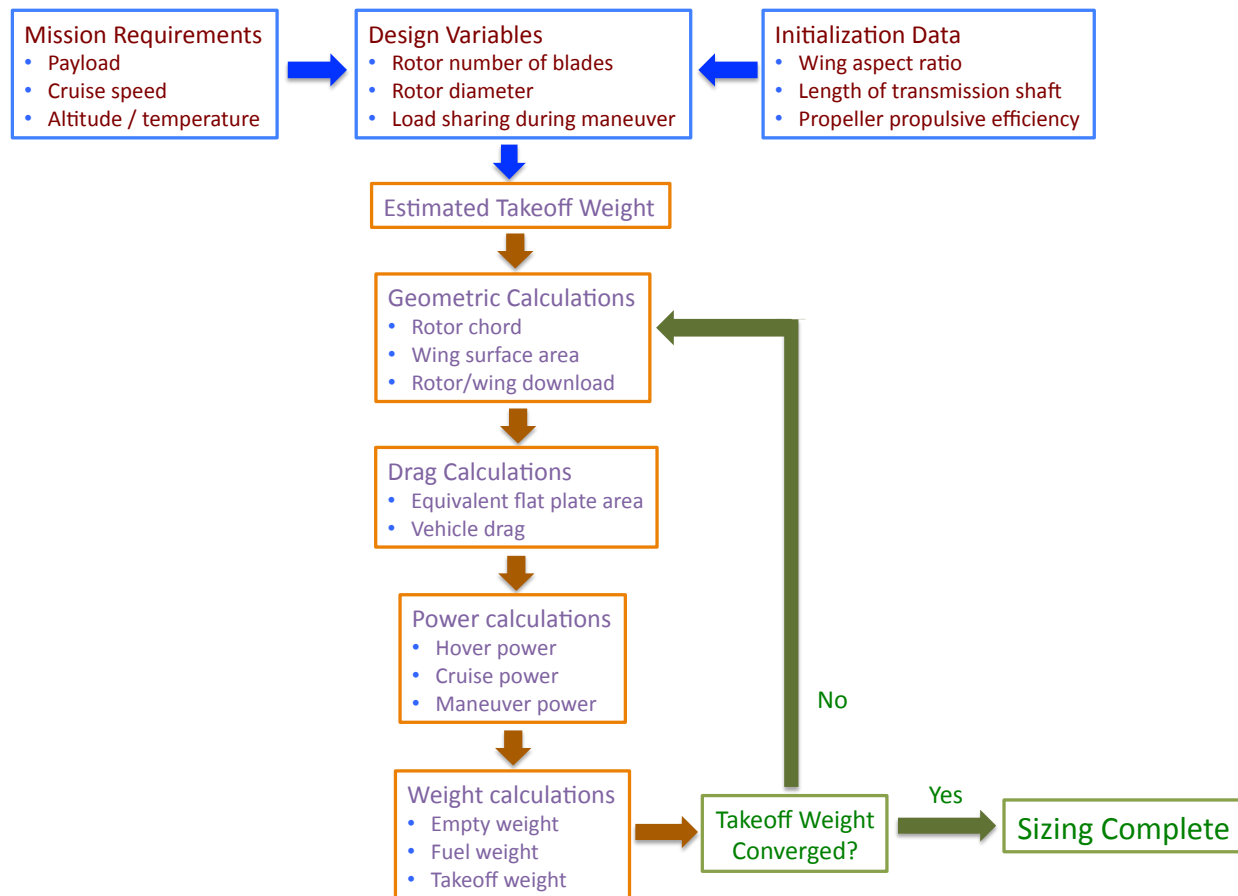


FIGURE 4.1: Block diagram of sizing algorithm.

11. Takeoff weight is calculated from the empty weight and the weights of the fuel, crew, and payload. If the weight has converged according to the criteria of less than a 0.05% change in takeoff weight between successive iterations, then the procedure ends. If not, then a new iteration begins, starting with Step 3.

Later in the design process, more detailed analyses were performed to determine wing characteristics, propeller characteristics (see Chapter 7), parasitic drag area, and required power (see Chapter 13), and these values were used in the sizing to obtain better vehicle weight estimates.

4.2 Sizing Considerations

As shown by the results in Section 2.2.4, the highest load factor on the vehicle occurs during the short stop 5g maneuver at 110 kts. This 5g maneuver requires the largest contribution from the wing to offload the rotor and, therefore, is the limiting factor in determining the minimum surface area of the wing. The load sharing between the rotor and wing during the short stop maneuver was one of the key mission parameters set in the sizing method because it determines the maximum lift required from the rotor, as well as the wing.



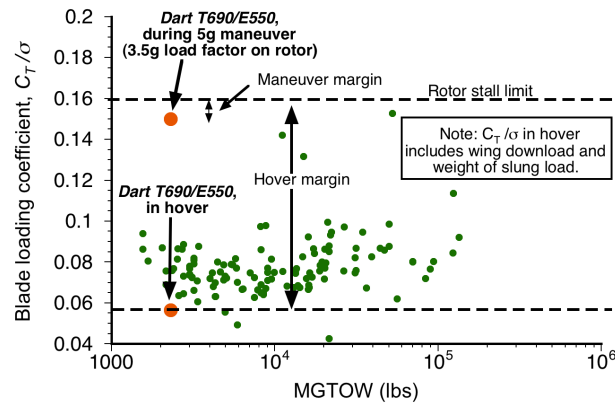


FIGURE 4.2: Historical data for blade loading coefficient versus MGTOW. MSL ISA.

The rotor was sized to have acceptable stall margins while lifting its share of the 5g load. Figure 4.2 shows historical data for C_T/σ , as well as the C_T/σ selected for the *Dart T690*. To give acceptable maneuver and propulsive margins, most helicopters operate at values of C_T/σ in hover close to 0.08 at MSL ISA. As part of the sizing initialization data, the maximum C_T/σ during the short stop maneuver was set to 0.15 to ensure that the rotor will not stall during this maneuver. Initially, a tip speed of 611 ft s^{-1} was desired so that the rotor would not have to be slowed at high airspeeds to avoid advancing blade compressibility effects. However, the tip speed was increased to 680 ft s^{-1} to decrease the blade loading coefficient, ensuring that the aircraft could perform the 5g maneuver. As a result of this tip speed selection, the *Dart T690* linearly slows its engine rpm at airspeeds greater than 159 kts so that the advancing tip Mach number never exceeds 0.85 at MSL ISA. According to an equation given in the RFP, when the engine rpm is slowed by 10% at the design cruise speed of 200 kts, the power available is only reduced by 2.5%.

Because the course can be completed well within the 30 minute duration for the intermediate rated power (IRP) of the engine, it was assumed that the *Dart T690* could be operated at its IRP during both hover and high-speed cruise. It was also assumed that the vehicle could perform the short stop maneuver at its maximum rated power.

4.3 Trade Studies

The sizing algorithm was used to determine the optimum combination of rotor diameter, number of blades, and load sharing during the 5g short stop maneuver. Specifically, the effects of these design parameters on takeoff weight, engine size, wing span, and blade aspect ratio were all taken into account. These parameters were determined using the sizing methodology before performing a more detailed analysis of the other design variables. For a sweep of maneuver load sharing scenarios, the best combinations of rotor diameter and number of blades were determined. The results were then compared to determine the optimum combination of the three design variables.

4.3.1 Rotor Diameter and Number of Blades

The effects of variations in rotor diameter and number of blades are shown in Fig. 4.3 for the load sharing scenario where the rotor sustains a 3.5g load factor during the 5g short stop maneuver, with the remaining 1.5g being carried by the wing. This flight condition was eventually selected for the design of the *Dart T690*, and is discussed in detail in Section 4.3.2. Figure 4.3(a) shows the trades on takeoff weight from variations in diameter and number of blades. Notice that the takeoff weight is reduced by increasing the number of



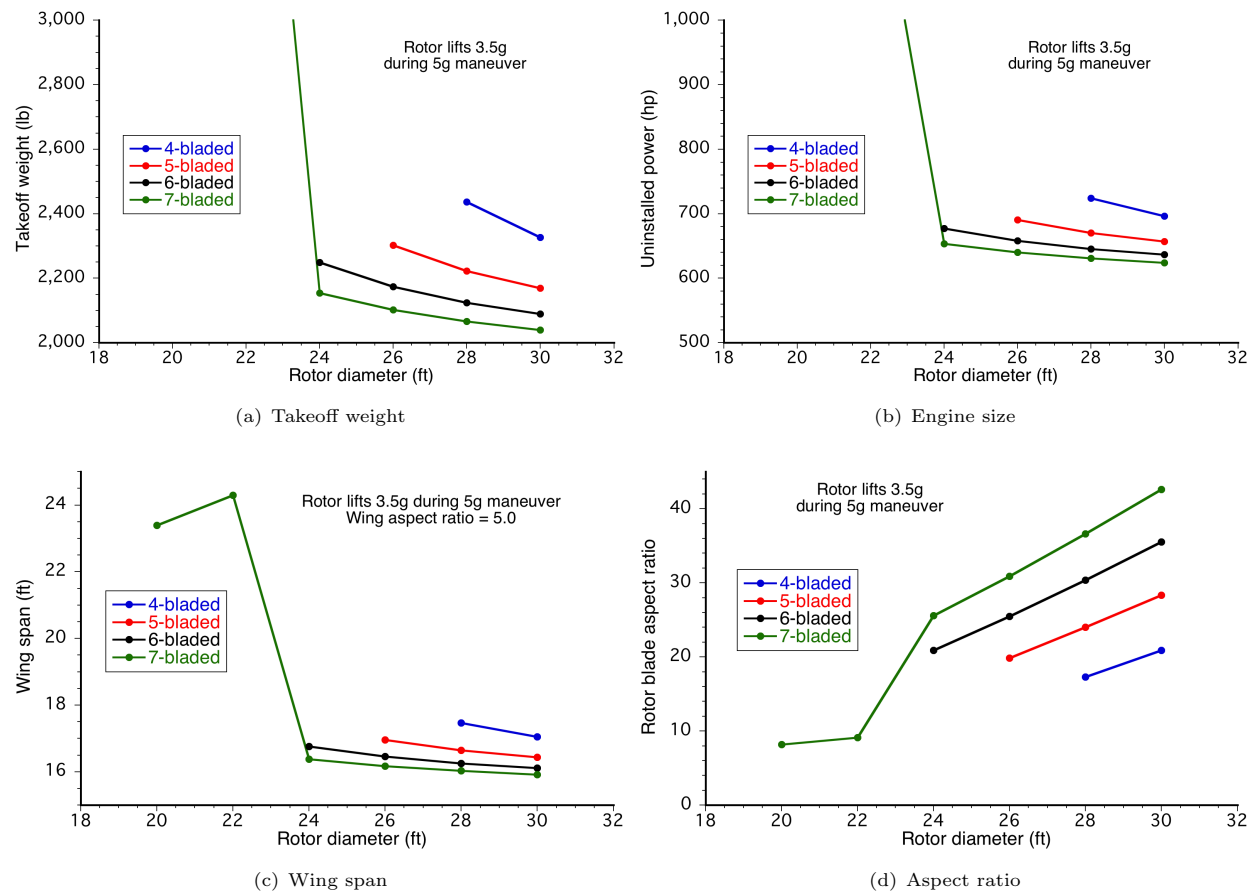


FIGURE 4.3: Parametric study of the effects of rotor diameter and number of blades on vehicle characteristics.

blades. Increasing the number of blades also allows for smaller rotor diameters. While decreasing diameter increases takeoff weight to some extent, a smaller diameter has the benefit of increasing the clearance with the pylons during the race, making it easier for the pilot to navigate the course. The same trends for takeoff weight are also apparent for engine size (i.e., uninstalled power) and for wing span, as shown in Figs. 4.3(b) and 4.3(c), respectively. A larger wing span is undesirable because of the greater download from the rotor wake, which reduces hover efficiency and also decreases performance in sideward flight.

Figure 4.3(d) shows the corresponding effects on blade aspect ratio. Aspect ratios greater than 20 were deemed undesirable from a structural standpoint. A 6-bladed rotor with a 24 ft diameter was initially determined to give the smallest diameter while maintaining an appropriate aspect ratio, as well as relatively low weight and power requirements. However, a 5-bladed rotor with a 26 ft diameter decreases the cost and complexity of the rotor system with only marginal increases in takeoff weight and engine size. For this reason, five blades and a 26 ft diameter were selected for the flight condition where the rotor carries a 3.5g load factor during the 5g maneuver.



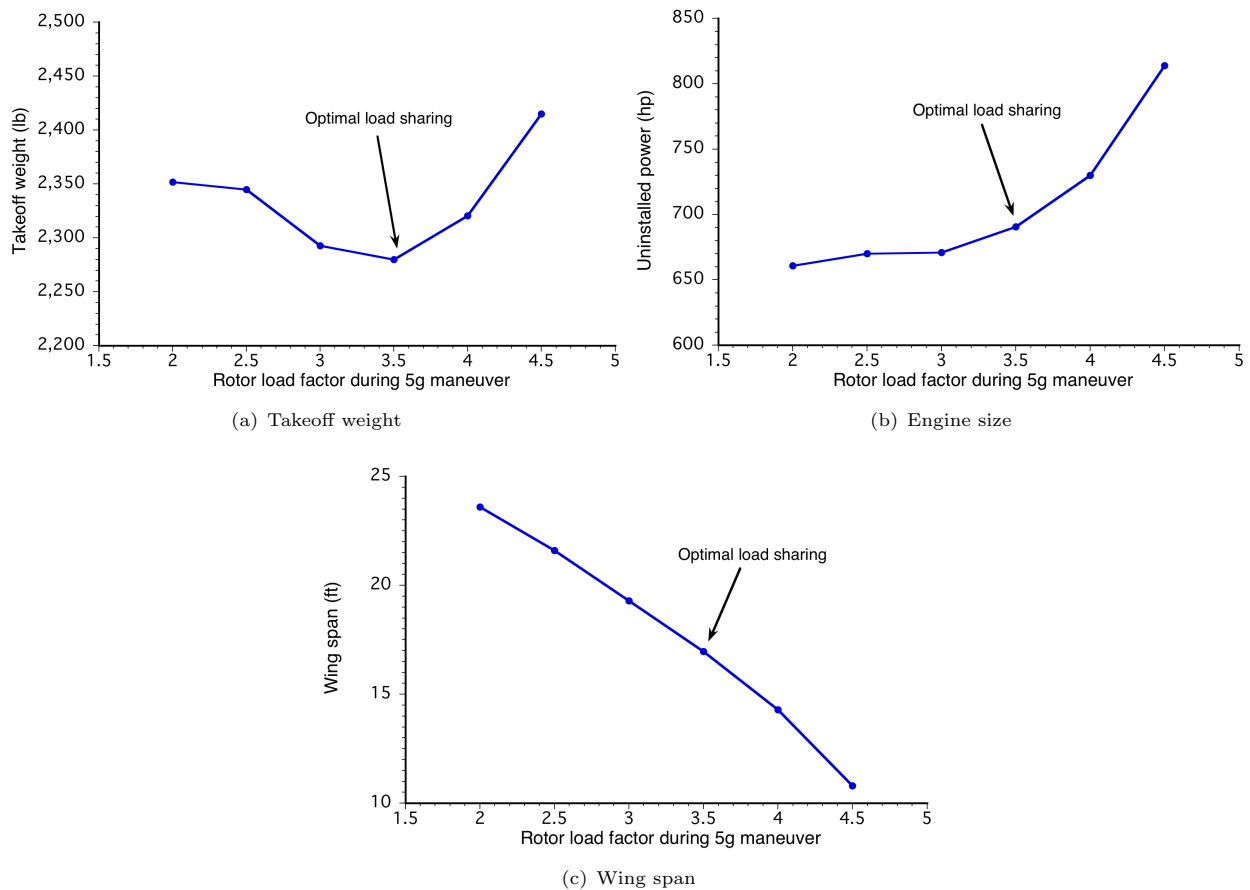


FIGURE 4.4: Trade study of the effects of maneuver load sharing on vehicle characteristics.

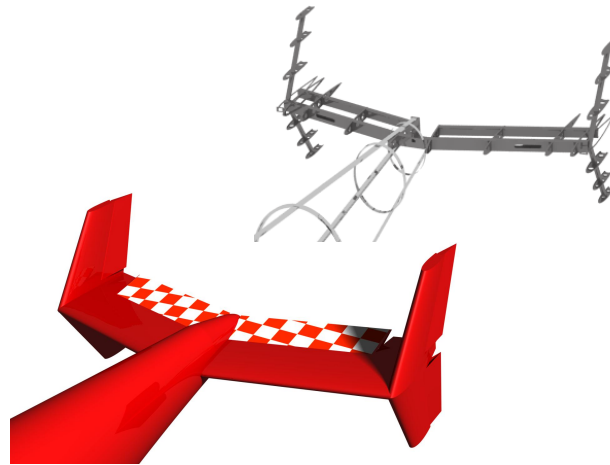
TABLE 4.1: Preliminary sizing results.

Rotor diameter	Rotor N_b	Rotor solidity	C_T/σ , hover	C_T/σ , maneuver	Wing span	$P_{\text{uninstalled}}$	Empty weight	Takeoff weight
26 ft	5	0.08	0.0565	0.15	17.9 ft	690 hp	1,584 lb	2,999 lb

4.3.2 Rotor/Wing Load Sharing during Maneuver

The best combinations of rotor diameter and number of blades for a range of maneuver load sharings are shown in Fig. 4.4. In general, increasing the load factor on the rotor during the short stop maneuver increases the rotor diameter and number of blades, but decreases the wing span. As shown in Fig. 4.4(a), the takeoff weight reaches a minimum when the rotor pulls a 3.5g vertical load factor. Figure 4.4(b) shows that engine size increases with load factor on the rotor, and begins to increase considerably above 3.5g. For these reasons, a rotor load factor of 3.5 during the 5g short stop maneuver was chosen as the critical design point; this combination of design variables resulted in the best overall vehicle performance. Some key aircraft characteristics from the preliminary sizing are shown in Table 4.1.



FIGURE 4.5: Empennage of the *Dart T690*.

4.4 Tail Selection and Sizing

The empennage of the *Dart T690/E550* was carefully designed to provide adequate stability and control to the aircraft. Figure 4.5 shows the chosen configuration, along with the different control surfaces (elevators and rudders) and their actuation mechanisms.

4.4.1 Empennage Configuration

Several different tail configurations were considered during the design of the *Dart*. Initially, an H-tail was selected, which is an ideal configuration when using two wing-mounted propellers because higher levels of control authority can be produced by the effect of the propeller wake on the vertical stabilizers. Furthermore, H-tails give a larger surface area for a lower height, decreasing the likelihood of tail strikes. The H-tail also provides redundancy and directional control if one of the vertical stabilizers is damaged after a pylon or water strike. Another possible configuration considered was the V-tail. This design offers good aerodynamic advantages because of its lower effective wetted area and smaller interference drag. However, such a design requires an increased level of flight control complexity from cross-coupling between pitch and yaw, although it could be manageable using a fly-by-wire system. To reduce adverse roll-yaw coupling, an X-tail was also explored. However this tail generates higher pitching moments when inside the wake of the rotor at low forward speeds. While the X-tail may be a more aesthetically pleasing choice and is consistent with the name “*Dart*”, from an engineering perspective it is not as good as the H-tail. Therefore, the trade study resulted in the selection of the H-tail configuration for the *Dart*.

4.4.2 Empennage Sizing

The size of the empennage has a significant impact on the performance of an aircraft. It affects the range of center of gravity (c.g.), with a smaller tail reducing the allowable c.g. travel. The *Dart* has only one pilot, no internal payload, and a low fuel quantity, so the c.g. position remains relatively constant during flight and a smaller tail is possible. In addition, tails with lower surface area generate lower drag. However, a small tail reduces static stability and makes the aircraft harder to fly to obtain adequate handling qualities, which is critical in high load factor maneuvers.



Method	Horizontal stabilizer area (ft ²)	Vertical stabilizer area (ft ²)
Airplane historical data	8.3	4.0
Helicopter historical data	9.2	6.9
Stability analysis	18.7	12.4

TABLE 4.2: Summary of the tail sizing predictions.

The empennage sizing for an airplane can be conducted using the method developed by Raymer [7], which is based on historical data and tail volume coefficients (ratio of stabilizer dimensions and wing dimensions). The tail moment arm is constrained by the minimum distance required to avoid the rotor blades striking the vertical tails. The selected horizontal tail coefficient was 0.7 and the vertical tail coefficient was 0.07. These values resulted in a horizontal surface of 8.3 ft² and a vertical surface of 4.0 ft². Although this sizing approach is fairly standard, further considerations were required in the case of the *Dart* because it is such a unique aircraft. To this end, historical data for helicopters were also used to aid in empennage sizing.

Stabilizer surface areas as a function of vehicle gross weight are shown in Fig. 4.6. A trendline was fit to the data, and the appropriate tail size for the *Dart* was estimated. These new areas were slightly bigger than those determined using Raymer's method. However, note that the Eurocopter X³, which is of a similar configuration to the *Dart*, has much higher stabilizer areas than other helicopters in the same weight class.

Further sizing of the tail was performed by considering the dynamic stability of the aircraft. The analysis was performed for the most stringent flight conditions where control authority is critical. Tail effectiveness ratios were chosen to take into account the downwash of the wing on the empennage, which decreases its efficiency, and the slipstream of the propellers, which can increase the control authority of the tail.

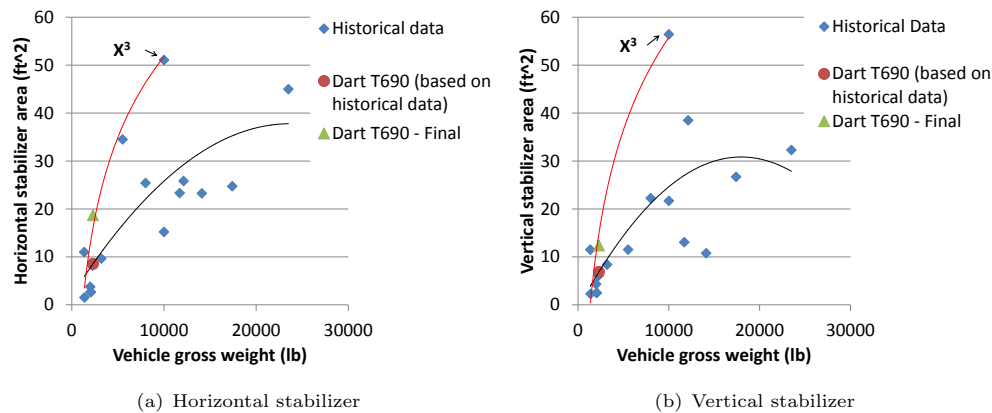


FIGURE 4.6: Helicopter stabilizer historical data.

The outcome of this analysis was that a horizontal surface of 18.7 ft² and a vertical surface of 12.4 ft² were required for the *Dart*. These values are higher than those predicted using historical data alone, but they are on the same trend line as the X³. Table 4.2 summarizes the tail area estimations that were made using the different approaches.

4.4.3 Control Surfaces Sizing

To give the aircraft additional control authority, ailerons, elevators, and rudders were also used. This decision arose because at higher forward speeds, the rotor is offloaded by the wing lift and propeller thrust, and has



reduced control authority. Therefore, additional control authority from aerodynamic surfaces on the wing and the empennage is required. The need for control authority was validated using the X-Plane simulation. Both the horizontal and the vertical tails have a preset angle of incidence of 0.5° and 1° respectively, so that trim can be achieved throughout the entire range of operating speeds using the elevators and rudders, while still preserving adequate elevator and rudder deflection margins to conduct maneuvers.

The flight path management analysis (Chapter 2) has determined the maximum pitch, roll, and yaw rates that the aircraft needs to achieve. Therefore, the control surfaces were designed to provide a maximum roll rate of $180^\circ/\text{sec}$, a maximum pitch rate of $20^\circ/\text{sec}$, and a maximum yaw rate of $60^\circ/\text{sec}$. Furthermore, the rudders were designed to provide all of the anti-torque at higher airspeeds to allow the propellers to operate at more equal thrusts (i.e., no differential propeller pitch), which is critical to reach higher accelerations and airspeeds. A NACA0012 airfoil profile was selected for the horizontal stabilizer, and a NACA0009 profile for both of the vertical tails.

4.5 Initial Aircraft

The sizing results were used to create an initial single seat aircraft (see Fig. 4.7). This preliminary design was the starting point for all the future design decisions. As the design progressed, significant changes were made to this aircraft, resulting in the fast, agile, and maneuverable pylon racer that is the *Dart*.



FIGURE 4.7: The preliminary aircraft design.



5 Performance Overview

Main Rotor Specifications	
Diameter	26 ft
Number of Blades	5
Chord	0.652 ft
Solidity	0.08
Disk Loading	4.5 lb/ft ²
Blade Twist (Linear)	7.8°
Blade Taper Ratio (outboard of 80% radius)	2
Blade Sweep (outboard of 90% radius)	25°
Shaft rpm	450-500
Root Cutout	20%
Airfoil Sections	SC1095
Maximum Vertical Load Factor	3.5g

Vehicle Dimensions	
Total Length	26.5 ft
Fuselage Height	4.9 ft
Fuselage Width	3 ft
Height	7.9 ft
Cockpit Width	2.7 ft
Cockpit Height	3.4 ft
Cockpit Length	4.7 ft

Wing Specifications	
Span	17.9 ft
Chord	3.6 ft
Aspect Ratio	5
C_{LMax}	1.5
Taper Ratio	2
Sweep	0°
Incidence	4°
Maximum Vertical Load Factor	1.5g
Airfoil Section	NACA4415

Weights	
Maximum Gross Weight (full fuel)	2,515 lb
Empty Weight	1,700 lb

Propeller Specifications	
Number of Propellers	2
Diameter	5 ft
Number of Blades	3
Chord	0.417 ft
rpm	3,200
Twist (Bilinear)	-32.6°/ft (inboard) -10.7°/ft (outboard)
Airfoil Section	Clark Y

Performance	
Cruise Speed	200 kts
Maximum Speed	225 kts
V_{be}	50 kts
V_{br}	165 kts
Maximum Acceleration	0.5g
Maximum Yaw Rate	60 °/s
Maximum Pitch Rate	20 °/s
Maximum Roll Rate	180 °/s
Maximum Vertical Load Factor	5g
Maximum Endurance	2.7 hr
Maximum Range	256 nm

Engine Specifications	
Number of Engines	1
Maximum Rated Power	740 hp
Intermediate Rated Power	690 hp
Maximum Continuous Power	564 hp
Operating rpm	18,000



6 Rotor Design

6.1 Aerodynamics

From the preliminary sizing (Chapter 4), a 5-bladed, 26 ft diameter rotor was selected for the *Dart T690/E550*. In the aerodynamic design of the rotor, the blade twist, tip shape, and airfoils were selected to achieve two major goals: high aerodynamic efficiency (i.e., low power requirements both in hover and forward flight) and the ability to provide a sustained normal load factor of 3.5g at 110 kts. Better rotor efficiencies reduce fuel consumption, and by using less power also improve forward acceleration by allowing the propellers to draw more power. A good load factor capability not only allows the *Dart* to quickly complete the course as described in the RFP, but also makes it a compelling option for use in other racing competitions.

In hover, the aerodynamic performance of the rotor was analyzed using blade element momentum theory (BEMT). In forward flight, blade element theory (BET) was coupled with the Drees model for linear inflow [8]. In the cases where results were obtained using formal optimization, the Broydon-Fletcher-Goldfarb-Shanno (BFGS) algorithm was used for unconstrained optimization, and the method of feasible directions (MFD) was used for constrained optimization. The power required at different speeds was calculated assuming the optimum lift sharing schedule (described in detail in Section 13.4). All results shown are for MSL and 103°F.

6.1.1 Blade Twist

Four different types of blade twist were examined for the *Dart T690*: untwisted, linear, bilinear, and a hyperbolic twist. For each twist shape, the optimizer was used to determine the twist rates that minimized hover power; the power required for each optimized blade twist is shown in Fig. 6.1(a). Also shown is the power required to complete the short stop maneuver at 110 kts, during which the rotor sustains a 3.5g load factor (the other 1.5g being lifted by the wing). After taking into account the power consumed by the propellers, the power available for the rotor to perform the maneuver was determined to be 481 hp based on the maximum rated power (MRP) of the engine. Rotor power requirements are considerably lower with forward speed than in hover, even more so than for a conventional helicopter. This outcome is because the rotor becomes increasingly offloaded by the wing as airspeed increases, and also because the propellers are providing nearly all of the forward thrust. Rotor power decreases sharply after exceeding 160 kts because the rotor is slowed at these speeds to avoid adverse compressibility effects.

In Fig. 6.1(a), notice that an untwisted blade gives the lowest power in forward flight, but at the expense of some loss in hover efficiency and an increase in power required to perform the maneuver. To perform the short stop maneuver, the use of an untwisted blade exceeds the power available by 100 hp. Of the other three twist shapes, the linear and hyperbolic twists give the best performance, and both designs allow the sustained maneuver to be performed. Ultimately, a linear blade twist was chosen for the rotor because of its better overall aerodynamic performance, low cost, and ease of manufacture. The effects of different linear twist rates is shown in Fig. 6.1(b); reducing blade twist decreases power during level flight but increases the power required during a sustained maneuver. A linear twist rate of -0.6 deg/ft (7.8° of total blade twist) was selected because this is the lowest allowable twist rate that provides the ability to perform the sustained maneuver.

6.1.2 Blade Tip Shape

Tapering the blade tips was found to decrease the power required for both hover and cruise flight, and increase the power required to perform the short stop maneuver. Tip sweep was found to have a negligible



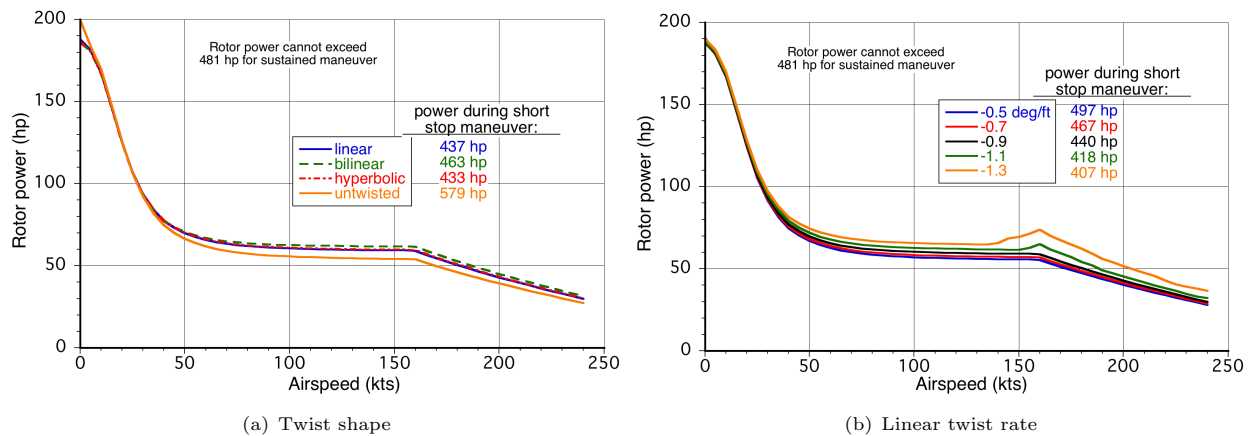


FIGURE 6.1: Trade study of blade twist and its effect on rotor power: (a) comparison of twist shapes; (b) comparison of linear twist rates. MSL 103°F.

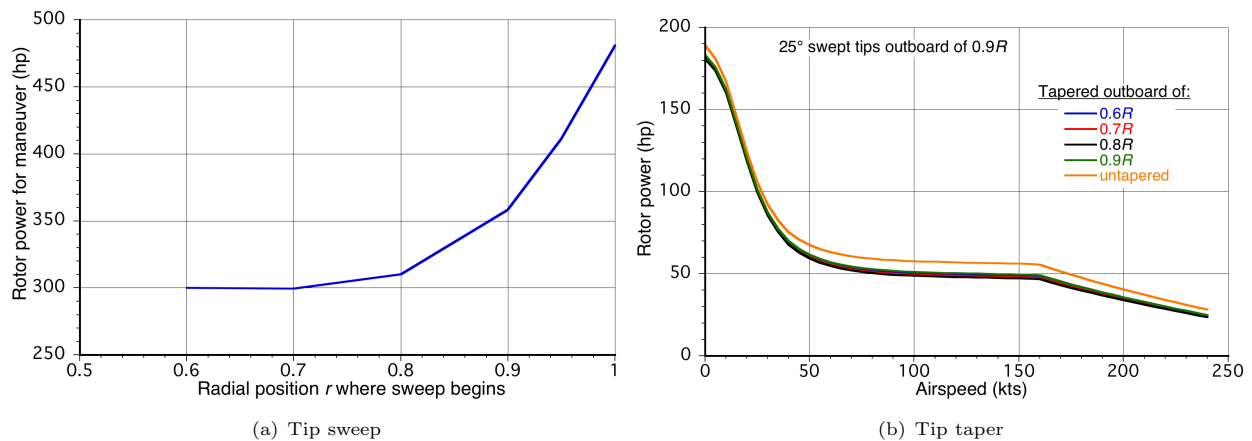


FIGURE 6.2: Trade study of blade tip shape: (a) tip sweep reduces power required for the short stop maneuver; (b) taper coupled with tip sweep can reduce power required. MSL 103°F.

effect on power during both hover and cruise flight, mainly because the rotational speed of the rotor is slowed at high airspeeds to keep the advancing tip Mach number below 0.85. However, as shown in Fig. 6.2(a), tip sweep does have a more significant effect on the power required to perform the short stop maneuver, where the blade lift coefficients are much higher, reducing the rotor power required from 480 hp to 300 hp. By using taper in conjunction with tip sweep, the power required was reduced at all airspeeds, while still maintaining the ability to perform the sustained maneuver. Figure 6.2(b) shows that the power in forward flight can be reduced by about 9 hp by introducing tip taper, with no benefit to tapering inboard of 0.8R. The tip sweep was kept constant at 25° outboard of 0.9R, a value less than the aerodynamic optimum, to minimize adverse effects on the blade c.g. balance. The taper ratio was optimized to minimize power with the constraint that the MRP of the engine would not be exceeded during the short stop maneuver. From this analysis, a tip taper ratio (inboard chord/tip chord) of 2.0 was selected, with the taper being applied over the outer 20% of the blade.



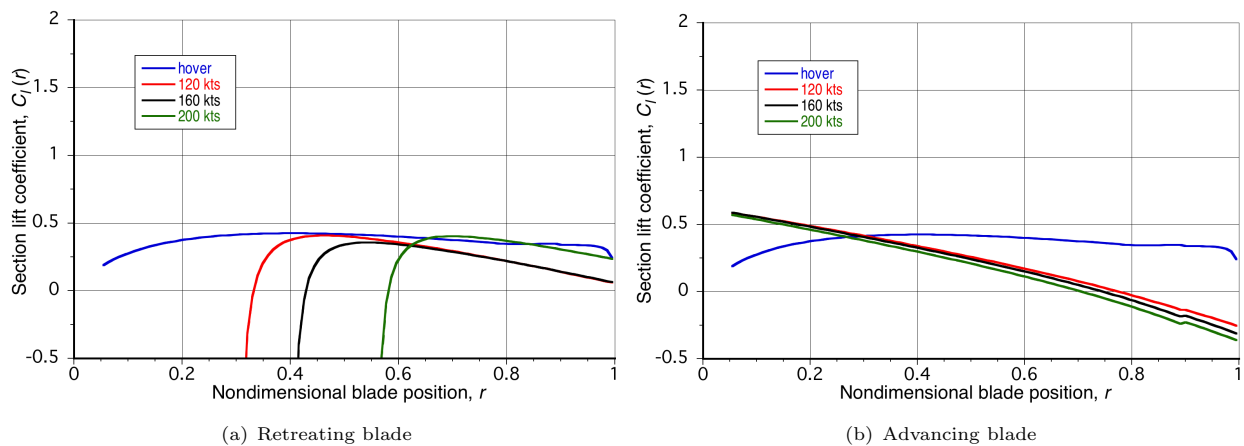


FIGURE 6.3: Lift distributions on the rotor blades at different forward speeds.

6.1.3 Blade Airfoils

Typically, a helicopter blade requires thicker airfoil sections near its root and midspan where the lift coefficients are higher, and thinner airfoil sections near the tip where the advancing blade Mach number is higher. Figure 6.3 shows that for the *Dart*, the lift coefficients are actually relatively low; this outcome is even more apparent in forward flight where some of the vehicle lift is shared with the wing. To perform maneuvers and achieve high load factors, however, the rotor blades must realize high maximum lift coefficients near the root and mid-span to prevent the rotor from stalling. The fact that the rotational speed of the rotor is slowed in high-speed flight eases the requirements to use thinner airfoil sections near the blade tips. Ultimately, the rotor airfoils for the *Dart* were derived from the SC1095, which has a thickness-to-chord ratio (t/c) of 9.5% and a $C_{l_{\max}}$ of 1.25. For the *Dart*, 15% t/c airfoils are used on the inboard sections. Outboard of $0.5R$, the airfoil t/c was linearly reduced to 12% at the tip. This thickness distribution gives structurally sound blades, and ensures that the *Dart's* rotor is able to sustain a 3.5g load factor without stalling.

6.2 Blade Structural Design

The 3.5g load factor on the rotor is a demanding design point. The blades are designed with appropriate strength and fatigue life for this aggressive load environment. Agility requirements also demand that the rotor system have a high hinge offset to transform the large lifting capability of the rotor into control effectiveness. A hingeless rotor is used to meet these structural, maneuverability, and agility concerns, while maintaining a clean aerodynamic profile and a compact hub. Continuous composite fiber placement connects the three primary structural sections of the rotor blade shown in Fig. 6.4. The lifting surface maintains the required aerodynamic shape and transmits the aerodynamic forces to the flexure, which in turn transmits the centrifugal loads while acting like a virtual flap and lag hinge. Finally the yoke transmits the loads to the hub.

6.2.1 Material Selection for the Rotor Blade

Composite materials are used for their high specific stiffness, excellent fatigue characteristics, and ability to manufacture complex shapes. Lay-up is performed using an automated fiber placement process and are





FIGURE 6.4: The three rotor blade structural sections.

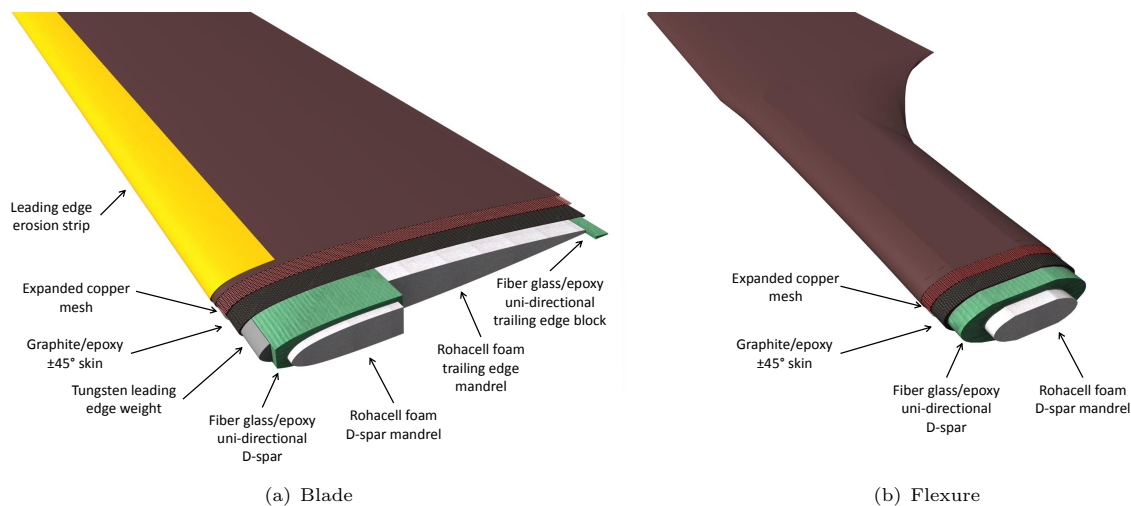


FIGURE 6.5: Internal structure of the blade and flexure. The D-spar from the blade forms the primary structure of the flexure as well.

cured in closed die molds. Both graphite and glass fibers were considered in the design process to form the skin and spar of the rotor blade. Graphite provides higher specific stiffness and ultimate strength when compared to glass, but at a higher cost [9]. Preliminary blade design showed that the required stiffness and strength can be achieved at 18.75 lb/blade by using unidirectional S-glass/epoxy composites in the spar. The larger area of the skin requires use of graphite to meet the weight target and torsional stiffness. Roahacell 75 (4.68 lb/ft³) foam is cut to shape by a hotwire and easily compressed to the required shape by the high pressure exerted by the closed die mold. Given the complex geometries at the flexure/D-spar junction and the tapered/swept blade tip, foam is an attractive solution over machining aluminum honeycomb.

6.2.2 Manufacturing the Rotor Blade

The internal structure of the blade shown in Fig. 6.5 is designed around two composite layups. The first layup forms the primary structural backbone of the blade by connecting the D-spar of the aerodynamic section, the flexure structure and the yoke. A central foam mandrel is cut slightly oversize and forms the core for fiber placement. Continuous unidirectional composite tapes are laid from the tip of the rotor blade, through the flexure, and all the way around the yoke by using automated fiber placement. These continuous unidirectional layers provide direct load paths for the centrifugal forces on the blade and also provide a



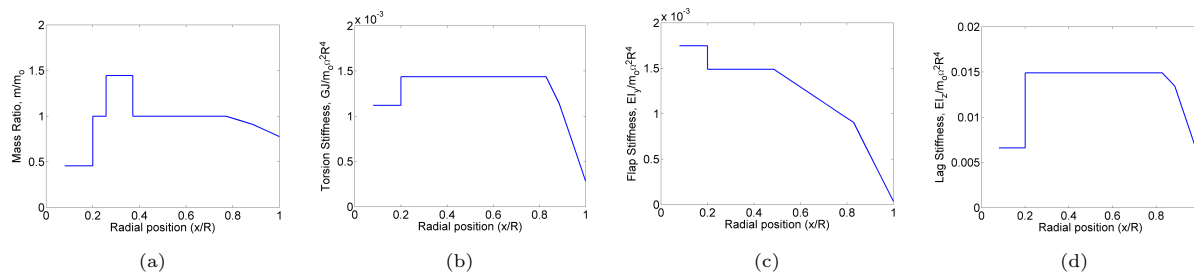


FIGURE 6.6: Sectional properties along the rotor blade. (a) Mass distribution (b) Torsional stiffness (c) Flap stiffness (d) Lag stiffness

majority of the bending stiffness. Additional layers of glass in the yoke section provide the required increase in stiffness and strength between the bearings.

The second layup creates the aerodynamic surface. A foam mandrel is placed behind the D-spar along the lifting surface of the blade. A small fiber glass block is placed at the trailing edge to add lag and flap stiffness while also stabilizing the trailing edge. Tungsten weights are placed in front of the D-spar to tailor the placement of the rotor blade center of gravity (c.g.) relative to its elastic axis (e.a.). This assembly is then wrapped in several layers of $\pm 45^\circ$ graphite/epoxy prepreg to contain the structure, maintain the proper aerodynamic shape, and add further torsional stiffness. The final layer is a 141.6 g/m^2 ($.029 \text{ lb/ft}^2$) expanded copper mesh providing a grounding path in the case of a lightning strike. This entire assembly is then placed in a second mold for the final cure. The final mold has a small step to produce a recess in the leading edge of the blade, around which is attached a S-glass/PEEK erosion cap that protects the blade from abrasion. A heating pad for de-icing is not needed in this design because of the relative warm weather defined by the RFP.

6.2.3 Sectional Properties of the Rotor Blade

The internal structure of the blade was designed by calculating the spanwise blade mass and stiffness properties accounting for the sectional thickness and chord. Significant parameters considered were airfoil D-spar thickness, D-spar chordwise length, skin thickness, and leading edge mass. Spanwise distributions of stiffness, mass, and inertia properties were then used as inputs in the structural dynamics module of the University of Maryland Advanced Rotor Code (UMARC) to calculate the first six blade vibratory modes. An iterative process varied the size of the trailing edge block, the thickness of the spar flanges, the thickness of the torsion layers, and added tuning masses until the desired structural frequencies were achieved across the full range of operational rpm.

Figure 6.6 shows the spanwise distribution of weight, torsional stiffness, flap stiffness, and lag stiffness. The rotor blade is slightly thicker at the root than at the tip. The continuous spar allows the weight and lag stiffness to remain constant, while the flap stiffness decreases noticeably. Beyond 80% span, the chord tapers as well, which causes a significant reduction in flap, lag, torsion, and mass properties of the blade. The local sectional c.g. location was controlled to balance the offset from the swept blade tip.

Figure 6.7 shows the fanplot for the *Dart's* rotor system. An equivalent hinge offset of 11% with a flap frequency of 1.1/rev was the target design. The rotor is soft in-plane, with a lag frequency of 0.63/rev. Stiff in-plane rotor blades alleviate concerns about ground and air resonance that are common in soft in-plane hingeless rotors. However, they do so at the cost of transmitting higher static and vibratory loads to the airframe, and therefore active vibration control may be required. Hence, a soft in-plane rotor was selected. The blade torsional frequency of 5.3/rev prevents interaction with the fundamental frequencies across the full range of operational rotor speeds.



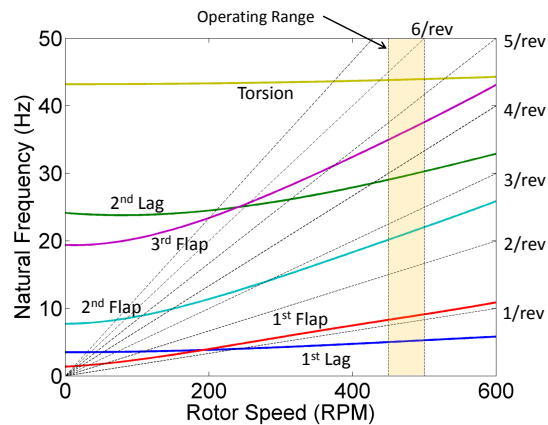


FIGURE 6.7: Fan plot showing rotor blade structural modes as a function of rotor rpm.

6.3 Rotor Hub Design

Various rotor hub systems were considered before deciding on the current *Dart* configuration. For a highly maneuverable racing aircraft, it was important to select a hub that both allowed for maximum control power through high hinge offsets and also high speed by causing low hub drag.

Articulated: Articulated hubs are mechanically complicated, and with a 5-bladed rotor, the part count is very high. Achieving the 11% hinge offset that was desired without making the hub a source of high drag is a significant challenge.

Semi-Articulated: Several modern helicopters use a semi-articulated hub utilizing flap flexures and the multi-functional nature of elastomeric bearings and dampers. While these hubs are mechanically compact, it is still challenging to achieve the high required hinge offset with a small hub size.

Hingeless: The Bo-105, Eurocopter Tiger, and HAL Dhruv all use a hingeless hub with a composite flexure and a bearing pack close to the hub. The Bo-105 has two radial bearings and a tension-torsion bar while the Tiger and Dhruv carry the loads through only one conical and one radial elastomeric bearing.

Bearingless: Bearingless rotors include the torsional degree of freedom in the flexure design and add a torsion tube to transfer pitch link loads to the far end of the flexure. While mechanically simple, this design adds a significant level of complication to the structural aspects of the flexure. Also, while the central hub is compact, the drag from the torque tube must also be considered.

The hingeless configuration of the Tiger and Dhruv was selected for its compact design and because it allows the rotor blade to directly interface with the pitch bearings, as shown in Fig. 6.8. However, the bearing arrangement was modified. The resulting lift force and moment the bearings transmit to the shaft were resolved into reaction forces on the two bearings. A conical elastomeric bearing was designed [10] to react the centrifugal rotor loads and the flap force. Near the rotor mast, a sealed self lubricating radial needle bearing [11] provides the second reaction force. In this location, the needle bearing is as capable as an elastomeric bearing, and is a more cost effective choice. A maintenance free, sealed hydraulic damper bridges the flexure between the yoke and the trailing edge of the lifting surface to provide the required in-plane damping for aeroelastic stability. The long length maximizes the deflection for a given lag travel.



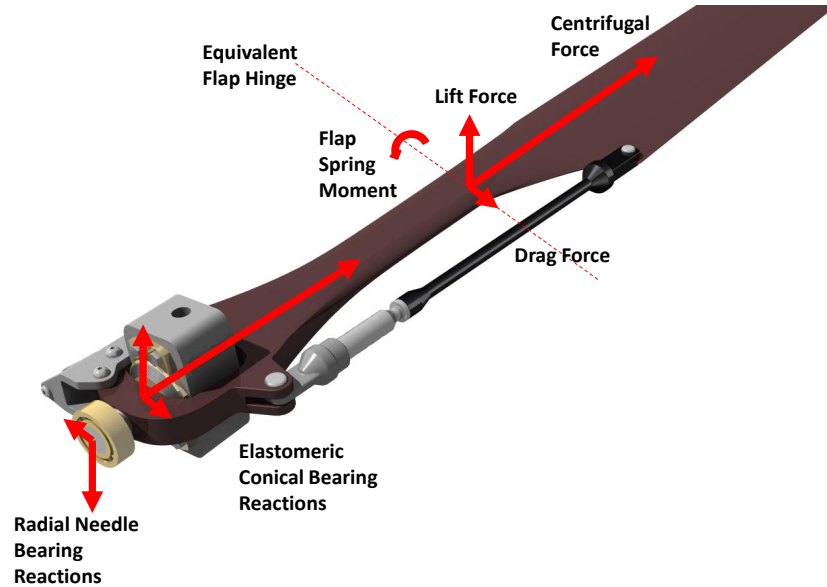


FIGURE 6.8: The pitch bearings are designed to take the high loads that result from close spacing.

6.4 Rotor Dynamics

Rotorcraft are susceptible to a number of unique aeromechanical considerations that require careful design. To evaluate aeroelastic areas of concern for the isolated rotor, an eigen-analysis was performed on the mass, damping and stiffness matrices that govern each instability as described in Johnson [12]. For ground and air resonance, the coupled rotor and body dynamics were accounted for in the dynamic analysis described in Section 12.2 and was used to ensure system stability. In the case of ground resonance torsional springs and dampers in the pitch and roll axes were added to model landing gear. The rotor was determined to be aeroelastically stable, with a margin of safety in all areas of concern.

6.4.1 Rotor Flap-Lag and Pitch-Flap

Pitch-flap flutter and pitch divergence are related phenomena that couple pitching motion of the rotor blade with its flap motion. The most effective way to manage pitch-flap instability is by placing the blade c.g. near the quarter-chord (the aerodynamic center). Figure 6.9(a) shows the stability boundary as a function of torsional frequency and c.g. location. The blade is stable from pitch-flap flutter with the c.g. of the blade at 25% chord and a torsional frequency of 5.2/rev.

Flap-lag flutter is an undesirable coupling of the flap and lag modes coming from perturbation aerodynamic forces and the limited aerodynamic damping in lag. An in-plane damper added to the rotor system gives sufficient damping to prevent any such instability. The root locus of the system is shown in Fig. 6.9(b) across the full range of thrust conditions.



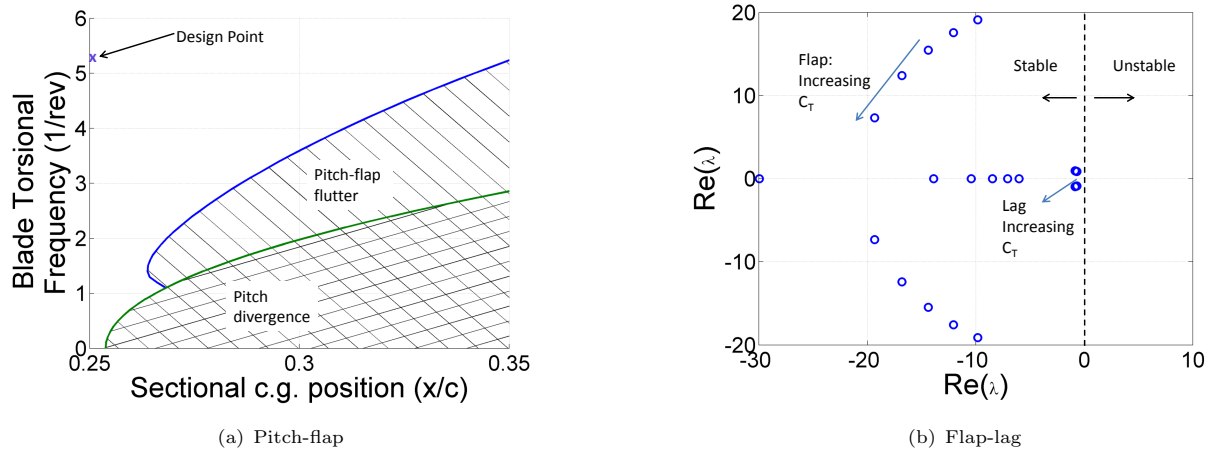


FIGURE 6.9: Results from the aeroelastic analysis of the isolated rotor. (a) Pitch-flap flutter and pitch divergence boundaries are plotted for various c.g. locations and torsional frequencies. (b) Flap-lag flutter eigenvalues for a variety of loading conditions are all in the stable left half plane.

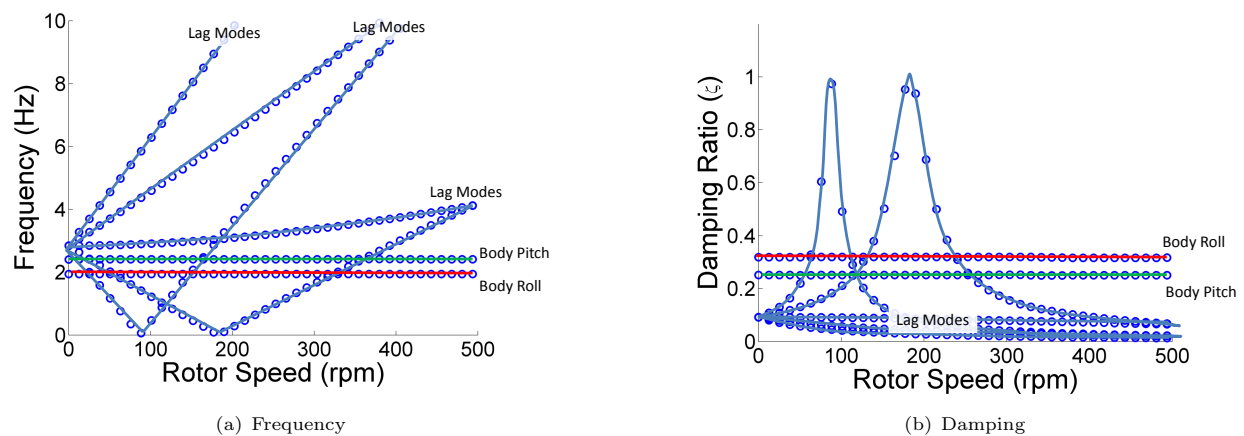


FIGURE 6.10: Stability analysis of ground resonance.

6.4.2 Ground Resonance and Air Resonance

Ground resonance is an explosive instability that comes from a coupling of the fuselage landing gear modes with the regressing lag modes of the rotor. This issue is particularly problematic with soft in-plane hingeless rotor systems and when operating from soft landing surfaces. The landing gear (see Section 9.6) are designed to increase the resonant rigid body frequencies, and the in-plane damper is tuned to ensure that the aircraft has a sufficient margin from this instability. Figure 6.10 shows that the rigid body modes are separated from the fixed frame lag modes at the operational rotor speed with no mechanical damping.

Air resonance is an airborne phenomenon where a number of rotor modes can couple with the rigid body modes and create limit cycle instabilities. The stability analysis performed in Section 12.2 included rotor flap and lag degrees of freedom and therefore also provided insight into air resonance. The vehicle is stable in all rotor modes and in the coupled rotor/body.



Main Rotor: Blade and Hub



DART T690



7 Propeller Design

7.1 Aerodynamics

Two factors drove the aerodynamic design of the propeller: propulsive efficiency and forward acceleration. Increased emphasis was given to maximizing the forward acceleration of the aircraft, which can help significantly to reduce the time needed to complete the course. The focus on dash capability is a unique design requirement for the *Dart T690/E550*, which sets it apart from all existing rotorcraft. Aerodynamic loads were calculated using blade element momentum theory specially formulated for propellers [13], which takes into account the high axial speeds and swirl velocities encountered by propellers and their effects on blade loads and overall performance.

7.1.1 Propeller Diameter

A larger diameter can produce more thrust for higher acceleration and also improve propulsive efficiency. Figure 7.1 shows that increasing the propeller diameter improves propulsive efficiency, but with a point of diminishing returns. A 5 ft propeller diameter was selected because larger diameters required that the landing gear and/or rotor shaft be extended to give the propellers adequate clearance with the ground and rotor; such changes were deemed unacceptable in terms of increasing the weight of the aircraft and its parasitic drag. Furthermore, a propeller diameter larger than 5 ft shows only limited gains in propulsive efficiency.

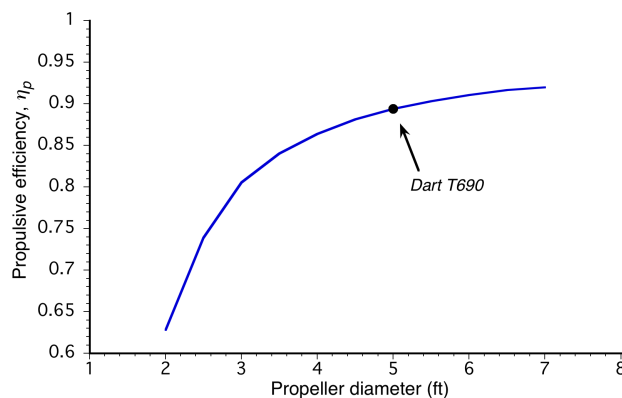


FIGURE 7.1: The effect of propeller diameter on propulsive efficiency.

7.1.2 Number of Blades and Rotational Speed

The shaft speed and number of blades were selected concurrently because these two parameters both contribute to the value of the blade loading coefficient. To prevent the helical tip Mach numbers from exceeding 0.85, an upper limit of 3,475 rpm was placed on the rotational speed of the propeller. For a range of shaft speeds, an optimum number of blades was chosen based on both translational acceleration and efficiency requirements; these optimum combinations are shown in Fig. 7.2(a). Varying the number of blades and shaft speed has a significant effect on maximum acceleration at lower airspeeds, but a negligible effect at higher airspeeds. This outcome is because the maximum acceleration of the vehicle is limited by available engine power at higher airspeeds and by propeller stall at low airspeeds. In this case, the combinations with



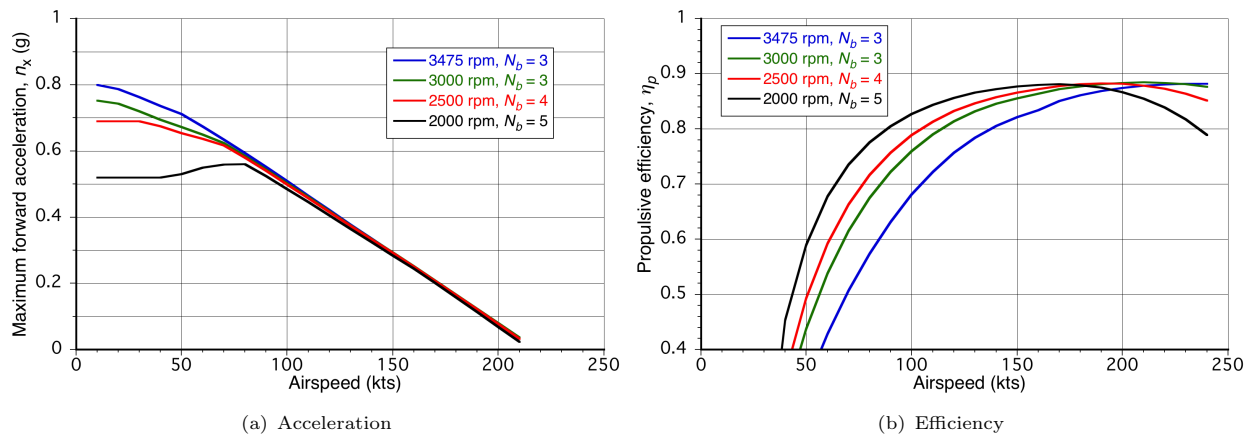


FIGURE 7.2: Performance of optimum combinations of propeller rotational speed and number of blades. MSL 103°F.

higher shaft speeds and fewer blades give greater levels of translational acceleration. Figure 7.2(b) shows that the opposite trend is true of propulsive efficiency, resulting in a trade between maximum translational acceleration and propulsive efficiency. Initially, the propellers for the *Dart* were chosen to be 3-bladed with a nominal operating speed of 3,000 rpm. However, the rotational speed was increased to 3,200 rpm so that the fundamental frequency of the propeller would not be an integer multiple of the fundamental frequency of the rotor (500 rpm), thereby avoiding the potential for high vibratory loads.

7.1.3 Anti-torque Requirements

Because the *Dart* does not use a tail rotor, anti-torque is obtained by using differential thrust from the propellers. Because the two propellers generate different thrusts, they also require different torques and, therefore, generate a rolling moment on the aircraft. One of the key decisions for the propellers with regard to anti-torque was their placement on the wing. The closer the propellers are to the wingtips, the less differential thrust they must provide to counteract the torque reaction from the rotor. Placing the propellers further outboard on the wings gives a small effect on total power required, but does reduce the rolling moment. However, placing the propellers at the wingtips reduces clearance with the ground and rotor, increases the length of the transmission, and increases the bending moment on the wing. For these reasons, the propellers were placed roughly halfway between the fuselage and wingtips, with 14 ft of separation between their axes of rotation.

A second design decision was whether or not to operate the propellers at different shaft speeds. Operating the higher thrusting propeller at higher rotational speeds could result in lower rolling moments by decreasing the torque reaction. Figure 7.3 shows the effects that differential rpm has on power required and the rolling moment on the aircraft. Differential shaft speed causes power to increase by increasing the profile power on the faster rotating propeller. Rolling moments can be decreased by introducing differential shaft speed, but only at airspeeds greater than about 100 kts; at these higher airspeeds, most of the anti-torque can be provided by the vertical tail. The results show that there is no practical benefit to operating the propellers at different shaft speeds, and so the propellers on the *Dart* operate at the same rpm.



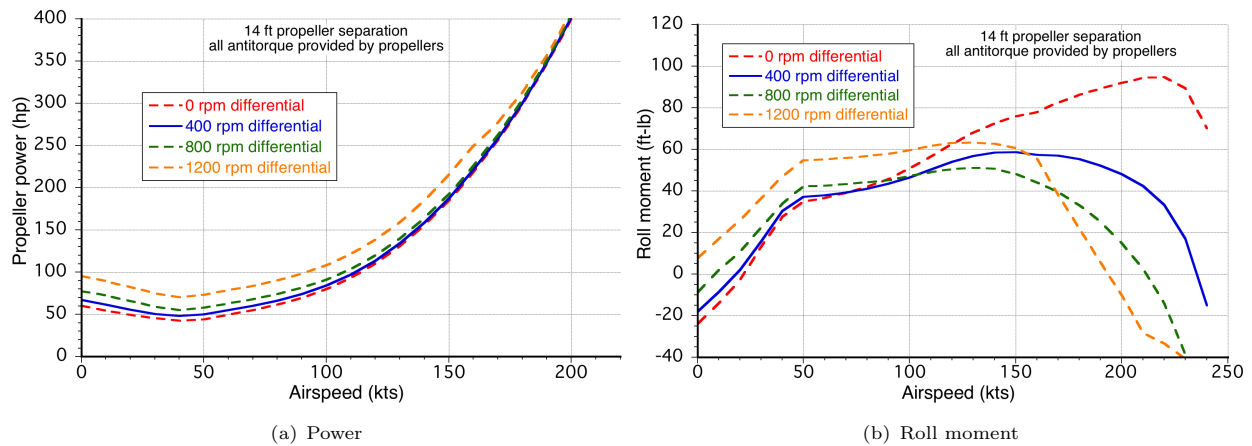


FIGURE 7.3: Effect of differential propeller shaft speed on power and roll moment. MSL 103°F.

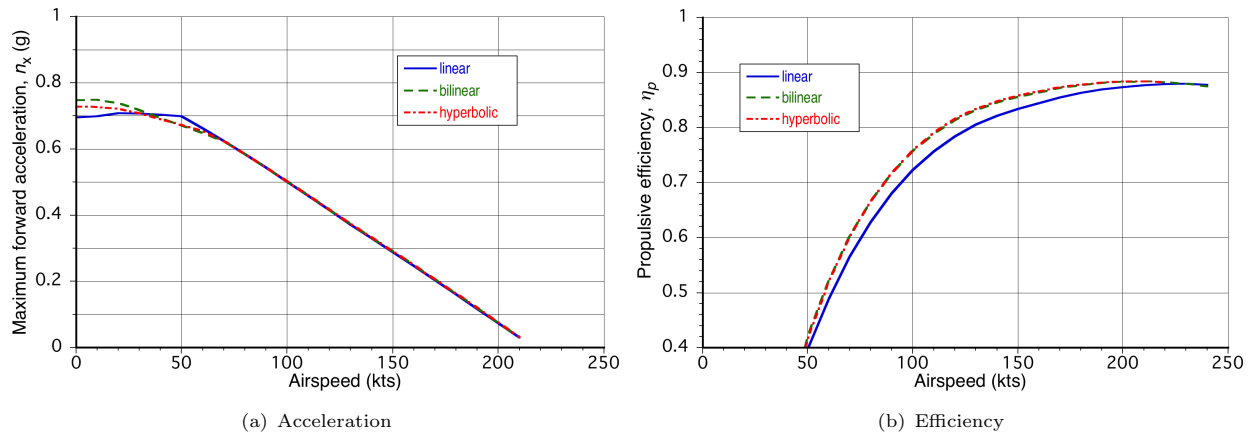


FIGURE 7.4: Trade study on propeller blade twist. MSL 103°F.

7.1.4 Blade Twist

Three blade twist shapes were considered for the *Dart*: linear, bilinear, and a hyperbolic twist. For each type of twist, the twist rates were optimized to minimize power requirements in cruise at 125 kts; this airspeed was determined to be the best design point to maximize overall propeller performance at all airspeeds. Figure 7.4 shows that all three types of blade twist can achieve similar maximum translational accelerations, but linearly twisted blades show lower efficiencies. Bilinear twist was selected because of its good performance characteristics, as well as its low manufacturing cost compared to a blade with hyperbolic twist. The *Dart's* propeller blades have a $-32.6^\circ/\text{ft}$ inboard section and a $-10.7^\circ/\text{ft}$ outboard section (42.4° total blade twist). The twist rate changes at $0.52R$.



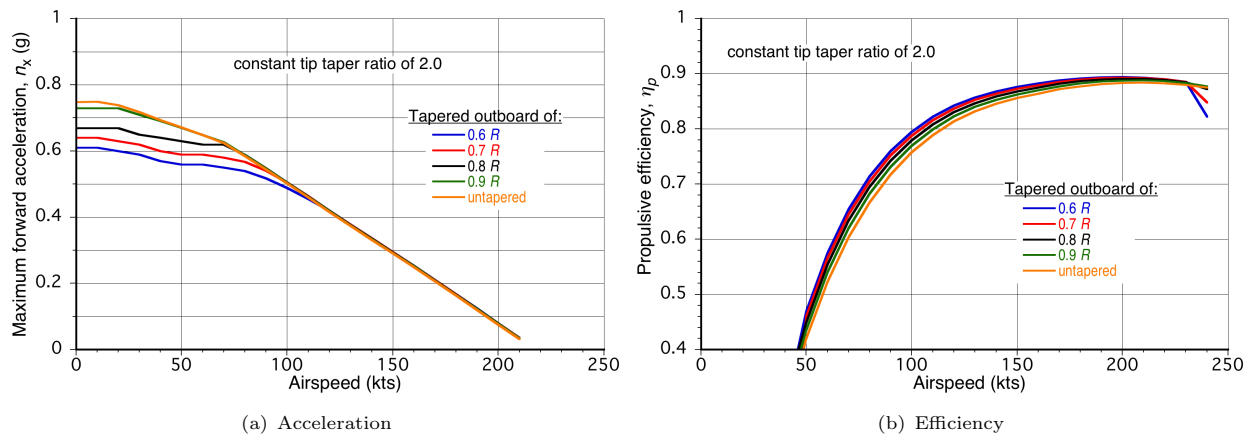


FIGURE 7.5: Trade study on propeller taper. MSL 103°F.

7.1.5 Blade Tip Shape

Tip sweep was found to have a negligible effect on propeller performance. The slowed engine rpm at high airspeeds ensures that the propeller never exceeds a helical tip Mach number of 0.79 at MSL ISA, thereby eliminating the need for sweep. Tapering the propeller blade tips, as shown by the results in Fig. 7.5, produces a minor improvement in cruise efficiency but decreases the maximum attainable translational accelerations. Therefore, the *Dart*'s propeller blades are unswept and untapered.

7.1.6 Propeller Airfoils

Airfoil selection for the propeller was based partly on the requirements for the maximum attainable lift coefficient. Figure 7.6 shows the lift coefficients over the propeller blades at both zero acceleration and maximum acceleration. The largest requirements for airfoil maximum lift coefficient, $C_{l_{max}}$, arise when the propellers are operating at their maximum thrust in hover. This thrust is achieved with the inboard part of the blade in a semi-stalled condition because the propeller twist was designed for forward flight and is larger than desired for maximum static thrust. The airfoils for the *Dart* were derived from the Clark-Y, which has an 11.7% thickness ratio and a $C_{l_{max}} = 1.3$. The blade has a circular cross section near the spinner, and blends into a 15% thick airfoil by $0.5R$. The airfoils further blend into a 12% thick section at $0.8R$ and a 6% thick section at the tip. This distribution gives large values of $C_{l_{max}}$ at the blade root and mid-span with minimum drag at the tip.

7.2 Propeller Blade Structure

Composite rotor blades were selected to reduce total propeller system weight and the resulting wing weight. The propeller blade has two primary sections, the shank and the blade. The shank is a metallic plug, which transmits the centrifugal and bending loads from the blade to the hub and helps in pitch actuation for propeller control. The blade itself consists of a Rohacell foam core, a $\pm 45^\circ$ wrap, an intermediate unidirectional section, and an outside $\pm 45^\circ$ wrap. Bending, lag and centrifugal loads are all carried primarily by the unidirectional layer, while the $\pm 45^\circ$ layers provide a majority of the torsional stiffness. The final layer is a 73 g/m^2 ($.015 \text{ lb/ft}^2$) expanded copper mesh for lightning protection. A glass/PEEK erosion shield,



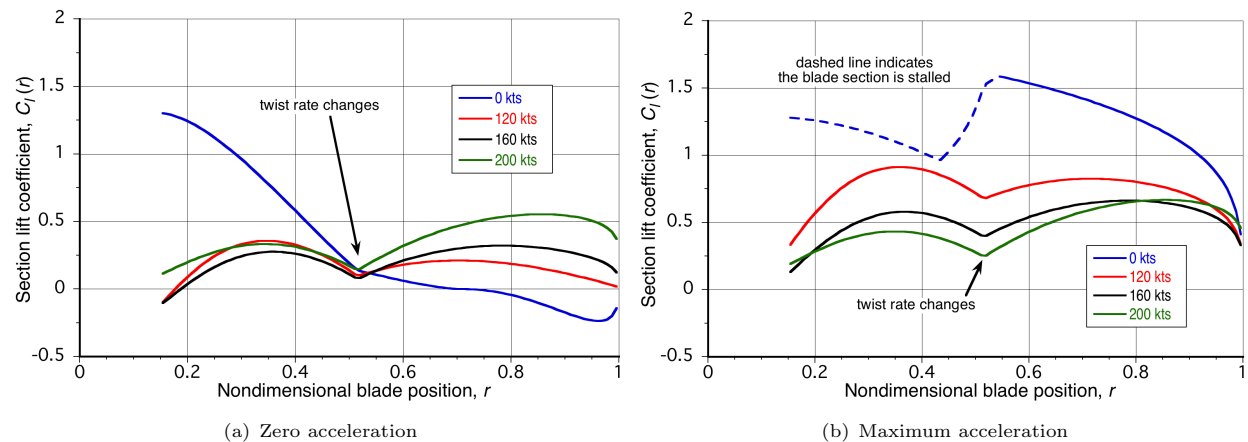


FIGURE 7.6: Propeller lift coefficients at zero acceleration and maximum acceleration. MSL 103°F.

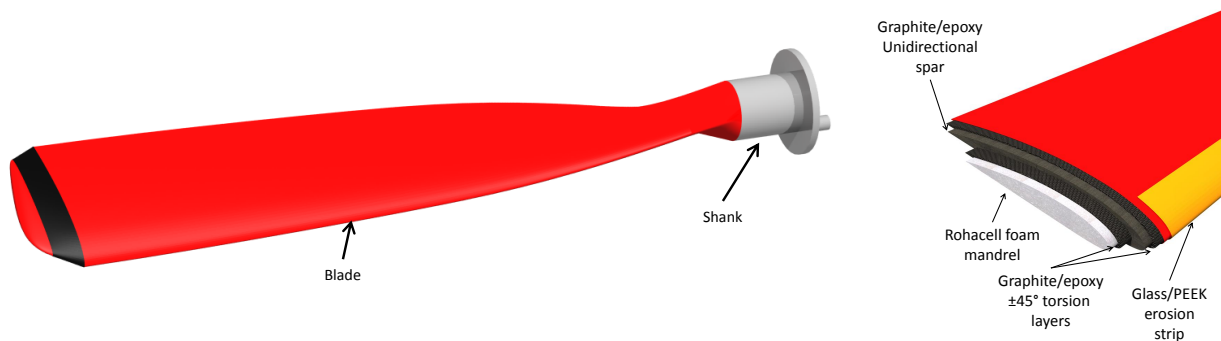


FIGURE 7.7: Propeller blade structure. (a) Exterior features (b) Internal structure

similar to the one used in the main rotor blade (Section 6.2.1) is bonded to the leading edge of the propeller to protect the propeller from any impact with debris.

7.3 Propeller Hub

The *Dart T690* propellers are directly interconnected with the main rotor, and an electric actuator controls the collective pitch of the propeller through a swashplate and slider mechanism in the propeller hub (Fig. 7.8). This system gives the pilot direct control of the propeller thrust, while the rpm of the entire system is maintained by the FADEC system (Section 8.1). Counterweights are added near the root to reduce the centrifugal moments, alleviating pitch loads. A streamlined spinner covers the inner 15% of the rotor radius, including the hub, to minimize the drag caused by the hub.



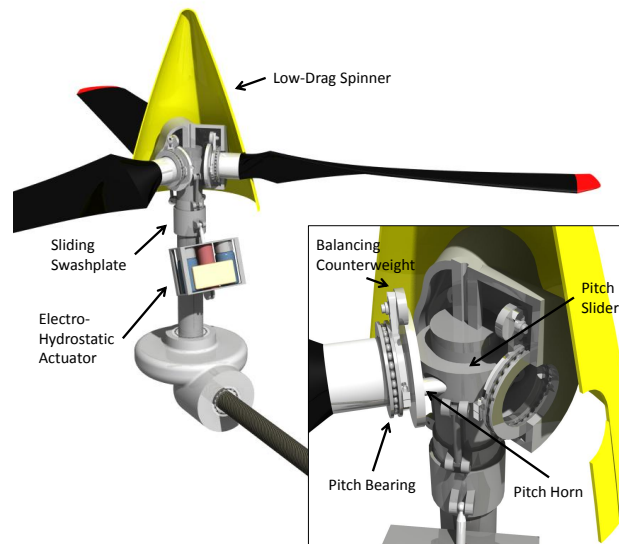


FIGURE 7.8: Propeller hub and collective pitch actuation mechanism.

7.4 Compatibility with the *Dart E550*

In the *Dart E550* option, each propeller has its own electric motor and is not directly connected to the main rotor. However, the electric motor control system was designed so that the system responds in the same manner as the turbine option. This allows for a common propeller and hub design between the two aircraft models.

7.5 Propeller Dynamics

Propellers operate primarily in axial flow, but when flying in a nose-high attitude or in rotor downwash, the propeller experiences a small component of edgewise flow. To ensure propeller stability, a study of material choice and thickness of the various composite layers was performed. The stiffness of the propeller blades was calculated for each configuration and the resulting propellers were then evaluated as described in Section 6.4 (Fig. 7.9). The first three bending modes show significant blade motion in both the flap and lag direction. This is expected because the blade has 42° of twist between the root and tip, and the lag stiffness is more than ten times higher than the flap stiffness.

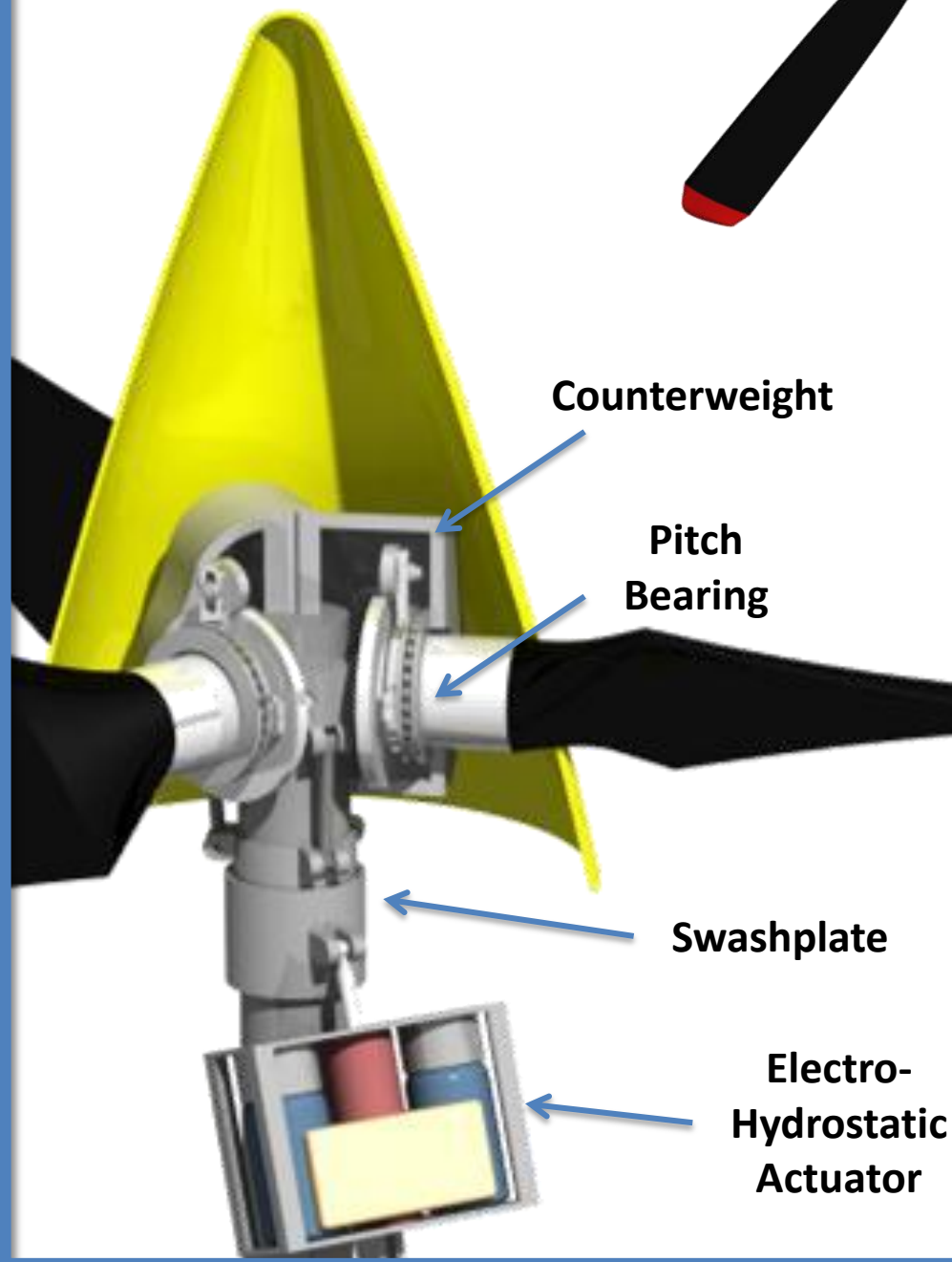
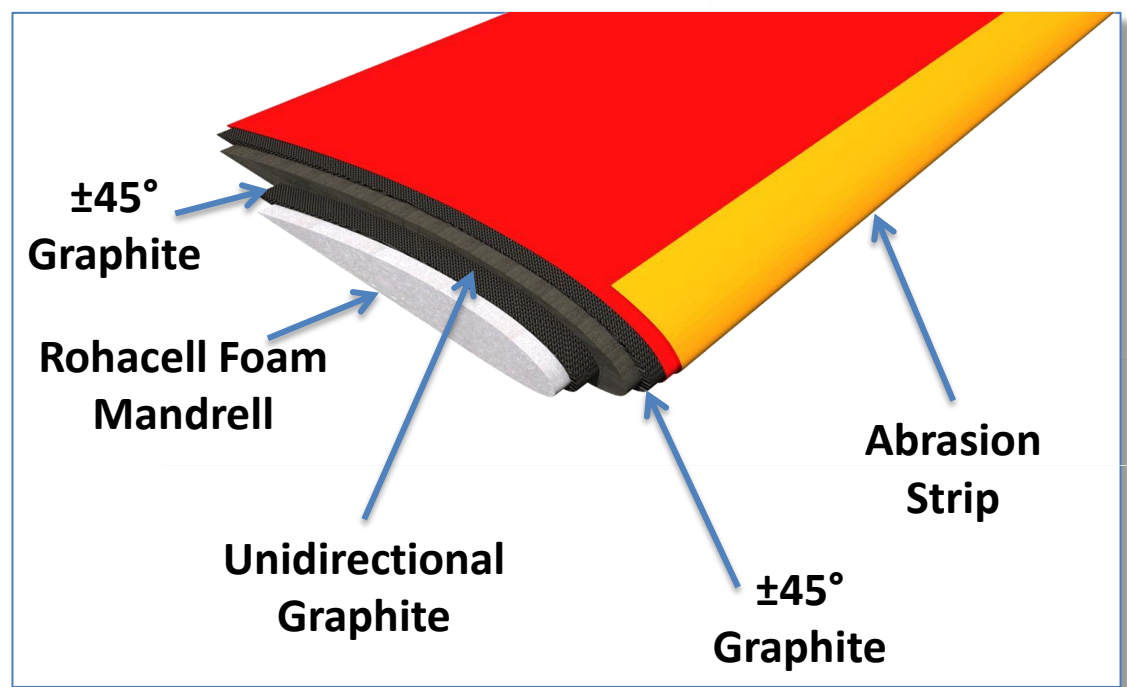
Overall, there is no possibility of any aeroelastic instability or mechanical resonance with any of the rotor harmonic. The propeller rpm is set to be 6.3/rev of the rotor, and the expected vibratory loads due to edgewise flow are very low (far below the threshold levels) at all operating conditions. Whirl flutter is also not an issue; see Section 9.9.5.



Propellers

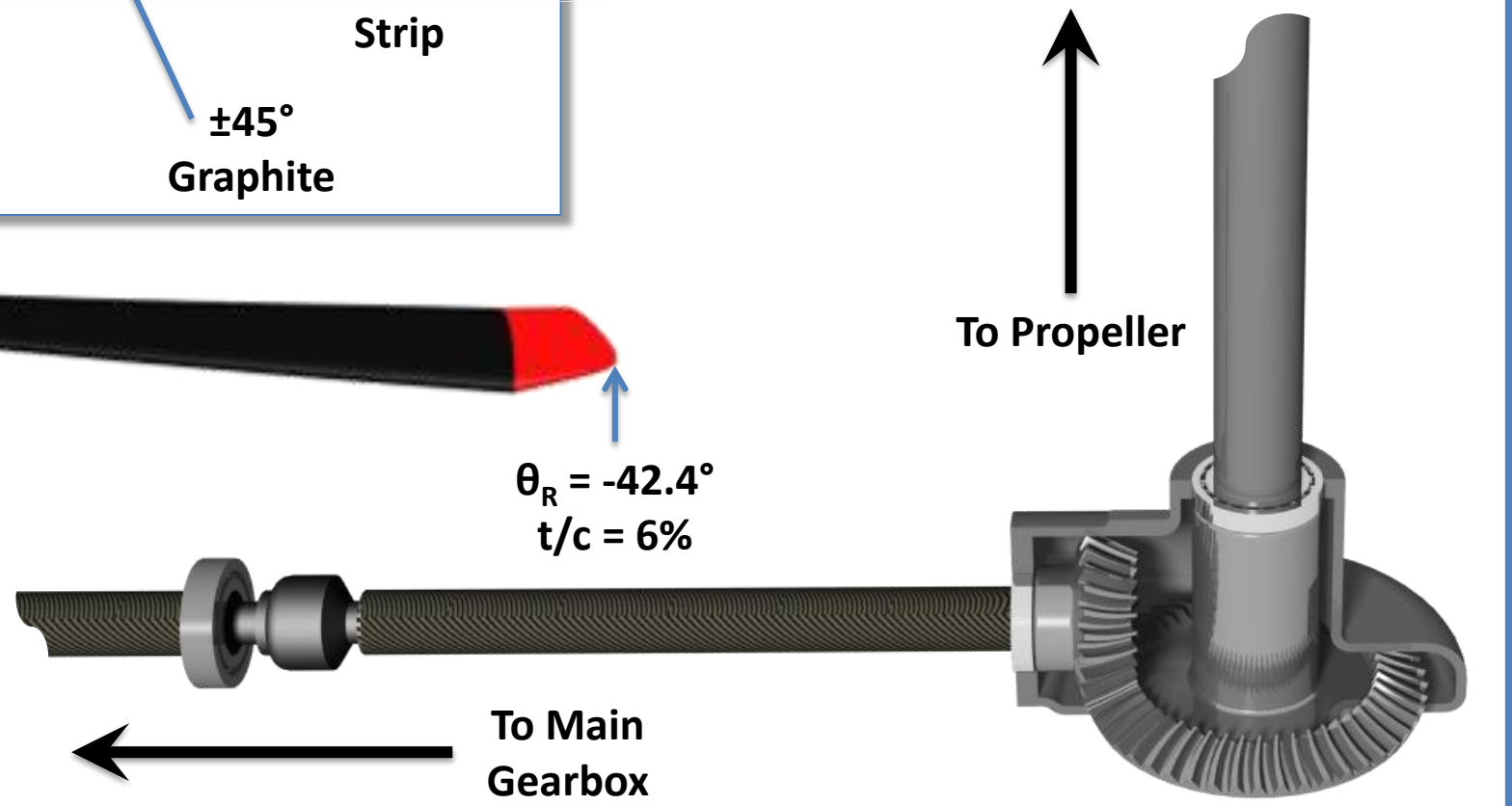


DART T690



$\theta_{0.5R} = -30.2^\circ$
 $t/c = 15\%$

$\theta_R = -42.4^\circ$
 $t/c = 6\%$



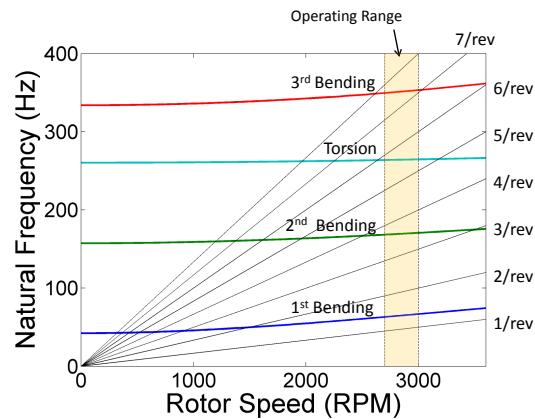


FIGURE 7.9: Propeller blade fan plot.

8 Power System and Transmission

8.1 Turboshaft Engine

The RFP has provided a theoretical “rubber” engine, scalable by power rating and SFC. Engine weight and dimensions (i.e., length and diameter) are computed based on the maximum continuous power of the engine. These numbers reflect a high level of advanced technology, as shown in Fig. 8.1, which compares the *Dart T690*’s engine dimensions to data for contemporary civil turboshaft/turboprop engines. While the provided engine clearly deviates from historical trends, it is sized in accordance with the equations provided in the RFP. The designation *T690* stands for a turboshaft engine with an intermediate rated power of 690 hp. Figure 8.2 shows the *Dart T690*’s turboshaft engine and Table 8.1 gives its dimensions. The aircraft uses dual Full Authority Digital Engine Controllers (FADEC) to regulate the turbine throttle in order to maintain a constant engine rpm.

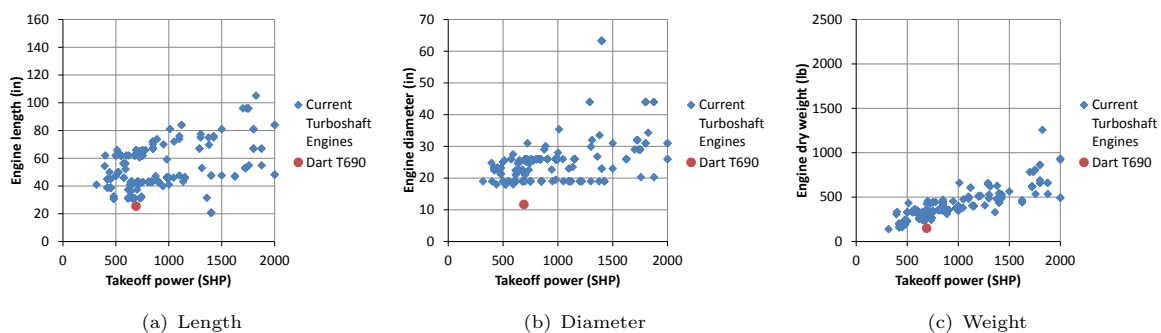


FIGURE 8.1: Historical data for engines compared to that given in the RFP.

Correction factors for power and SFC, with equations for ram power and residual thrust estimation, were provided in the RFP to account for operations at different engine speeds. For performance at altitudes and temperatures other than MSL ISA, the lapse rates were calculated and the results are shown in Fig. 8.2. Notice that a 1°C increase in temperature leads to a 0.76% decrease in MCP and a 0.26% increase in SFC. An increase in altitude of 1,000 ft reduces the MCP by 3.14% and increases the SFC by 0.13%.



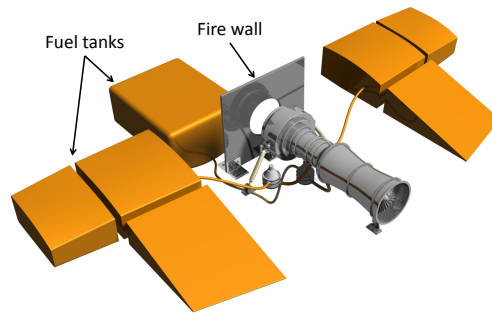
FIGURE 8.2: Turboshaft engine and fuel tanks of the *Dart T690*.

TABLE 8.1: Engine characteristics.

Maximum Rated Power (HP)	Weight (lb)	Length (ft)	Diameter (ft)
690	150	25.5	11.7

TABLE 8.2: Lapse rates of the given engine.

Power Loss	OEI	MRP	IRP	MCP	Part	Idle
For 1°C (HP)	-7.28	-7.28	-7.04	-5.8	-3.64	-1.44
For 1°C (%)	-0.69%	-0.73%	-0.75%	-0.76%	-0.73%	-0.72%
For 1,000ft (HP)	-32.73	-32.07	-30.37	-24	-16.03	-6.37
For 1,000ft (%)	-3.12%	-3.20%	-3.25%	-3.14%	-3.20%	-3.18%
SFC Loss	OEI	MRP	IRP	MCP	Part	Idle
For 1°C (lb/hp/hr)	5.2×10^{-4}	6.4×10^{-4}	7.6×10^{-4}	1.0×10^{-3}	1.6×10^{-3}	4.5×10^{-3}
For 1°C (%)	0.14%	0.18%	0.21%	0.26%	0.38%	0.67%
For 1,000ft (lb/hp/hr)	1.0×10^{-4}	3.7×10^{-4}	4.7×10^{-4}	5.0×10^{-4}	8.3×10^{-4}	2.6×10^{-3}
For 1,000ft (%)	0.03%	0.10%	0.13%	0.13%	0.20%	0.38%

8.2 Alternative Propulsion System: The *Dart E550*

For the alternative propulsion system, there are three main considerations: 1. The choice of power plant for the system, 2. Transmission of power to the rotor and propellers, and 3. Provision of power for the on-board electrical systems. Additionally, the performance requirement used for the *Dart E550* is that it must be able to complete the course in the same amount of time as the *Dart T690*.

Based on these requirements, it was decided that the *Dart E550* would be driven by an electric propulsion system. The *Dart E550* uses a fully electric hybrid PEM Fuel Cell/Li-ion power plant with Halbach Array motors. Previous electric aircraft, such as the Sikorsky Firefly, were only able to achieve a flight time of 15



TABLE 8.3: Power required for the different mission segments.

Mission Segment	Time (min)	Max Power Required (hp)	Energy Required (hp-min)
Warm-up	10	50	500
Rotors turning	5	131	655
Wait till start	10	250	2500
Course	5	550	2,750
Staging	15	97	1,455

minutes. The *Dart E550* boasts a flight time of 40 minutes with the same aggressive maneuvering, agility, and speed capabilities of the *Dart T690*.

8.2.1 Propulsion System Selection

Three types of power plants were considered: piston engines, hybrid gas-electric, and fully electric power plants.

Piston Engine: Piston engines save weight when the vehicle has high range capability because the specific energy of gasoline is high. However, the *Dart E550* has a low range requirement, so this system would be heavier than the turboshaft option.

Gas-Electric Hybrid: This system uses batteries to augment the power of the gasoline-fed piston engine during high power loads. A generator is used to power an electric motor which runs a drive shaft. While this system is more environmentally friendly than a piston engine, it tends to be heavy due to the inclusion of a generator to convert the mechanical output of the piston engine into electrical power.

Fully Electric Vehicle: There are three ways of implementing this system: fully battery driven, fully fuel cell driven, and a hybrid battery-fuel cell power plant. These systems are simpler to implement since there is no need for a generator, and there are no emissions, making the vehicle environmentally friendly. The disadvantage is that batteries and fuel cells have lower power and energy densities than turbine engines, so the power plants are heavier than a comparable turbine engine. However, this weight deficit can be overcome by including lightweight electric motors in place of heavy transmissions and shafting.

It was decided that the alternate version of the aircraft would be a fully electric vehicle. Of the three options considered, a fully electric vehicle has the main advantage of having no carbon footprint, making the vehicle a “green” aircraft. Given recent advances in battery and fuel cell technology, this system is feasible with a minimal weight penalty and a reasonable TRL.

8.2.2 Power Requirements

The maximum power required to complete the course at MSL 103° F is 550 hp and, therefore, the power requirement for the *Dart E550* was also set to 550 hp. Table 8.3 shows the power schedule for the vehicle based on the power requirements for each mission segment. The power schedule shows that the aircraft must maintain idle power (50 hp) for 10 min during warm-up and staging, power at V_{be} (97 hp) for 25 min, hover power (250 hp) while waiting to start the course, and maximum speed/acceleration power (550 hp) for 5 minutes during the race course. Based on the performance analysis in Section 13.5, it is apparent that the maximum power is set by the maximum speed the vehicle is required to attain (see Section 2.2.4 for the flight path planning results). Table 8.3 also shows the energy requirement for the mission, which was found by taking the product of the flight time with required power, yielding a total energy requirement of 8645



TABLE 8.4: Maximum power required by the rotor and propellers.

	Main Rotor	Propeller (each)
Required power (hp)	200	260
Operating rpm	500	3,200
Flight condition	Hover	Maximum speed

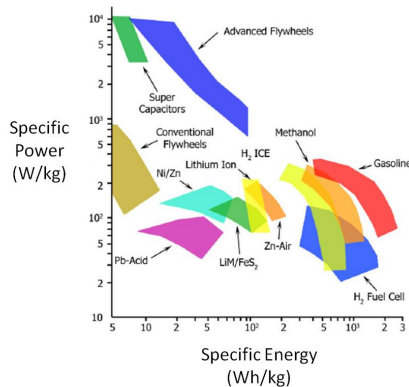


FIGURE 8.3: The specific energies and powers of various power generation technologies[14].

hp-min. Of this energy, one third are used during the course and the remaining two thirds are used for the other mission segments.

Table 8.4 summarizes the maximum powers required by the propellers and the main rotor, as well as what flight conditions set those powers. The maximum power required by the rotor (200 hp) is set by the power required to hover, and the maximum power for each propeller (260 hp) is the power required to reach a maximum speed of 225 kts.

8.2.3 Power Plant Trade Study

Possible Power Plants

In Section 8.2, it was concluded that the alternate power plant would be fully electric, for which there are three types of implementations: batteries, fuel cells, or battery/fuel cell hybrid. The weights of these systems, which is a major design consideration, is dictated by their specific powers and specific energies.

Figure 8.3 shows a Ragone plot of the specific powers and energies of various technologies available today [14], with a higher specific energy and specific power indicating a lower system weight. Of the technologies identified in Fig. 8.3, the most advanced battery technology is Lithium-ion (Li-ion) and the most advanced fuel cell technology is the hydrogen fuel cell, also known as a Proton Exchange Membrane (PEM) fuel cell. Projected values of specific power and energy, along with other useful quantities are shown in Table 8.5 [15, 16]. The values in the table are the expected values for the specific power and energy for a Li-ion battery and PEM fuel cell technology that would be available between 2017 and 2020.

Lithium-ion Batteries

Li-ion batteries have three main components: a negative electrode, a positive electrode, and an electrolyte. The negative electrode is made from carbon, the positive electrode is a metal oxide, and the electrolyte is a



TABLE 8.5: Battery and fuel cell properties projected to expected values for 2017 [15, 16].

	Li-ion Battery	PEM Fuel Cell
Density (kg/L)	2.0	1.19
Specific Power (W/kg)	2500	2000
Specific Energy (Wh/kg)	200	2250
Efficiency	90 %	85 %

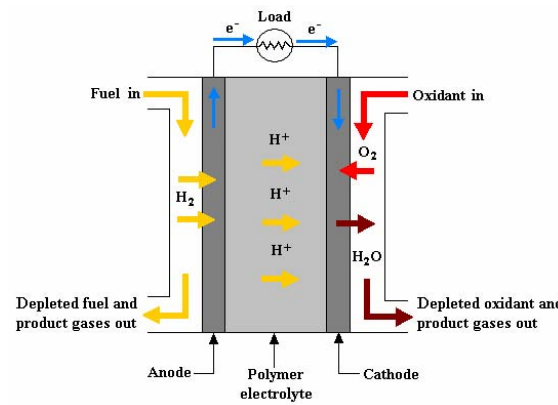


FIGURE 8.4: Description of a PEM Fuel Cell.

lithium salt in an organic solvent [17]. The Lithium ions in the electrolyte carry electrons from the negative electrode to the positive electrode, producing a current that is used to power a circuit; for the *Dart E550*, this circuit is the electric motors that run the propellers and main rotor.

PEM Fuel Cells

A PEM fuel cell stack consists of a stack of hydrogen fuel cells [18]. Figure 8.4 shows a diagram of a single PEM fuel cell. Each fuel cell consists of two platinum impregnated porous electrodes (an anode and a cathode). The electrodes are thin films that are bonded to a hydrated, proton conductive polymer membrane. Hydrogen gas is directed from an onboard storage tank to the anode side of the cell, where the catalyst (generally platinum) separates the gas into protons and free electrons. Electrons cannot pass through the polymer membrane and are forced through the external load, in this case, the electric motors. The protons diffuse through the membrane to the cathode, where they react with the oxygen in the air coming from the intakes and the returning electrons to produce water, which is directed out of the exhaust.

Power Plant Sizing

The goal behind the alternate propulsion design is to develop an aircraft to fly the course in the same time as the *Dart T690*. This means that the weight and airframe of the *Dart E550* cannot change with the installation of an electric power plant. Hence, the electric system must only use replaceable weight and volume onboard the *Dart T690*. Items that are replaceable include the engine, oil system, fuel, transmission, gearboxes, etc. The total replaceable weight was determined to be 850 lb (Chapter 10) and the replaceable volume is about 12 ft³.

Both Li-ion batteries and PEM fuel cells were sized to determine whether they were viable options as electric power plants for the *Dart E550*. Using the flight times and power requirements in Table 8.3, along with the specific powers/energies listed in Table 8.5, it was determined whether the full battery or fuel cell systems



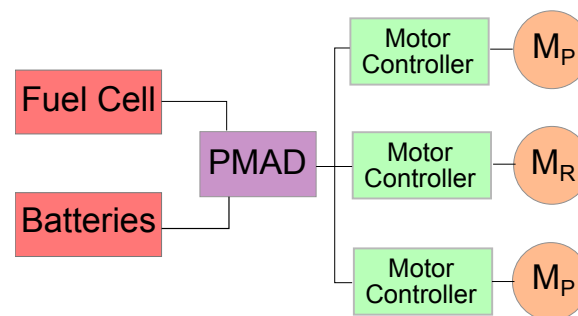
TABLE 8.6: Weight and volumes for a pure battery and a pure fuel cell vehicle.

	Li-ion Battery	PEM Fuel Cell
Weight (lb)	3,100	730
Volume (ft ³)	24.6	16.3

were power or energy limited, from which a system weight and volume can be calculated Table 8.6 shows the weights and volumes for pure Li-ion battery and PEM fuel cell power plants using this methodology.

The values in Table 8.6 show that a Li-ion system is too heavy and both Li-ion and PEM fuel cell systems require higher volumes than are available. However, the volume needed for a PEM fuel cell system is driven by the amount of hydrogen that must be stored in the aircraft. Therefore, if the amount of hydrogen could be reduced, the PEM fuel cell system could be a viable power plant. The amount of on-board hydrogen can be reduced by augmenting the fuel cells with batteries during heavy power loads, i.e., using a fully electric hybrid vehicle, where in this instance, “hybrid” refers to the use of two different power plants.

A schematic of a fully electric hybrid is shown in Fig. 8.5. Power is generated by the batteries and the fuel cell. This power is fed into a power management and distribution unit (PMAD) that sends the required power to the motor controllers, which transfer the power to the electric motors.

FIGURE 8.5: Flow of power through the system. M_R is the main rotor motor and M_P is a propeller motor.

8.2.4 Fully-Electric Hybrid Power Plant Design

Power Sharing Between Li-ion Batteries and PEM Fuel Cell

Based on the results of the previous section, the power plant on the *Dart E550* must be a fully-electric hybrid system, where the power load is split between PEM fuel cells and Li-ion batteries. In the previous section it was shown that a fuel cell system on its own takes up too much volume, however, its weight is within the replaceable weight of the *Dart T690*. The reason that the volume is high is because of the amount of hydrogen that must be stored to run the five minute course, which is a high power condition (see Table 8.3). Therefore, by augmenting the fuel cells with batteries, the amount of hydrogen carried can be reduced.

The minimum power that the fuel cell must provide is 250 hp (from Table 8.3), which allows the vehicle to complete the warm-up, takeoff, and taxiing parts of the mission. However, during the course, the power plant must produce up to 550 hp, of which the fuel cells must provide at least 250 hp so that the vehicle can hover. To determine the amount of power the fuel cells should provide, a study was conducted to determine the fuel cell/battery power sharing that minimizes overall weight and volume. The weight and volume of the fuel cell system were calculated by assuming that the fuel cell provides 250 hp during all mission segments,



except for the race course itself. During the race course, the power provided by the fuel cell varied from 250 hp to 550 hp. The weight and volume of the battery were determined to make up the deficit of power that the fuel cells did not supply during the race itself.

Figures 8.6(a) and 8.6(b) show preliminary weights and volumes of the power plant as a function of the power provided by the fuel cell. The dashed line represents the minimum power from the fuel cell (250 hp). To minimize total system weight and volume, the amount of power provided by the PEM fuel cells

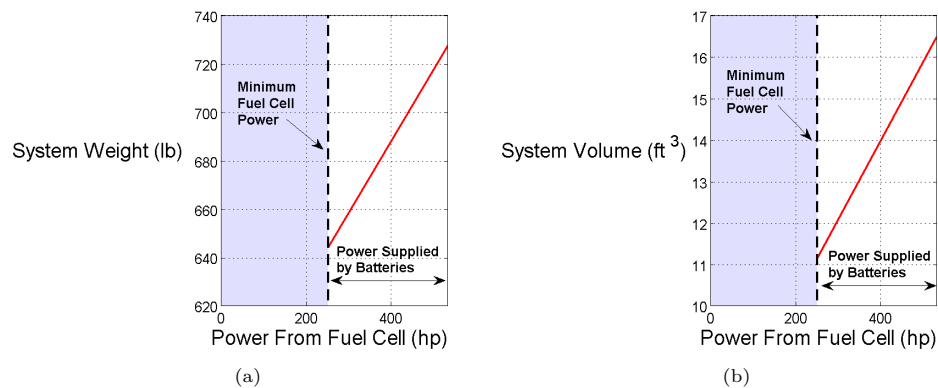


FIGURE 8.6: (a) Preliminary system weight and (b) Preliminary system volume.

during the race should be a minimum of 250 hp, and that should be augmented by batteries that supply the remaining 300 hp (of the total 550 hp required).

Fuel Cell and Battery Design

The preliminary sizing showed that the PEM fuel cell for the *Dart E550* provides 250 hp and the batteries supply 300 hp. To size the fuel cells, the polarization curve from [18], as shown in Fig. 8.7(a), is used. The polarization curve gives the potential of each cell versus the current density, which is the current divided by the active area of the cell. The current required per cell is determined by using the fuel cell power (250 hp)

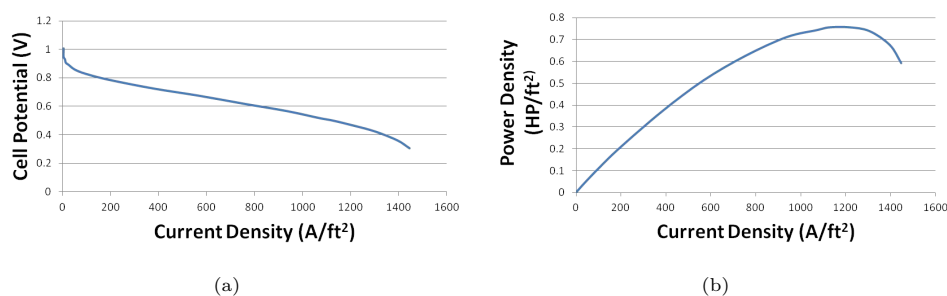


FIGURE 8.7: The (a) cell potential and (b) power density as a function of current density.

and the operating voltage, which was chosen to be 300 V. With the required current and operating voltage, the area of each cell and the total number of cells needed in the fuel cell stack can be calculated as a function of the current density by using the polarization curve. The power density curve, as shown in Fig. 8.7(b), is obtained by taking the product of the cell potential and the cell density. The peak of the power density curve gives the current at which the weight of the fuel cell is minimized.



TABLE 8.7: Design specifications for the PEM fuel cell and Li-ion batteries.

PEM Fuel Cell	
Num. cells	517
Stack weight (lb)	180
Active area (ft ²)	0.64
Hydrogen flow rate	1 × stoichiometric
Oxygen flow rate	1 × stoichiometric
Hydrogen weight (lb)	28 lb
Stack dimensions (ft)	0.82 × 0.82 × 2.6
Voltage (V)	300
Power (hp)	250
Li-ion Batteries	
Weight (lb)	212
Power (hp)	300
Volume (ft ³)	1.7

However, the hybrid system on the *Dart E550* must also consider the weight of other systems such as hydrogen, hydrogen storage tanks, electric motors (see Section 8.2.5), and transmission shafts (see Chapter 10). With the addition of these systems, Fig. 8.8 shows the total weight and volume of the propulsion system as a function of the cell density. The total system weight and volume achieve minimums at different current

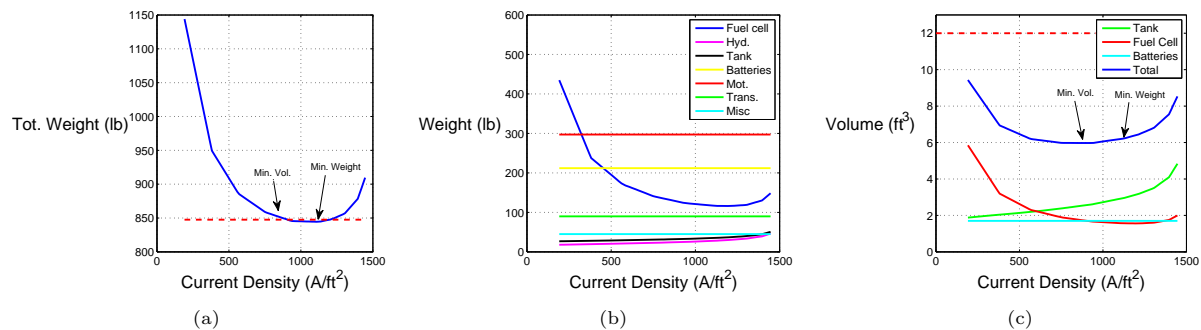


FIGURE 8.8: The (a) total system weight, with the red line being the replaceable weight on the Dart T690, (b) component weights, and (c) system volume as a function of current density.

densities. However, as shown in Fig. 8.8(c), the system volume (6 ft³) is well below the replaceable volume (12 ft³). As shown in Fig. 8.8(a), the minimum system weight is 845 lb, and is 5 lb less than the replaceable weight (850 lb). Therefore, the hybrid system can be sized to minimize the weight of the propulsion system while remaining below the replaceable weight. The designs that minimize the weight are summarized in Table 8.7.

With this fully-electric hybrid power plant, the *Dart E550* meets all the power and energy requirements stated in Section 8.2.2 within the replaceable weight (850 lb) and volume (12 ft³) available in the *Dart T690*. Therefore, the *Dart E550* can perform the required mission without any degradation in performance. As such, the *Dart E550* has the same maximum speed, acceleration, deceleration, and attitude rates of the *Dart T690*, while also resulting in a truly environmentally friendly rotorcraft.

Hydrogen Storage



The reactants supplied to the fuel cell are hydrogen and oxygen. Oxygen is provided from the air using the intakes already on board the *Dart E550*. Hydrogen, however, must be stored on board the aircraft. To decrease the total system weight, the required hydrogen weight of 28 lb (Table 8.7) is stored in a single composite tank at 15,000 psi. The hydrogen is stored at a temperature of 77°C. These storage properties lead to a storage tank with a length of 2.7 ft and a radius of 0.65 ft, and weighing 35 lb.

8.2.5 Motor Selection and Design

Electric Motor Options

For any electric propulsion system, motors are needed to convert the electrical power to mechanical power. Three types of motors were considered for the *Dart E550*: AC, Brushless DC (BLDC), and Halbach Array (HA)

AC: AC motors are used for domestic applications as they work using readily available alternating current. On electric vehicles, an inverter is needed to transform the DC output of the power plant to AC. As such, the maximum power-to-weight ratio of the motor/inverter combination is 1 hp/lb.

Brushless DC: Brushless DC motors run off of direct current and are useful for electric vehicles. Specifically, wheel-hub motors, which are motors that sit directly in the hub of a wheel on a bicycle, motorcycle, or electric car, are advantageous because they reduce weight by eliminating gearboxes, differentials, drive-shafts, etc. High power BLDC motors have a power-to-weight ratio of 2-3 hp/lb.

Halbach Array: HA motors have similar components to DC and AC motors, but have the benefit of running off of both alternating and direct current. They have all the benefits of BLDC motors and are lighter from the inclusion of a Halbach Array permanent magnet section (explained in more detail next). These motors can have a power-to-weight ratio of up to 5 hp/lb [19].

Because HA motors have the highest power-to-weight ratio, they were chosen as the motors for the *Dart E550*. Figures 8.9(a) and 8.9(b) show the two main components of a HA motor: a stationary section (stator) and a rotary section (rotor). The stator consists of several sets of wire windings and the rotor consists of a circular HA. In addition to the main components, there is also an impeller ring that draws air to cool the motor and a carbon fiber backing plate.

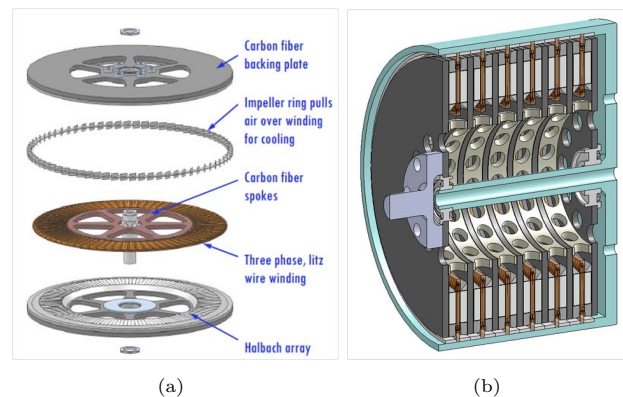


FIGURE 8.9: A (a) Halback array motor and (b) a cutaway of a Halbach array motor stack.[19]

Figure 8.10(a) shows a typical dipole HA [20]. The HA is on the outside, with permanent magnets oriented so that a concentrated uniform magnetic field is created in the center of the array with a near zero field



TABLE 8.8: LaunchPoint HA motor and motor controller properties. [1]

Motor Properties	
Motor specific power (hp lb^{-1})	5
Motor diameter (in)	18
Motor width (in)	1.5
Motor power (hp)	150 @ 3,200 rpm
Motor power (hp)	100 @ 2,700 rpm
Motor controller specific power (hp lb^{-1})	21

on the outside. Since the field is near zero outside the array, the power of the magnetic field is efficiently harnessed because there are no losses to having field lines away from the wire windings in the stator. When current (DC or AC) passes through the wire windings in the stator, a magnetic field is induced, which causes the HA magnets in the rotor to turn to align the fields, creating rotation to move a drive shaft or propeller.

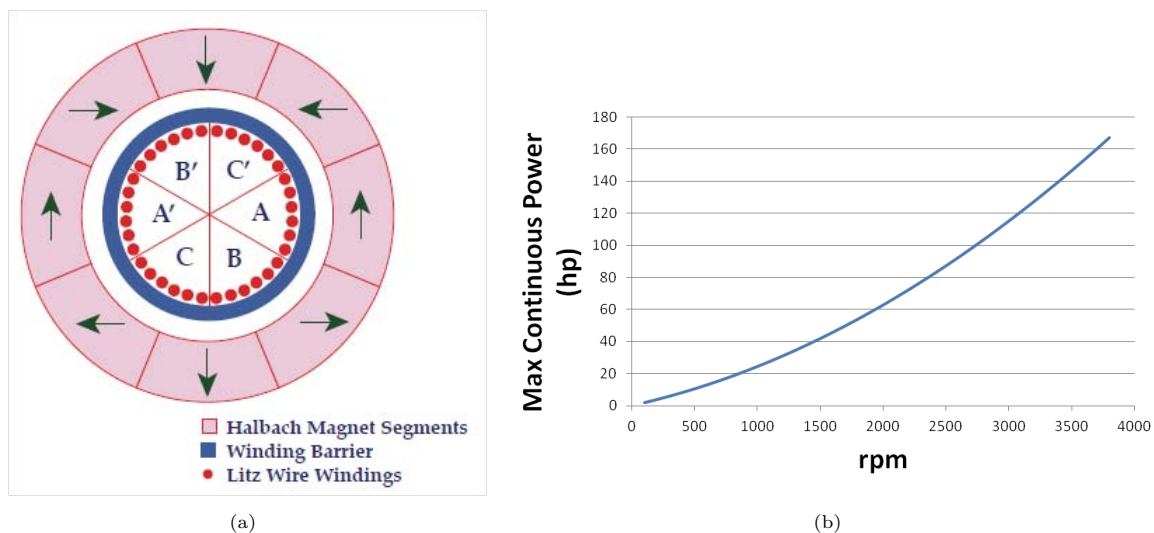


FIGURE 8.10: A (a) sketch of a Halbach array motor [20] and (b) the power curve for the LP HA motor.

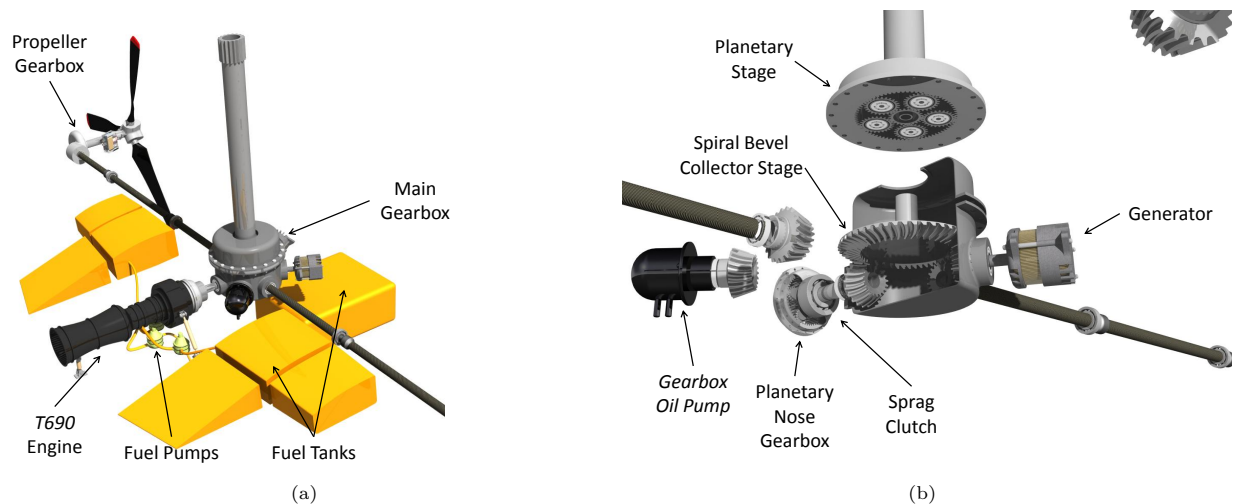
Electric Motor Selection

The HA motors selected for the *Dart E550* were based on the designs created by LaunchPoint Technologies. LaunchPoint has designed a scalable motor that can achieve 5 hp/lb [1], shown in Fig. 8.9(b). The properties of this scalable motor are listed in Table 8.8. Using the motor properties in table 8.8, the power curve, shown in Fig. 8.10(b), was calculated, which shows that the power that the motor is capable of transmitting reduces quadratically as the rpm is reduced. From Table 8.4 it is seen that the main rotor must operate at 500 rpm, for which the power output of this motor is only 15 hp, well below the required 200 hp. This amount of power would require 14 motors in the stack, with a total weight of 510 lb, which is infeasible. So instead, the motors for the main rotor on the *Dart E550* operate at 2,000 rpm, which gives an output power of 60 hp power per motor in the stack, and four motors are needed in the stack to produce the required 200 hp. From Table 8.4, it is clear that the propeller motors must operate at or below 3,200 rpm. At 3,200 rpm, the LaunchPoint motor produces 130 hp. To achieve the required power, there needs to be two motors at each



TABLE 8.9: HA motors used on the *Dart 550*.

	Main Rotor	Propeller (each)
Required Power (hp)	250	260
Operating RPM	500	3200
Weight (lb)	120	60
Diameter (in)	18	18
Stack Depth (in)	6	3
Controller Weight	29	15

FIGURE 8.11: *Dart T690* transmission layout. (a) complete transmission system with shaft rotation directions (b) Central transmission detail

propeller, producing 260 hp at each propeller. The electric motor stacks on the *Dart E550* are summarized in Table 8.9, where the weights and dimensions were calculated using the specifications in Table 8.8

8.3 Transmission

The transmission for the *Dart T690*, shown in Fig. 8.11, is a variation of the classic SMR transmission where the output for the tail rotor is exchanged for the two propeller shafts. Each propeller has a gearbox in the wing to reduce the shaft speed to the required propeller speed. This configuration is somewhat simpler than a traditional SMR because the horizontal alignment between the main gearbox and the propeller gearboxes alleviates the need for intermediate gearboxes that turn the tail rotor shaft. Because of the limited number of gear stages, the transmission efficiency is a relatively high 98%.

8.3.1 Transmission Selection

Many early compound helicopters and autogiros have added propulsive devices on the wings or on either side of the fuselage. Forgoing the precedent of adding additional engines, the Eurocopter X³ recently demonstrated how relatively simple the transmission layout for a dual thruster configuration could be.



TABLE 8.10: Breakdown of transmission stage sizes and ratings.

	Rating	Input rpm	Gear Ratio	Stage Type	Diametral Pitch	Gear	# of Teeth
Main Gearbox	654	6000	3:1	Spiral Bevel	5	Pinion Gear	20
			4:1	Planetary	8	Sun Planet Ring	60 25 75
Propeller Gearboxes	327	6000	15:8	Spiral Bevel	6	Pinion Gear	24 45

For the *Dart T690*, two configurations were considered for the main gearbox:

Split Torque: Split torque transmissions divide torque among more than one pinion, allowing for large gear reductions in the final stage, thereby removing an intermediate stage and decreasing system weight. This design was first demonstrated successfully on the 23,000 hp Mil Mi-26, but it has also been shown to be viable in transmissions of only 442 hp [21].

Planetary Gear: Planetary gears have a number of advantages, including compactness and the fact that the input and output are collinear. Because the planetary gear is symmetrically arranged around the input, all radial forces are reacted as a hoop stress in the ring gear rather than as radial forces in large bearings.

A planetary system was the ideal choice for the *Dart T690*. The weight savings in a split torque transmission are achieved when high gear ratios in the final stage allows one of the intermediate stages to be removed. However, the 18,000 rpm output speed of the *Dart T690* and the high operational rpm of the main rotor means that an overall gear ratio of only 36:1 is required. This goal is obtained in a three-stage planetary transmission: a 3:1 nose gearbox, a 3:1 collecting spiral bevel gear, and a 4:1 planetary stage.

8.3.2 Main Gearbox

The main gearbox contains two of the three transmission stages, including the 3:1 spiral bevel collecting and distribution stage, as well as a 4:1 planetary stage that performs the rpm reduction for the main rotor. Figure 8.11 shows the 500 rpm output to the main rotor, two 6,000 rpm shafts leading to the right and left propeller gearboxes, and three 6,000 rpm auxiliary outputs used to run the two electric generators and oil pump. All actuators on the aircraft are electrically operated, alleviating the need for a hydraulic pump.

The individual gear sizes were selected using the ANSI/AGMA 2001-C95 standard for the fundamental equations, with special application to helicopter transmissions from AGMA 911-A94. The diameter and face width of the individual gears were calculated from compressive stresses, and then the diametral pitch was selected based on the required tooth bending strength. Larger teeth are stronger, but smaller gears run smoother. The gears are to be manufactured from AISI 9310 high strength gear steel with magnesium gearboxes.

Gears are splash fed oil from a series of nozzles placed around the gear-sets and collected at the bottom of the case. The oil is pumped through an oil cooling unit that provides the primary cooling of the transmission. A chip detector is located in the oil system to help identify any internal damage and is connected to the HUMS. The main gearbox is rated to 2,500 hours of life and designed to survive 30 minutes after any loss of lubrication.



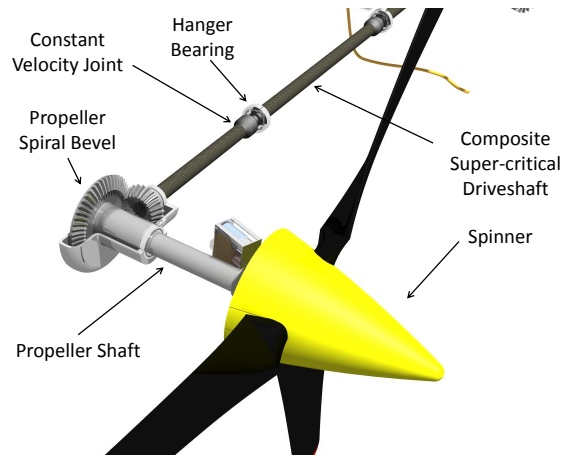


FIGURE 8.12: Propeller Gearbox.

8.3.3 Nose Gearbox and Overrunning Clutch

A planetary nose gearbox was designed to perform an initial speed reduction to 6,000 rpm before entering the main gearbox, allowing the main gearbox to survive 30 minutes after any loss of lubrication. A planetary configuration was chosen because it allows the engine to remain collinear with the input to the main gearbox. The nose gearbox feeds into a sprag clutch that automatically disengages the engine from the rotor and propellers in the event of any engine power failure and disengages below a set operational engine rpm, allowing the engine to warm at idle without turning the rotor.

8.3.4 Propeller Gearboxes

The propeller gearboxes (Fig. 8.12) provide a 15:8 gear reduction and a 90° turn from the 6,000 rpm driveshafts to the 3,200 rpm of the propellers themselves. The two gears are spiral bevel gears, which provide larger contact area and smoother running than straight bevel gears. The gearboxes use splash lubrication and have a chip detector connected to the HUMS. A nacelle over the wing reduces the aerodynamic drag of the gearbox.

8.3.5 Main Rotor Shaft

The main rotor shaft is cast from AISI 4340 steel and designed to meet dynamic axial, radial, and side shearing loads. The 11% hinge offset also contributes a mast moment. The maximum load factor of 3.5g is set by the 5g pull up maneuver. The forces are reacted against the transmission casing through radial bearings in the standpipe and a thrust bearing on the carrier section.

8.3.6 Propeller Driveshafts

Carbon/epoxy composite, 6,000 rpm, super-critical driveshafts connect the main gearbox and the propeller gearboxes. Each propeller shaft is segmented into three sections to tune their natural frequencies and to allow for misalignment between the main and propeller gearboxes caused by wing bending. The segments are connected by constant velocity joints and are supported by hanger bearings at the wing ribs.



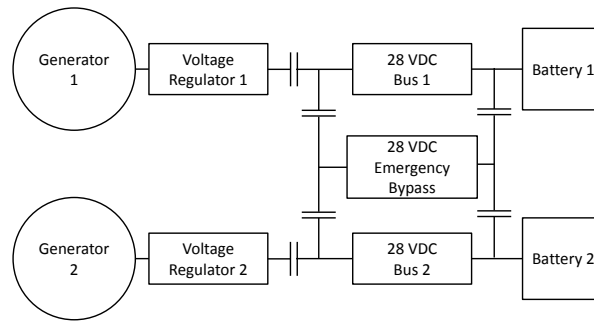
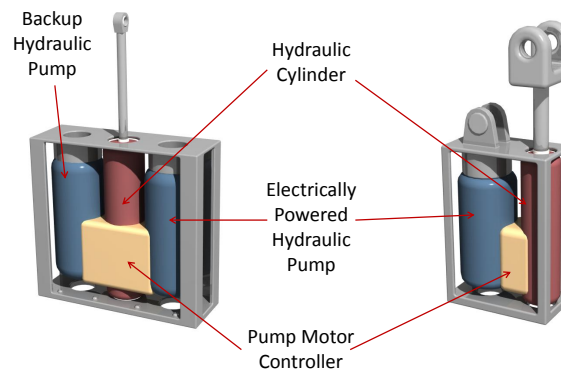


FIGURE 8.13: Power distribution schematic. The generators and DC buses are isolated by the relays in the case of a short circuit.



(a) Single EHA

FIGURE 8.14: The two electro-hydrostatic actuators (EHA) used in the *Dart*. Dual and single units are included.

8.3.7 Electrical Power Distribution System

The *Dart E550* is designed from the ground up to be a power-by-wire system to maximize compatibility with the *Dart T690* (see Section 8.2). All systems are designed to run on 28 VDC. For safety, a triple redundancy electrical power system (see Fig. 8.13) is built into the power train and all flight critical actuators are double redundant. Two generators are attached to the main gearbox and are governed by voltage regulators; they supply three parallel, independent 28 VDC buses and charge two batteries. In the event of a loss of engine power, autorotation of the main rotor can still generate power. In the event of a component failure, a series of relays can isolate the failed components and connect any unpowered buses to a viable power source. Each generator is capable of powering the entire system while maintaining the battery charge. If both generators fail, then the batteries together are capable of powering all systems. Each battery alone is capable of powering the mission critical equipment for a minimum of 30 minutes.



E550



DART T690



Hydrogen Tank

PEM Fuel Cells

Main Rotor Shaft

Halbach Motors

Li-ion Batteries

T690 Turbine Engine

Main Rotor Shaft

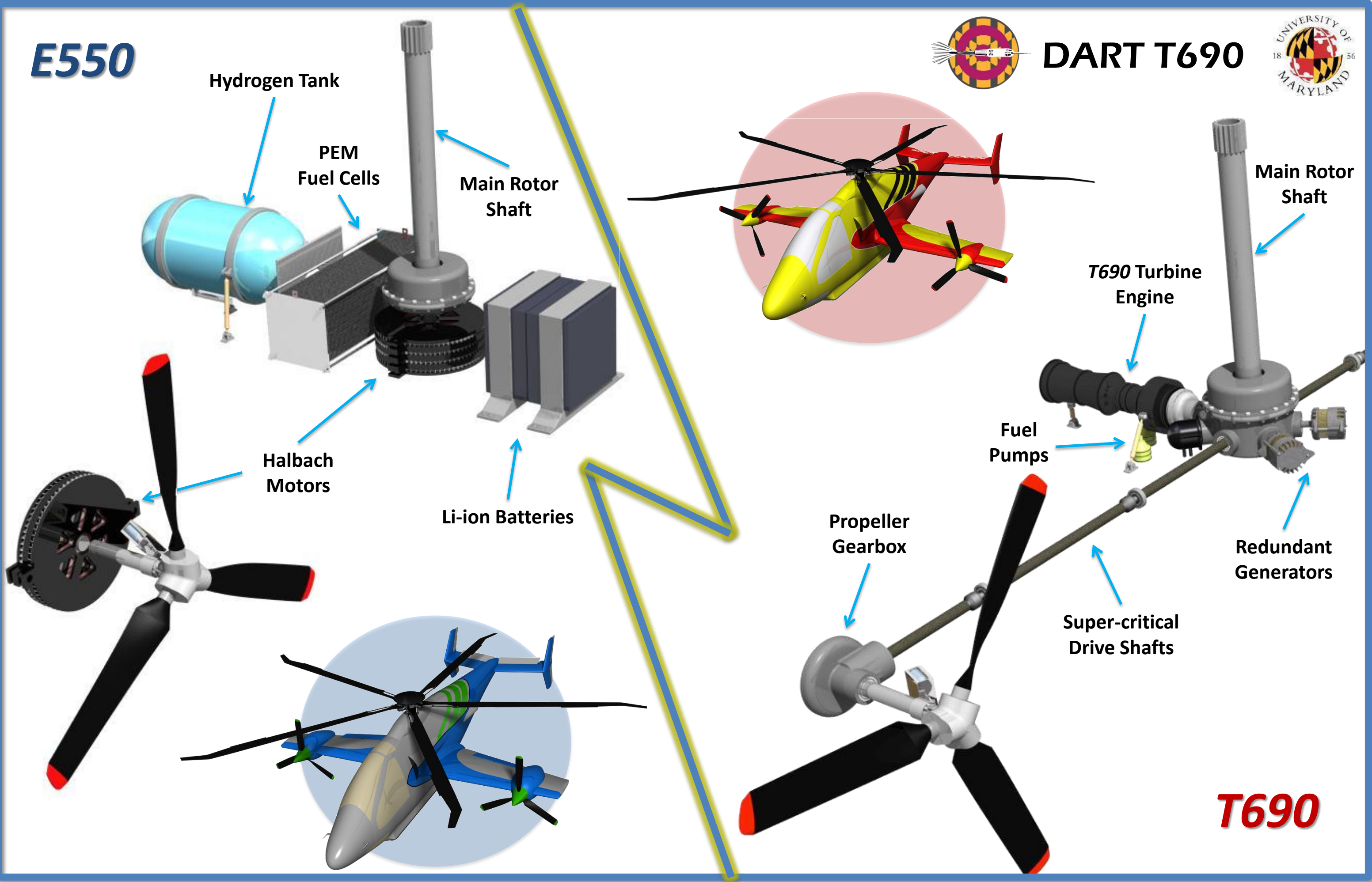
Fuel Pumps

Redundant Generators

Propeller Gearbox

Super-critical Drive Shafts

T690



8.4 Power-By-Wire

Fly-by-wire controls require a more complex actuation system than simple push rods. In aerospace applications, this goal is commonly achieved by the addition of hydraulic actuators. Recently, electro-hydrostatic actuators (EHAs) have been used as the primary control in the F-35 Lightning II to create a power-by-wire control system that does not need a centralized hydraulic system. EHAs are self contained hydraulic pumps and actuators that are powered by electric motors and allow for all-electric power transmission throughout the aircraft [22]. They can come as a single actuator or in the redundant dual actuator configuration; see Fig. 8.14. Dual actuators have a second electrical pump and are used in the propellers and the swashplate controls, which are flight critical controls. Single actuators are used for the ailerons, elevators, and rudders, which are secondary flight controls. Power is supplied to this system through the triple redundant power supply.

8.4.1 Transmission for the *Dart E550*

One significant advantage of an electrical power system is that the motors are compact and can be placed at or near the locations where power is required. For that reason the *Dart E550* option trades a significant part of the transmission weight for battery and fuel cell weight. The optimum rpm of the Halbach array motors is close to the nominal propeller speed of 3,200 rpm. However, the power density is reduced significantly at lower rotational speeds. The same final planetary stage and rotor mast with a smaller gearbox and oil cooling system is used for the main rotor drive in this configuration. The common gearbox allows for uniform attachment to the transmission deck. Notice that because the drive system is all electric in the *Dart E550*, the generator components are not needed.

9 Airframe Design

The turbine powered *Dart T690* and electric-powered *Dart E550* share a common airframe, a semi-monocoque design composed of an aluminum frame with a load bearing composite skin. A cut away of the *Dart T690* is shown in Fig. 9.1. The only differences between the fuselages of the two aircraft are where the powerplants are mounted and the nacelles in the wing. The fuel cells and hydrogen tank of the *Dart E550* are attached to the transmission deck at different points than the turboshaft used on the *Dart T690*. All other attachment points are identical, including the main rotor transmission. By designing a single airframe for both aircraft variants, the development, manufacturing time and costs can be reduced.

As a racing aircraft required to carry no payload, the largest interior component of the vehicle is actually the pilot. The fuselage, therefore, must be sized around the cockpit, while maintaining appropriate positioning for the main rotor, propellers, and empennage. The cockpit of the *Dart* is designed to fit a pilot up to 6 ft 3 in. tall. With a width of 33 inches, it provides more room than racing airplane cockpits. The fuselage of the *Dart* measures 3 ft across at its widest point to allow adequate space for the landing gear mechanism. The overall height of the fuselage is 4.9 ft, allowing enough vertical space to fit a pilot and allow the crashworthy seat to stroke 12 inches. From the tip of its nose to the tail of the empennage, the *Dart* is 26.5 ft long.

To eliminate the risk of the rotor blades striking the propellers, the wing is positioned low enough on the fuselage to provide the 5 ft diameter propellers with sufficient clearance even when the rotor blades flap down to a maximum angle of 12°. The skid landing gear of the helicopter has a 5 ft track and extends downward 2.1 ft from the lowest point of the fuselage, allowing the propeller blades to clear the ground by 6.5 in if the aircraft had a ground roll angle of 5°. The wide track of the fuselage gives the helicopter a tipover angle of 56°; the pitch over angle of the helicopter on the ground is 32° (see Fig. 9.2(a)).



FIGURE 9.1: Cut away view of the internal components of the *Dart T690*.

The required height of the empennage above the ground is a balance between several requirements. The empennage is positioned high enough to allow a flare angle of 10° on landing without the tail striking the ground. It is also positioned low enough to allow the horizontal stabilizer to remain out of the separated flow wake behind the wing in a deep stall. Finally, the tail boom is low enough to prevent a tail strike when the blades flap down at an angle of 12° , the maximum expected from the stiff rotor. The taper angle of the tail boom on both the top and bottom is shallow (less than 12°) to minimize flow separation, thereby reducing parasitic drag (see Fig. 9.2(b)).

On top of the fuselage is a rotor control fairing, which streamlines the swashplate and a portion of the pitch links to reduce drag. Each side of the fuselage has an air intake for the turboshaft engine or the fuel cell. The exhaust is via an outlet on either side of the fuselage aft of the engine compartment.

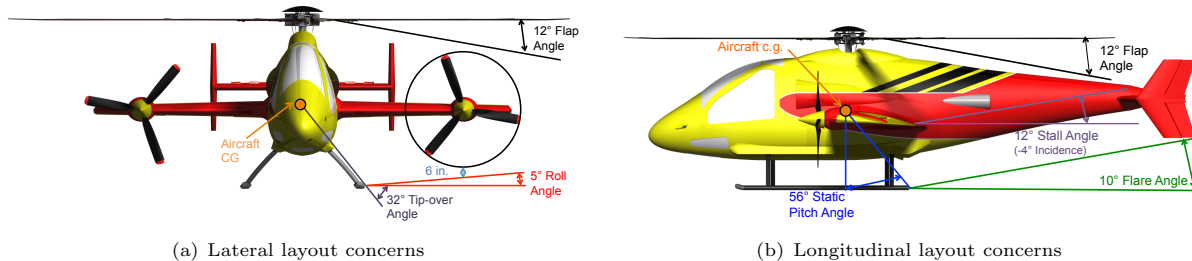


FIGURE 9.2: Layout considerations of rollover, tail strike etc.

9.1 Material Selection for the Airframe

The demanding nature of the pylon racing flight environment means that the airframe of the *Dart* must be capable of withstanding frequent high load factor maneuvers. Using aluminum for the main structural elements gives high reliability and reduces the cost of manufacturing. Composites are advantageous, and are used in the fuselage and wing skin where large continuous panels can contribute to stiffness and crash-worthiness, as well as having low weight.



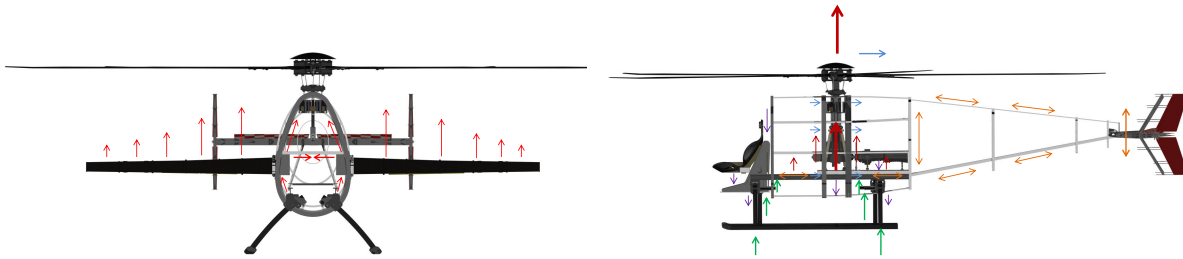


FIGURE 9.3: Load paths viewed from the (a) front and (b) side of the aircraft.

A carbon fiber and Nomex honeycomb composite sandwich skin is used for the fuselage, wing, and tail boom. Carbon fiber composites allow for high stiffness with minimum weight, and utilize a sandwich structure to greatly increase resistance to buckling loads. Composite construction also has the benefit of allowing large structural panels to be manufactured, minimizing the number of fasteners and stringers needed to attach the skin to the primary structure. The use of carbon fiber necessitates that cadmium plated fasteners be used to prevent galvanic corrosion.

The skin panels are constructed using out of autoclave (OOA) pre-pregs. Traditional composite manufacturing techniques require expensive tooling that can survive the high temperature and pressure within an autoclave. The use of OOA manufacturing allows the use of less costly tooling, savings that are especially critical for a limited production aircraft, and enables the construction of larger panels as a single element than would be possible with autoclave size restrictions. Larger panels also increase overall stiffness and reduce the number of fasteners required.

The disadvantage of using OOA technology is the potential for air bubbles in the composite. High pressures within an autoclave force air into solution with resin, eliminating flaws in the final composite. OOA composites require air to be drawn from between the fabric layers by vacuum and, therefore, requires frequent and time consuming debulking cycles, where a vacuum is applied to the part in work without curing. The use of automated fiber placement (AFP) technology can prevent these issues. AFP utilizes pre-pregs that are almost completely impregnated with resin on both sides, and applies them with consistent force, increasing the quality of the composite while obviating the need for debulking cycles. AFP also provides the benefit of automating the manufacturing process, improving quality control of the composites. It also allows the same machinery to be used to make all of the composite components, including the tail and wing surfaces.

The skin over the fuselage and wings consists of layers of $\pm 45^\circ$ and $0/90^\circ$ carbon fiber in a sandwich structure about a Nomex core. The tail boom has a similar structure with additional unidirectional reinforcements running aft along the structure to resist the bending loads experienced during flight maneuvers.

9.2 Primary Load Paths

During the most intense maneuver required, a 5g turn, there is a load factor of 3.5g on the rotor and 1.5g on the wing. The airframe was designed with a safety factor of 1.5, for a proof load factor of 7.5. Most of these loads are transmitted to the remainder of the airframe by the two main bulkheads, one fore and one aft of the transmission. The primary load paths are highlighted in Fig. 9.3. At the top of the fuselage, these bulkheads react the bending loads on the mast as they are passed through the standpipe. The rotor thrust is carried by a thrust bearing from the main gear box carrier through the transmission case and into the standpipe. From the standpipe, the load is transmitted by means of four struts to the longitudinal beams supporting the engine deck. A reinforcing band is fastened around the four strut connection points to react



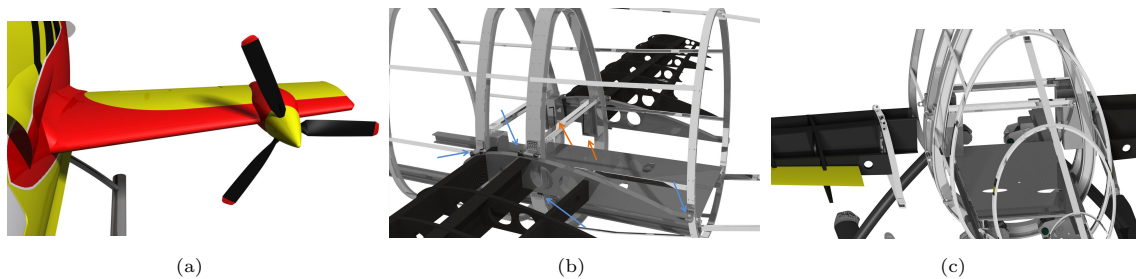


FIGURE 9.4: *Dart T690* wing removal process. (a) Wing in flight condition with the fairing attached. (b) Wing structure with fairing removed, 4 bolts secure each wing. (c) Wing removed from the *Dart T690* for transport.

the bending moments. The longitudinal deck beams for the engine are fastened directly to the main fuselage keel beams, which carry the thrust load to the remainder of the airframe, including the main bulkheads.

9.3 Wing to Fuselage Attachments

The wing loads are transferred directly to the main fuselage bulkheads. Each wing has a solid machined rib at the root, which features four connection points to the fuselage (Fig. 9.4). The two main connection points are located on the top and bottom of the root rib at the main spar, and carry wing bending in compression and torsion, respectively. Another attachment point is provided above the forward spar and takes a portion of the bending load. This forward connection point, as well as a fourth at the trailing edge of the root, transmit wing torsion and chordwise bending loads to the fuselage. Each of these connection points is bolted to a corresponding cleat attached to the bulkheads. To reduce the load carried through the entire bulkhead, reinforcement beams link the left and right halves of the two main bulkheads to save weight. These beams are attached to the bulkheads at the same point as the wing connections above the forward and aft main spars, allowing the loads from the wings to react against each other.

The wings are attached to the fuselage by first slotting the roots of the fore and aft spars into guide blocks that are attached to the fore and aft bulkheads. Once aligned appropriately, the connection points are securely fastened by means of four bolts, which then transmit the wing loads to the fuselage. A removable fairing covers these attachment points.

9.4 Tail Boom Structure

Adequate structure is needed to carry the maneuver loads, as well as to mount the elevator, rudder, and their actuators. Three longerons and a series of bulkheads provide extra strength to the composite skin. Two of the longerons extend aft and up from the keel beams, attaching to each of the tail bulkheads, and, finally being fastened to the spar and root ribs of the horizontal stabilizer. The third longeron is fastened to the top of the last fuselage bulkhead, and runs along the top of the tail boom before meeting with the vertical member that supports the spar of the horizontal stabilizer.





FIGURE 9.5: Landing gear (a) extended and (b) retracted.

9.5 Cockpit Structure

The front section of the *Dart* is cantilevered from the forward cockpit support bulkhead, as well as the keel beams, which extend all the way to support the frame of the pilot's seat. The pilot seat is contoured to provide optimal support during intense maneuvers, with a focus on preventing slipping during high lateral g maneuvers. Two doors are provided: a main door on the left-hand side of the pilot and an emergency exit to the right. The doors hinge forward and up to allow a large exit area for the pilot. The nose cone of the aircraft houses the backup batteries, as well as flight computers and sensors. The cockpit is also designed to provide maximum pilot visibility and easily meets MIL-STD-850B.

9.6 Landing Gear

As shown in Fig. 9.5, the *Dart* utilizes a novel, retractable skid landing gear system. The design of these skids is based on a Eurocopter patent for skids with fixed crosstubes that slide into the fuselage [23]. On each side of the vehicle, the skid is attached to two struts. These struts follow a curved path up and into the fuselage, where they are each cantilevered on two rollers. Rollers, which are allowed to pivot to follow the path of the landing gear strut, are fastened to a mount that is directly bolted to the keel beams to carry the loads to the remainder of the aircraft. Each landing gear strut is machined with a series of teeth along its length, and an electric motor inside the fuselage creates a rack and pinion mechanism to retract the gear. The motor is also attached to a torsional spring, which the motor must wind to retract the skids. This spring provides a fail-safe mechanism; if the motor fails, the spring will drive the gear to the down position. To ensure against accidental sliding of the skids into their retracted position on landing, a locking pin is used, which passes through the strut of the skid and acts in double shear with the landing gear mounting block. The pin is operated by a spring-loaded solenoid. The spring maintains pressure on the pin, causing the device to lock whenever the skid is in its fully deployed position. The gear can only be retracted by triggering the solenoid, which pulls the pin out and allows the retraction motor to be activated. Once the gear has begun to retract, the current to the solenoid is cut, allowing the spring to apply pressure to the pin, which has a low friction PTFE tip to allow it to slide along the strut without gouging.

9.7 Transportability

Although it is capable of being ferried over a distance of 250 nautical miles with a full auxiliary fuel tank, an easy ground transportation capability is a key feature of the aircraft. The helicopter is designed to be transported in a single standard, 28 ft trailer. The wings are removable and can be stowed along the walls



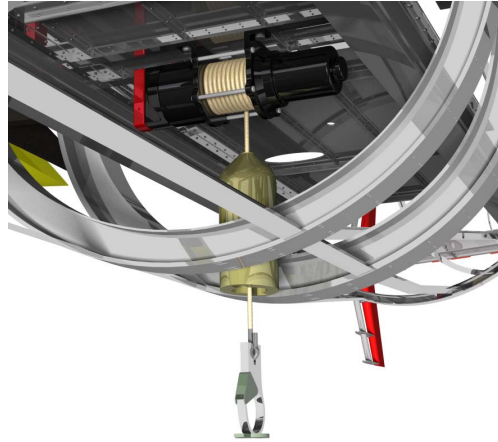


FIGURE 9.6: Slung load support consisting of an electric winch, a hook, and a housing with ensures the hook properly retracts into the fuselage.

of the trailer. The propeller shafts are designed to be removed at their connection to the main gear box. The main rotor blades can be easily unbolted from the rotor and, at only 19 lb each, can be stowed in the trailer along with the propeller blades. With the wings, propellers, and rotor blades removed, the widest point of the aircraft is its tail, which has been sized to fit within the doors of a standard 8.5 ft trailer. With the landing gear extended and ground handling wheels attached, the overall height of the *Dart* is under 8.5 feet, leaving half a foot of clearance to the ceiling of the trailer.

9.8 Slung Load Capability

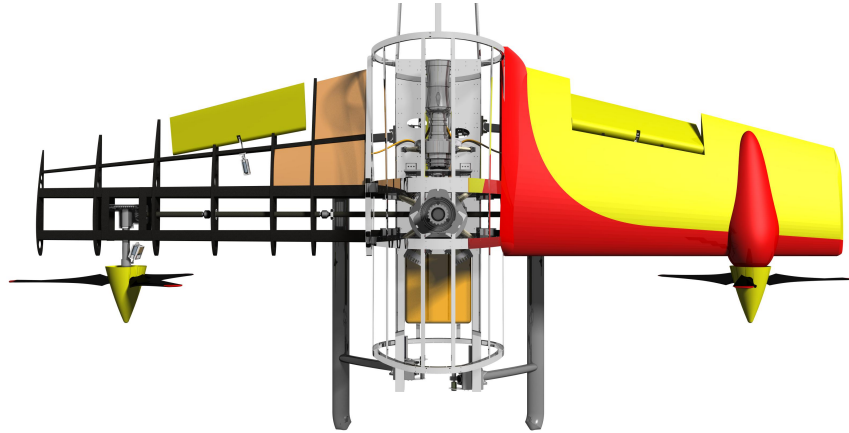
As required for the defined RFP race, the *Dart* is equipped with a hook and a winching mechanism for carrying a slung load. The commercially available winch is electrically operated and runs off of the same 24 VDC power as all of the other helicopter systems. The winch is positioned in the lower fuselage, directly below the rotor mast near the center of gravity of the aircraft, and is bolted to the engine deck right where the transmission is attached (see Fig. 9.6). The winch reels in a Kevlar rope, which is attached to a hook provided by the race organizers, for picking up a slung load. The aircraft is equipped with a customizable retraction pock so that, when retracted by the winch, the hook will retract within the lower fuselage. A circular fixture designed to mate with the cavity opening and provide a seamless external surface to reduce aerodynamic drag can be attached to the bottom of the hook.

9.9 Wing Design

9.9.1 Wing Geometry

The wing of the *Dart* has a 17.9 ft span and an aspect ratio of 5, which are values set by the sizing; it has an unswept leading edge and a 2:1 taper ratio (see Fig. 9.7). No sweep was used because of the low free-stream Mach numbers that are encountered. The relatively high taper ratio means that the wing could be more prone to tip stall, so a small amount of washout was added to the wing. The selected taper ratio and washout also help to reduce the structural weight by decreasing the root bending moment. No dihedral was used because of concerns about ground-to-propeller and propeller-to-rotor clearances. Finally, the wing incidence was fixed to 4° relative to the waterline of the fuselage; this angle was chosen to generate enough



FIGURE 9.7: Wing of the *Dart*.

lift across the range of operating airspeeds based on the optimum lift sharing between the rotor and the wing (see Section 13.4).

9.9.2 Airfoil Selection

To perform high load factor maneuvers, it was necessary to use an airfoil with a high maximum lift coefficient. It was also important that the chosen airfoil have a wide drag bucket with a low drag coefficient and gradual stall characteristics. Furthermore, a forgiving airfoil that is insensitive to manufacturing inaccuracies and profile distortions under maneuver loads is ideal for an aircraft such as the *Dart*. Some high performance airfoils with high maximum lift coefficients were immediately discarded because their drag characteristics were unsuitable. The NACA4415 airfoil profile was chosen for its good maximum lift coefficient ($C_{l_{max}} = 1.5$), high maximum lift-to-drag ratio ($C_l/C_d = 51$), and larger drag bucket ($C_{d_0} = 0.0075$) in the required range of Reynolds number (around 4×10^6). Its relatively large thickness-to-chord ratio (0.15) also provides higher bending and torsional stiffness. In addition, the camber-induced nose-down pitching moment helps to counter the nose-up pitching moment created by the thrust of the propellers.

9.9.3 Wing Structural Design

The wing box is made of two C-channel spars located at 15% and 35%, respectively, of the mean aerodynamic chord. The skin completes the torque box providing necessary torsional stiffness. A false spar is used to support the ailerons and the actuation mechanisms. Five ribs are positioned along the wing span. The propeller and its gear box are supported by the two end ribs. The transmission shaft runs through the main wing box.

9.9.4 Wing Finite Element Analysis

A finite element analysis was performed to determine the optimum dimensions and material for the wing box (Fig. 9.8(a)). The root of both spars was clamped and distributed forces and moments were used on the surface of the wing box to represent the wing lift and pitching moment, the propeller thrust, the weights of the wing, the propeller, propeller gear box, and the fuel tank. This calculation was carried out for an airspeed of 220 kts and under a 1.5g load factor, and with a 0.5g forward acceleration. A safety margin of 1.5 was applied. The sizing metrics were the maximum tip deflection, which is determined by the rotor/propeller



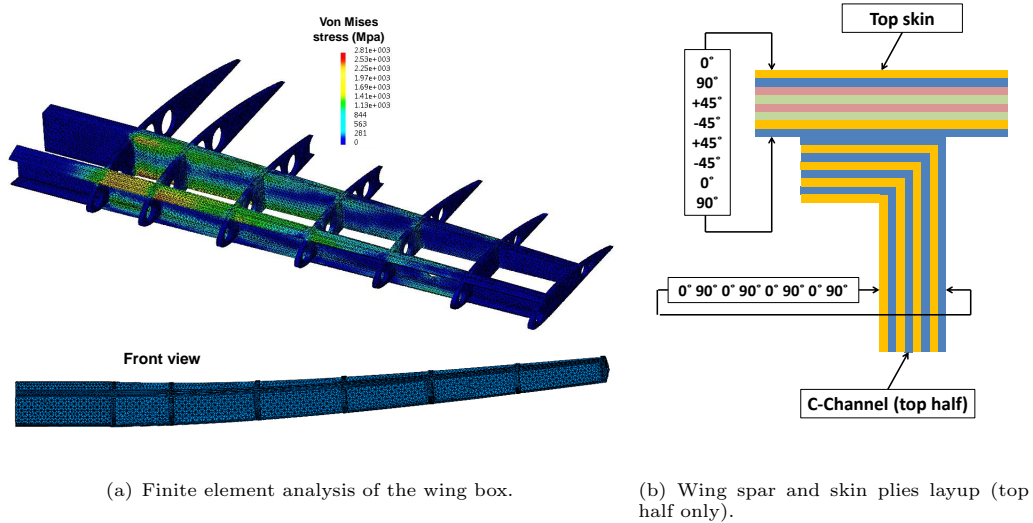


FIGURE 9.8: Finite element analysis of the wing box and plies layup.

and propeller/ground clearances, the minimum beam bending stiffness and torsional stiffness, which were all determined from a whirl flutter analysis.

A carbon/epoxy composite structure was chosen for the wing box because of the high rupture resistance and good fatigue strength, combined with the 35% lower weight compared to its metal equivalent. Each spar cap is constructed using 4 layers of carbon fiber with plies oriented at $0^\circ/90^\circ$. The shear web also has 4 layers at $0^\circ/90^\circ$. This arrangement helps keep manufacturing relatively simple, while providing the adequate bending stiffness. The skin was designed to give enough torsional stiffness to the wing; it is made of 4 layers of $\pm 45^\circ$ fabric with two layers at $0^\circ/90^\circ$ on each side. Figure 9.8(b) shows the top of the structure where the ply layup can be seen. The front and rear spar caps provide 22% and 27% of the bending stiffness respectively, while the skin provides 51%.

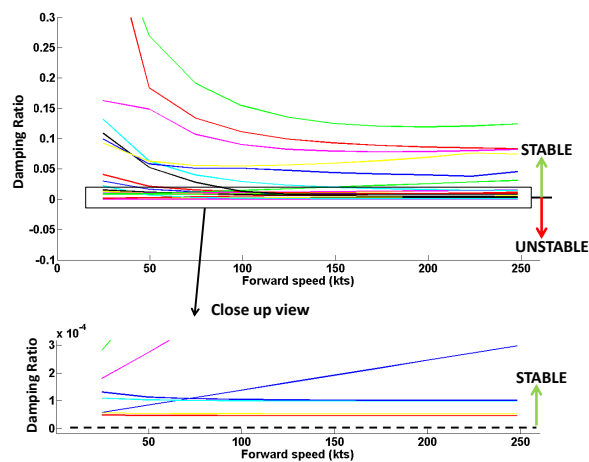


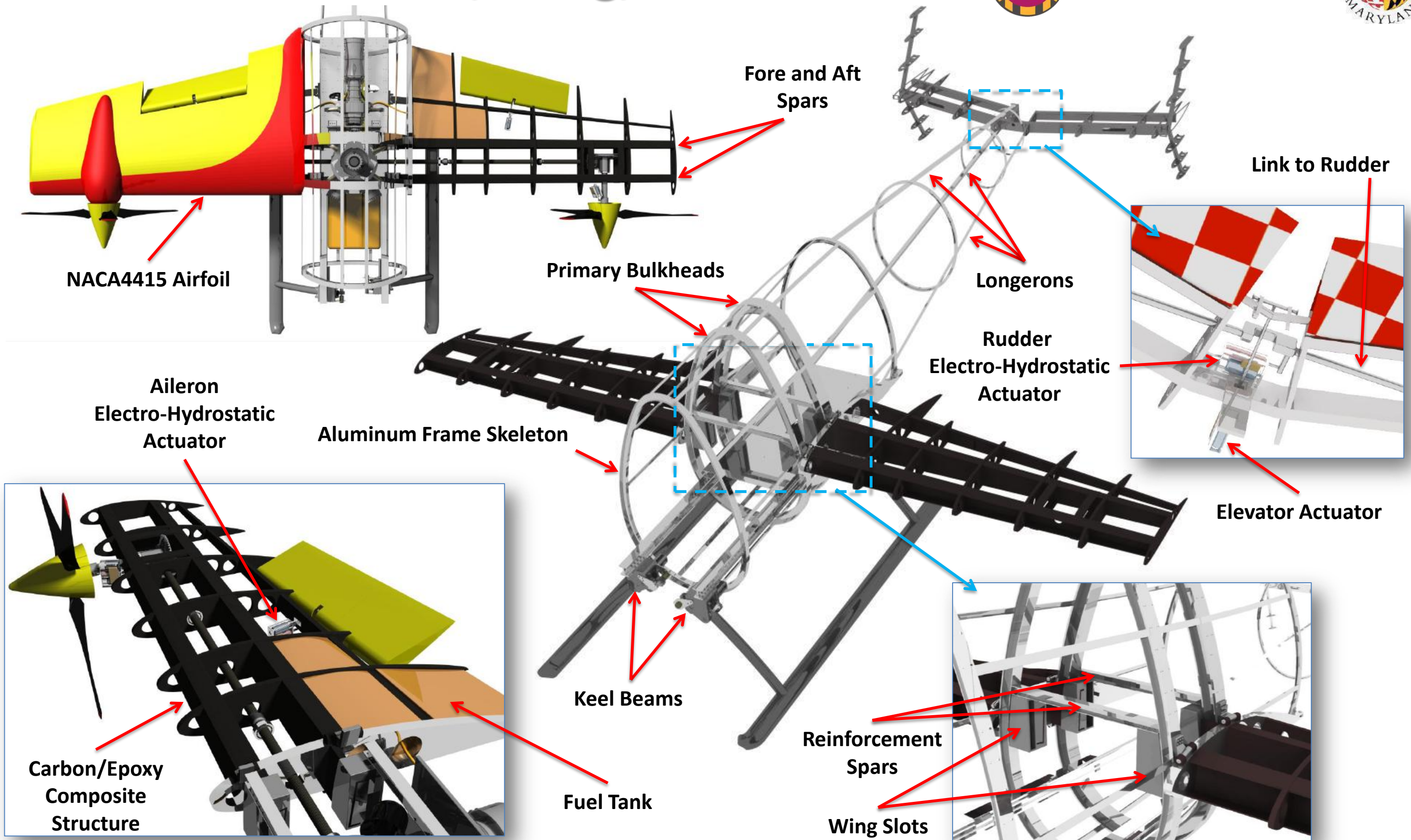
FIGURE 9.9: Damping of the different modes as a function of airspeed.



Structures: Airframe, Wing, and Tail



DART T690



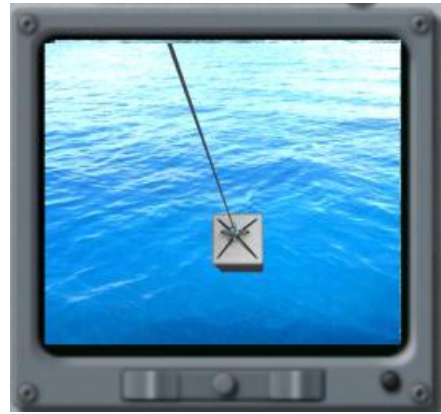
Undercarriage



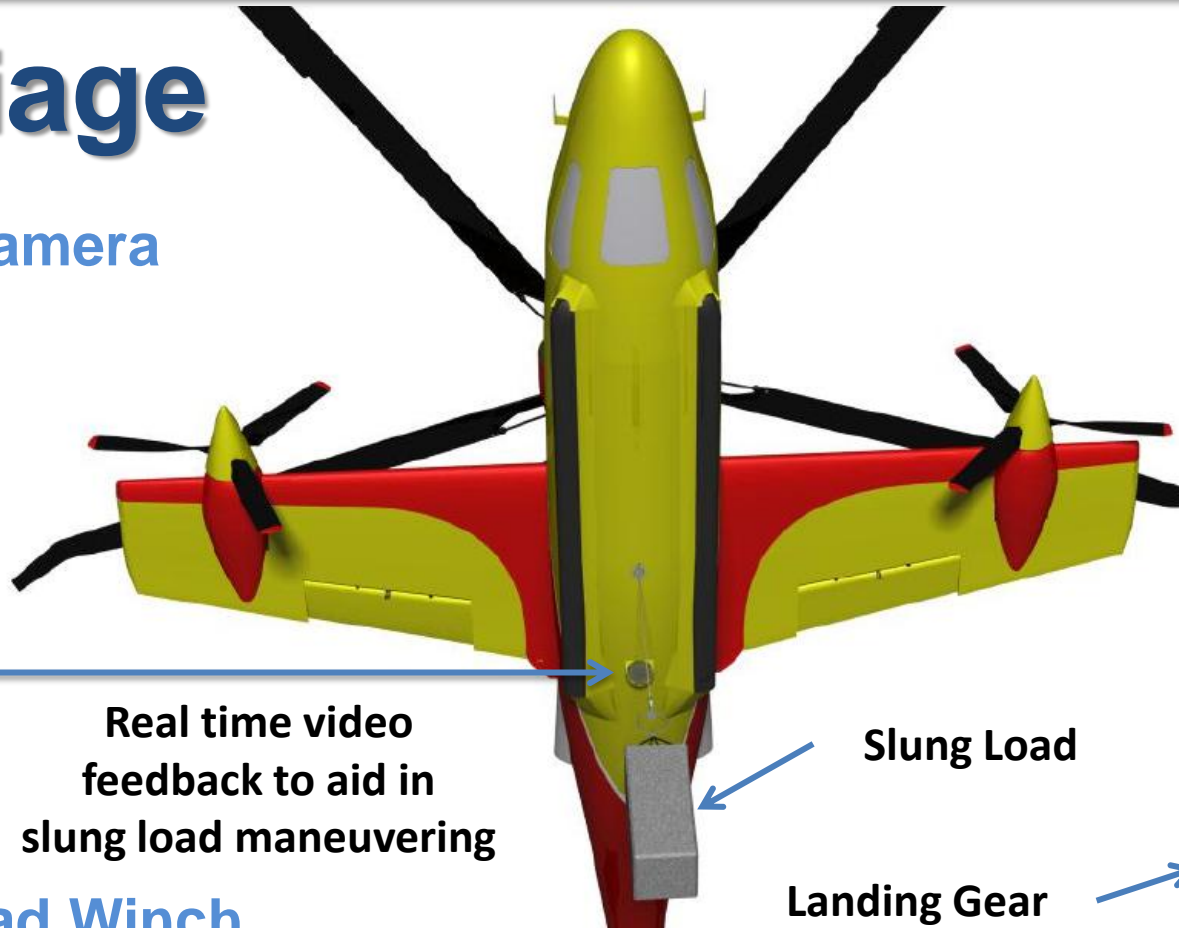
DART T690



Slung Load Safety Camera

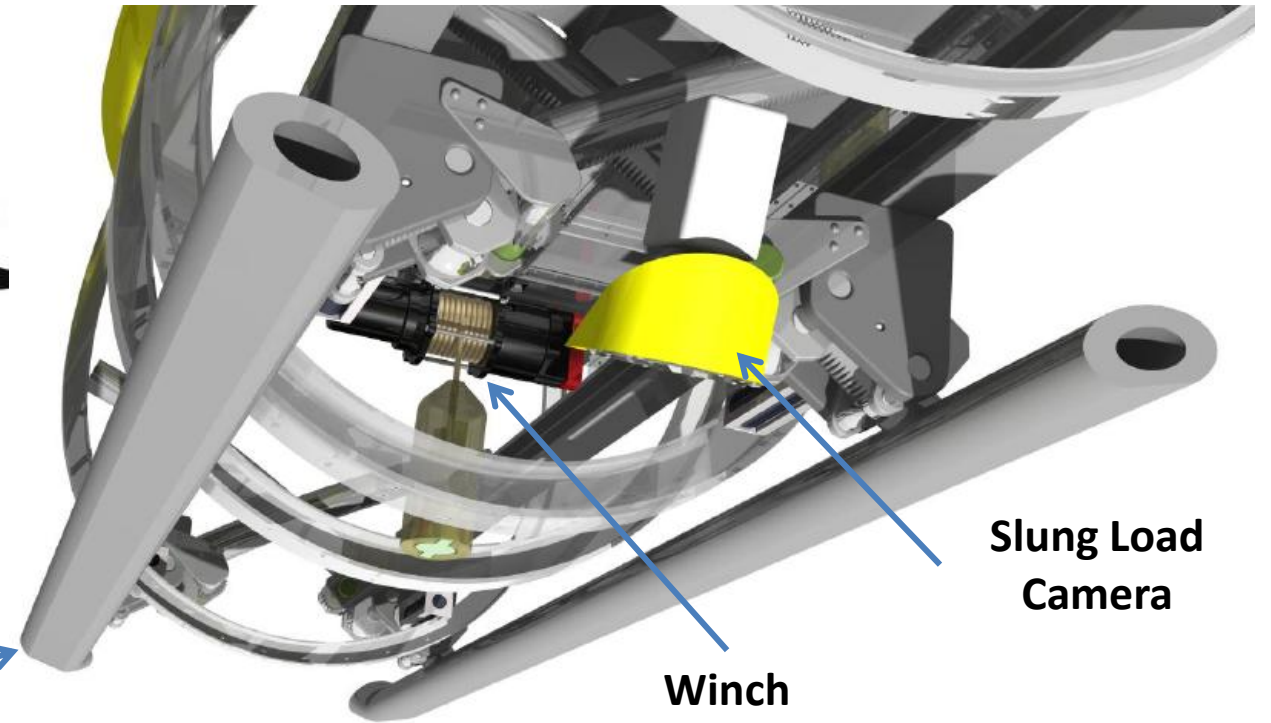


Real time video feedback to aid in slung load maneuvering



Slung Load

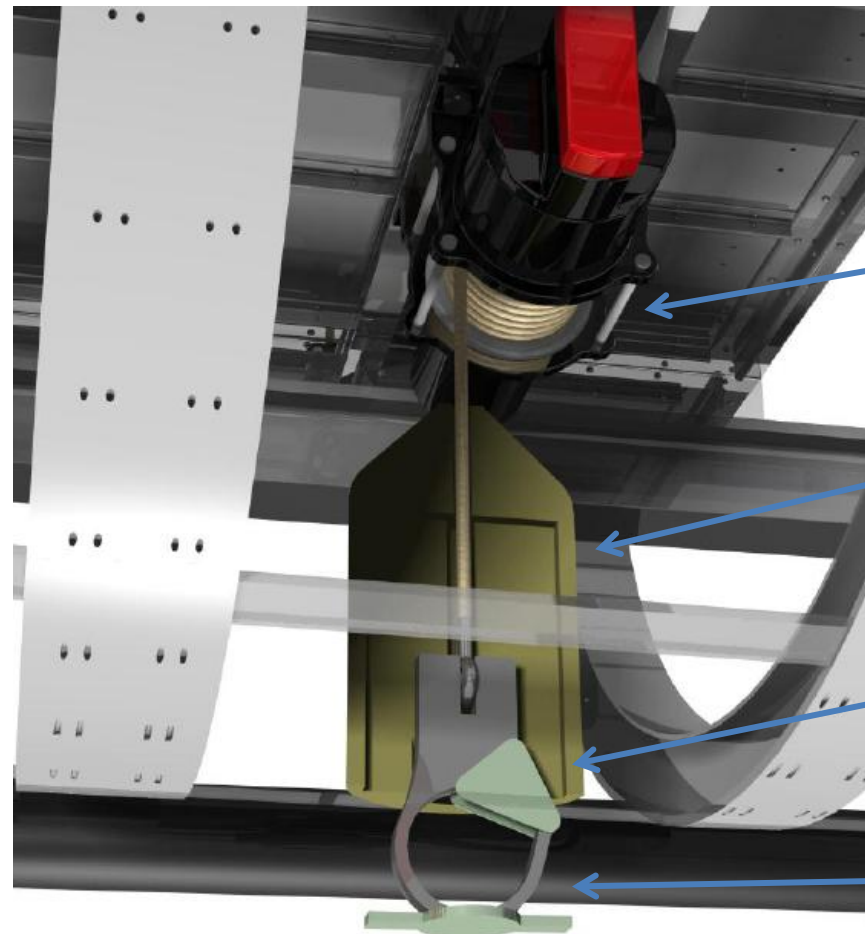
Landing Gear



Winch

Slung Load Camera

Electric Slung Load Winch



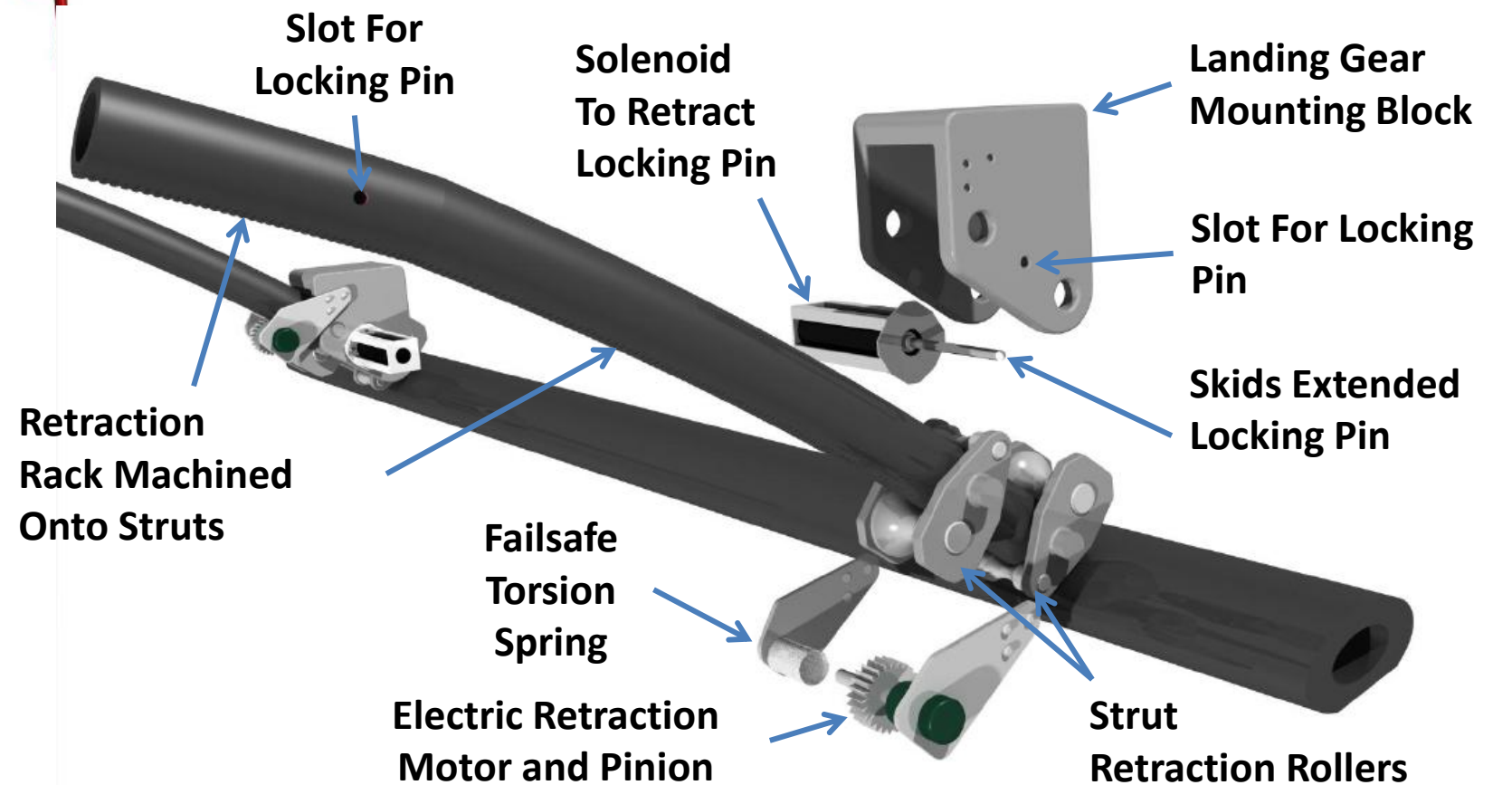
Electric Winch

Recessed Housing For Hook

Partially Retracted Hook

Smooth Cavity Fairing Feature

Retractable Skid Landing Gear



Slot For Locking Pin

Solenoid To Retract Locking Pin

Landing Gear Mounting Block

Slot For Locking Pin

Skids Extended Locking Pin

Retraction Rack Machined Onto Struts

Failsafe Torsion Spring

Electric Retraction Motor and Pinion

Strut Retraction Rollers

9.9.5 Whirl Flutter Analysis

A numerical analysis was performed to determine the *Dart*'s sensitivity to whirl flutter. Figure 9.9 shows the damping of the different modes as a function of airspeeds. All modes are stable for the entire range of airspeeds, and their frequencies are well separated. It should be noted that although some modes have a damping ratio below 2%, low values of structural damping were used in this analysis and the actual damping ratio of these modes is expected to be above 3%. In addition, these modes have a high frequency, which also explains the low damping ratios. Therefore, the *Dart* will not experience whirl flutter.

10 Weight Analysis

The weight estimates given in Table 10.1 are based on the preliminary sizing described in Chapter 4 and presented as in MIL-STD-1374A[24]. The positions of the individual components and systems within the aircraft are based on the analysis described in their respective chapters. The longitudinal center of gravity (x_{cg}) is referenced from the nose of the aircraft, and the vertical center of gravity (z_{cg}) is referenced from the ground plane. This breakdown is for the *Dart T690* engine option and is shown graphically in Fig. 10.1. The center of gravity (c.g.) location of each of the systems is shown by means of the blue circles, the area of each circle representing the relative weight of each system. The c.g. of the entire aircraft is shown by the smaller red circle. The *Dart E530* option, as described in Section 8.2, is designed to maintain the same c.g. location.

TABLE 10.1: *Dart T690* component weight estimates.

	Component Description	Weight (lbs)	% Empty Weight	x_{cg} (ft)	z_{cg} (ft)
1	Rotor Group	152.6	9.0	9.63	7.35
2	Propeller Group (No. 2)	95.7	5.6	8.08	3.44
3	Wing Group	125.0	7.4	9.63	3.44
4	Tail Group	36.0	2.1	23.85	4.44
5	Fuselage Group	289.2	17.0	12.08	3.88
6	Alighting gear group	85.6	5.0	9.88	2.03
	Structural Weight	784.1	46.1	11.02	4.26
7	Propulsion Group	160.5	9.4	11.96	3.44
8	Drive System Group	362.2	21.3	9.70	3.94
9	Oil and Cooling Group	128.3	7.5	9.63	2.94
10	Fuel System	10.6	0.6	11.29	2.94
11	Electrical Group	50.0	2.9	3.98	3.34
12	Flight Controls Group	84.5	5.0	8.34	5.43
13	Avionics Group	36.0	2.1	2.75	3.84
14	Furnishing and equipment group	83.4	5.0	8.02	2.68
	Empty Weight	1,699.6	100.0	10.06	3.95
15	Oil	69.0			
16	Fuel (Maximum Capacity)	221.2			
17	Pilot	225.0			
18	Slung Load	300.0			
	Payload + Fuel	815.2			
	Gross Weight	2,514.8			



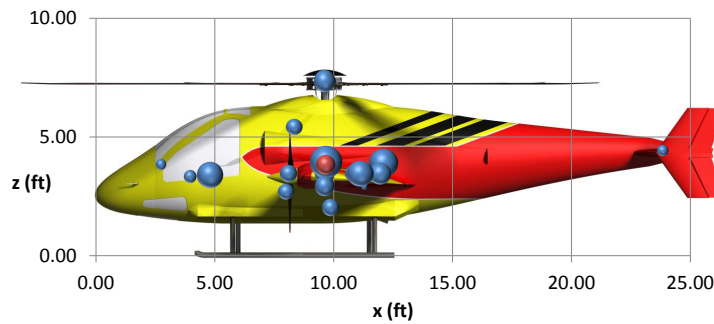


FIGURE 10.1: Distribution of the weight of primary systems throughout the helicopter, the c.g. is identified in red.

TABLE 10.2: Mass properties of the helicopter at various points in the course.

	Maximum Fuel Load	Racing Fuel Load	Landing Gear Retracted	Start of Course	End of Course	No Fuel
Weight (lb)	2,215	2,064	2,064	2,033	2,014	1,994
x_{cg} (ft)	9.6	9.7	9.7	9.7	9.7	9.8
z_{cg} (ft)	3.8	3.8	3.9	3.9	3.9	3.9
I_{XX} Roll (slug-ft ²)	663	550	537	512	495	478
I_{YY} Pitch (slug-ft ²)	878	880	867	864	863	861
I_{ZZ} Yaw (slug-ft ²)	1,306	1,169	1,169	1,142	1,124	1,106

10.1 Center of Gravity Location

The longitudinal position of the c.g. is nominally directly under the rotor. An iterative process was used to set the forward position of the pilot and cockpit systems so that they balance the weight of the empennage and tail structure. Vertically, the c.g. is located between the most massive components of the aircraft: the powertrain and the rotor. The vertical offset between the c.g. and the propellers results in a significant pitching moment proportional to propeller thrust. Therefore, the c.g. is positioned only 4 in. above the line of action of the propellers.

10.2 Center of Gravity Excursions During Flight

Table 10.2 shows how the mass, c.g., and inertia of the *Dart T690* change as it flies the course. The configurations presented do not include the slung load. The moments of inertia of the aircraft were calculated by combining the component offsets from the global c.g. and the component inertia about their own centers of mass. The maximum fuel fraction is 0.1, and the fuel fraction consumed during the course is only 0.01. The largest changes are in the roll and yaw inertia because of the location of the fuel storage in the wings; these changes do not substantially change the dynamics of the aircraft.



11 Avionics

The avionics and control system are the main interface between the crew and the aircraft. The goal of this system is to provide the pilot with all of the information necessary to fly the aircraft while reducing workload and improving overall efficiency. The *Dart T690/E550* achieves this goal using digital flight controls, modern sensors, and a minimalist approach to cockpit design. This architecture also provides the pilot with the largest possible view out of the cockpit, while providing all necessary aircraft information on the instrument panel. These systems are incorporated into the aircraft in a way that minimizes weight, costs, and maintenance.

11.1 Instrument Panel Layout

The *Dart* is designed for single pilot operation. The control panel is organized in a consistent manner with critical gauges placed in the pilot's peripheral vision when he/she is looking out of the cockpit. As shown in Fig. 11.1, the *Dart* is separated into three instrument groupings. The instrument grouping to the far left includes the engine status gauges, the middle grouping is the payload camera and artificial horizon, and the grouping to the far right is a modified version of the "standard six pack" of aircraft flight gauges. This layout minimizes the distance a pilot must move to quickly scan the instrument panel for critical aircraft information.

11.1.1 Glass versus Dial Cockpit Displays

Cockpit layouts for both Formula-1 cars and Red Bull[®] racing aircraft were studied. A picture of a Formula-1 car cockpit and the cockpit of the Zivko Edge 540 (the most common aircraft used in Red Bull[®] racing) are shown in Fig. 11.2. It is clear in both vehicles that the gauges and instruments were kept to a minimum. In a race, the pilot's focus is on the course and there is little time to look down at the instruments. Therefore, it is important to minimize cockpit clutter so that the pilot can focus on flying the aircraft.

Models of the *Dart T690* were flown in X-Plane[®] with both glass and dial cockpits. A number of pilots who flew the model found that dial gauges were much easier to read when flying the course. Based upon this information, a dial-based cockpit was used with one digital flight display that incorporates a slung load camera and a "Caution-and-Advisory" display. An image of the *Dart* cockpit as designed is shown in Fig. 11.1.

11.1.2 Baseline Equipment

The *Dart's* baseline avionics suite meets all FAA VFR flight requirements [25]. The cockpit panel displays and associated sensors provide airspeed, altitude, heading, engine rpm, internal engine temperature, oil temperature and pressure, and landing gear position. The aircraft is also equipped with the appropriate transponders and radios.

Through repeated test flights in the X-Plane simulator, additional instrumentation was included when it became apparent that the pilot required more information such as slip-rate, climb rate, and load factor to maximize performance.



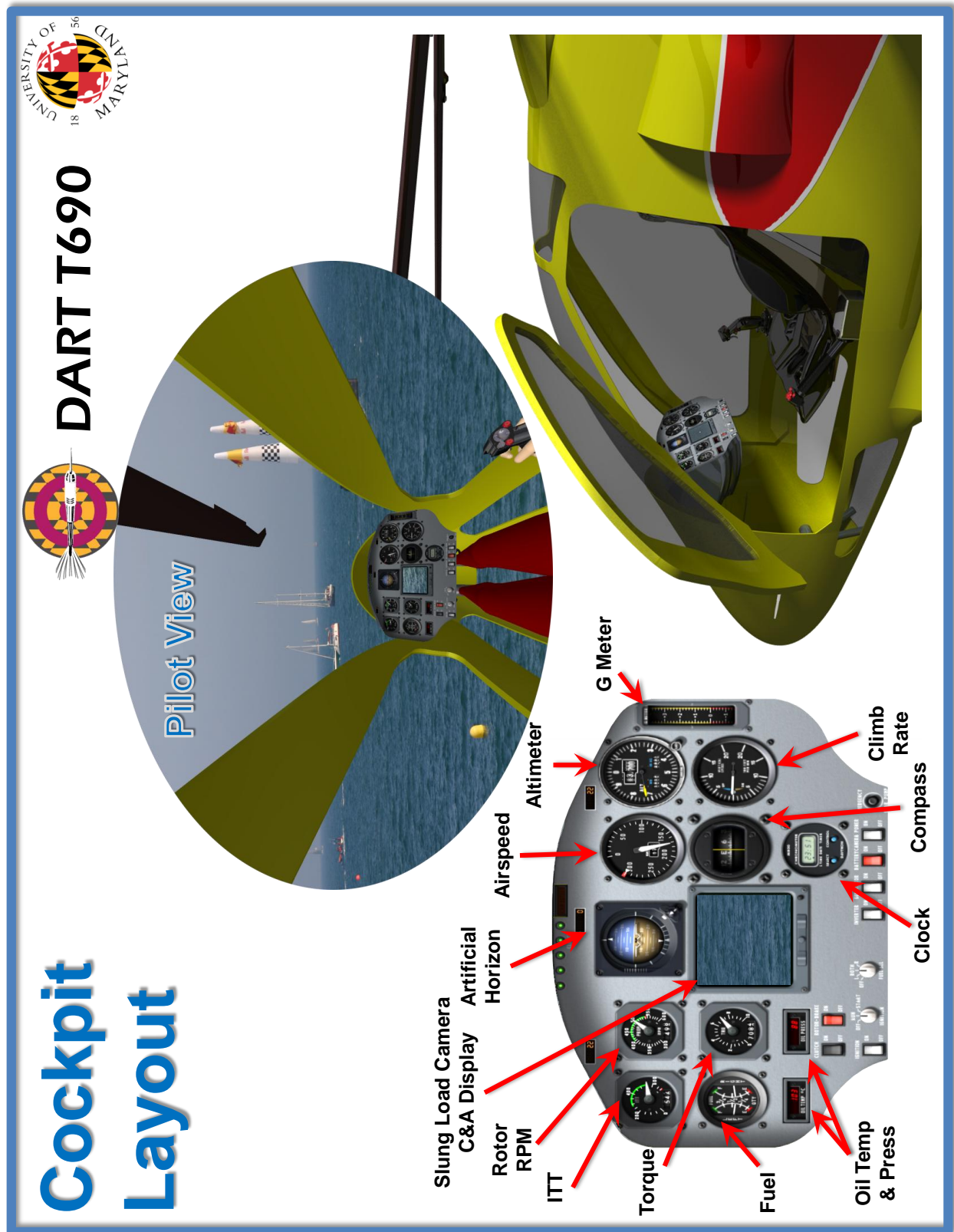


FIGURE 11.1: Dart T690 cockpit.





FIGURE 11.2: (a) Mercedes-Benz Formula 1 front panel (b) Zivko Edge cockpit.

11.1.3 Payload Camera and Caution-and-Advisory Display

Outward visibility for the pilot was given a high priority when the cockpit was designed. The large windows in the cockpit provide excellent forward and side viewing angles. However, it is difficult for the pilot to look down because of the restraint system to monitor the slung load. Therefore, a camera was installed in the aft of the aircraft so that the pilot could continue looking forward out of the cockpit while also watching the slung load behavior from a viewing screen in the cockpit.

While the camera is not being used, the electronic display can be switched to a Caution-and-Advisory Display. This display is a master caution board that will automatically display any aircraft warnings, faults, or other notifications to the pilot during flight. This dual-use display method reduces cockpit clutter while providing the pilot with the ability to monitor slung load behavior and centralize all aircraft warning systems.

11.1.4 Communications

Although the aircraft meets FAR 27 noise requirements, the pilot may still experience noise levels that may be uncomfortable or harmful after long periods (see Chapter 14). To mitigate noise, the pilot will wear a noise reduction *BOSE A20* aviation headset [26]. The headset will all but eliminate aircraft noise, and also allow the pilot to have easy communication with air traffic control and the ground crew. The headset is connected to the aircraft's radio system via a jack located behind the pilot's head.

11.1.5 Force Feel Stick Feedback System

The fly-by-wire architecture of the *Dart* eliminates the tactile feedback that a pilot receives through the control stick that is present in a mechanically linked system. It has been shown that tactile feedback to the pilot reduces overall pilot workload and increases pilot efficiency [27]. It was considered a necessity to reintroduce a tactile feedback system for the pilot.

A force-feel system was implemented on the aircraft by using a feedback loop built around a servo-actuator and the cockpit flight controller. The feedback loop performs the function of a feel spring and trim motor that is used in conventional feedback systems. The neutral flight controller position is determined by a trim switch. When the flight controller is deflected away from the neutral position, an error is produced. This error is processed through a shaping function to correlate the error with a corresponding displacement of the servo-actuator. The servo-actuator, which is comprised of an electric motor, a gearing device, and a clutch, generates a restoring force. The restoring force attempts to center the flight controller and provides the



pilot with tactile feedback. By manipulating the shaping function, the feedback and corresponding tactile feedback can be adjusted to reflect pilot preference [28].

11.2 Health and Usage Monitoring (HUMS)

The demanding flight environment to which the *Dart T690* is designed makes it imperative to diagnose problems before they cause failures in flight. Health and Usage Monitoring Systems (HUMS) continuously determine the status of flight critical systems that analyze the information to determine the system's overall health. Life-limited parts are automatically tracked by cycles or hours of operation. When a part approaches its life limit, the HUMS system can automatically notify the ground crew that the part is approaching its life expectancy. In addition to tracking the life of a part, the HUMS system can predict part failure by analyzing accelerometers, temperature sensors and strain gauges that are placed at key points along the aircraft and in critical systems. The HUMS monitors the sensor data and compares the outputs to a database of potential risks and failure modes that is compiled during the flight testing and certification portion of aircraft development. If the observed data matches the recorded failure mode behavior, the system can alert the flight crew and give the pilot early warning before the actual failure occurs. This life-cycle analysis occurs in real-time and improves aircraft safety dramatically. The cost increase associated with using a HUMS system was considered worthwhile because of the dramatic increase in aircraft safety and reliability [29-31].

11.2.1 Health Monitoring

The health monitoring systems ensures that all systems are operating at nominal performance levels. The system is comprised of six main tasks. These tasks include rotor track and balance, propeller track and balance, engine performance assessment, mechanical diagnostics, and recording of flight data to the flight data recorder. The rotor and propeller track and balance employs a variety of accelerometers and strain gauges to ensure that the rotor and propeller are constantly balanced and tracking correctly. The engine performance assessment function monitors the engine temperatures at the inlet, compressor, combustor, turbine, and exhaust. The system also records the engine torque and monitors the health of the Full Authority Digital Engine Control (FADEC) system that governs engine power. Dual FADEC's are used in the aircraft, and the HUMS system can automatically disable a faulty FADEC, if needed. The mechanical diagnostic system monitors all other mechanical systems on the vehicle, such as the main gearbox, propeller gear boxes, rotor and propeller shafts, control surface health, and the landing gear mechanism.

The final system is the flight data recorder. The recorder tracks all pilot inputs, control outputs, pilot radio communications, and aircraft sensor information, i.e, airspeed, time, altitude fuel, etc. These data are then stored and used for post-flight analysis. The entire health monitoring system also incorporates a failure modes library that is compared to aircraft sensor data so that failures can be predicted.

11.2.2 Usage Monitoring

The Usage Monitoring system acts as a recorder for the rest of the HUMS system. This system keeps a record of cycle counts for each life-limited part. Included in the Usage Monitoring system is an exceedance monitoring sub-routine that records any anomalous events, such as any in-flight warnings, and the total time spent above critical engine thresholds, such as power, temperature, and torque. The exceedance monitoring system also notifies the pilot and ground crew when the aircraft systems are approaching their operational limits or have exceeded them.



11.2.3 Maintenance Interface

The largest benefit of the HUMS system is the large amount of data that it provides operators and ground crew through the maintenance interface. This system allows the maintenance crew to analyze aircraft states in real time via a data-link that connects the HUMS system and flight management computer to a ground station. Crews can analyze trending data in conjunction with flight data to diagnose any abnormal behavior in flight. The interface system also provides a convenient graphical user interface that allows personnel to change aircraft configuration settings before, during, and post flight. All data from the HUMS and aircraft is sent to a ground station that archives a complete record of the aircraft performance. This system acts as ground-based flight analysis tool.

12 Stability and Control

12.1 Flight Control System

The *Dart T690/E550* is a unique rotorcraft and so the Flight Control System (FCS) must be carefully designed for the environment being flown by the aircraft. The control system must operate as a standard helicopter system using main rotor collective, cyclic, and anti-torque during hover and low-speed flight, and also utilizes conventional aircraft control surfaces such as ailerons, elevators, and rudders in forward flight. To optimize the in flight performance of the aircraft, a unique fly-by-wire flight control system was developed. This flight control system is a natural evolution of the current fly-by-wire systems utilized in advanced helicopters such as the Sikorsky X-2, the Bell 525 and the Sikorsky S-97. This type of digital control system provides a number of distinct advantages over a mechanical system:

- Complex control laws can be incorporated into the aircraft.
- Reduced weight – all signals are digital.
- Greater control accuracy – no mechanical control linkages that can wear and correspondingly reduce the accuracy and responsiveness of the system.
- Triple redundancy – wires that carry control signals are routed along multiple paths throughout the fuselage for increased safety.
- Improved ability to detect and correct system failures.

12.1.1 Cockpit Flight Controls

The advanced flight control architecture of the *Dart* allows for an innovative flight control arrangement. Using the traditional cyclic/collective/pedal configuration, it is possible to control the complete set of aircraft controls. A side-mounted control stick is incorporated for two-axis control. Pitch and roll control is obtained by using longitudinal and lateral displacements of the stick. Small displacement side-sticks have been shown to give Level-1 Cooper-Harper handling qualities ratings, and have been utilized in other aircraft designed for high maneuverability [32, 33]. Given the higher risk environment of racing, pilot safety is critical. The side-mounted control stick significantly improves the ease of ingress and egress out of the main door. In addition, the side-mounted joystick improves operator comfort, further increasing pilot safety and performance.

Conventional foot pedals are used to modulate the anti-torque thrust from the propellers. Located to the left of the pilot is a collective stick, which controls main rotor blade pitch. Multiple control methods were analyzed to control the propeller pitch. Three existing thrust compounded helicopters were examined to



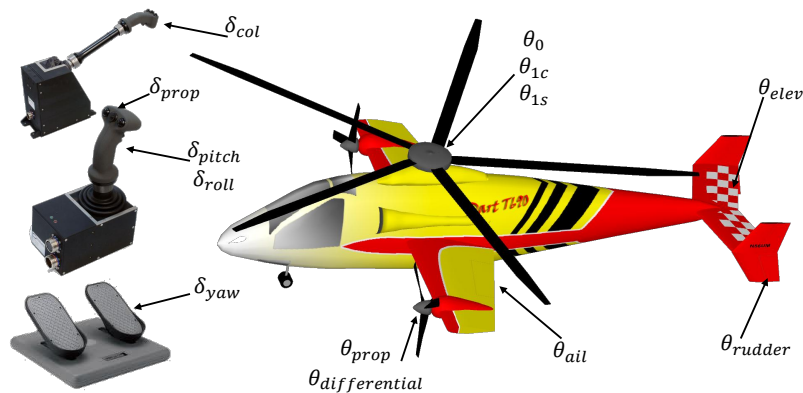


FIGURE 12.1: Dart T690 Flight Controls Diagram.

determine how past operators have controlled propeller pitch. The AH-56 Cheyenne uses a twist grip on the main rotor collective lever, the Sikorsky X-2 uses two buttons on the cyclic joystick to increase or decrease collective, and the Eurocopter X³ uses throttle controls similar to an airplane that were placed to the right of the pilot.

All three flight control options were tested on the X-Plane flight simulator at the University of Maryland by two helicopter pilots, and the preferred solution was two buttons placed on the cyclic stick. As shown in Fig. 12.1, this particular configuration allows the pilot to keep his/her hands on the controls at all times and to change the propeller pitch with one finger.

12.1.2 Control Mixing

The control mixing implemented on the *Dart* reduces pilot workload by coupling multiple flight control inputs that are inherently linked aerodynamically. Mixing the flight controls electronically provides a more robust control system and allows the control inputs to be modified in the field to reflect changing flight environments. To improve vehicle performance, reduce pilot workload, and also increase pilot effectiveness, some control inputs are mixed and scheduled as a function of flight speed.

12.1.2.1 Governing Propeller Pitch

The *Dart* uses two controllable pitch propellers to provide forward thrust and anti-torque. When using a controllable pitch propeller, the operator must manually change the propeller pitch with airspeed. This race course requires large changes in airspeed, so it is necessary to determine the optimum propeller pitch allowable. The propeller thrust limit in Fig. 12.2 corresponds to the stall limit of the propeller. Beyond the corresponding pitch angle, the propeller experiences a sudden decrease in thrust. To reduce pilot workload, the propeller pitch angles are scheduled so as to never exceed the stall limit; the maximum pitch is determined by the airspeed of the aircraft. Therefore, when the pilot commands the “max” propeller pitch at a given airspeed, the propeller will operate at the optimum pitch for that particular airspeed. The goal of this pitch scheduling is to prevent the pilot from ever stalling the propeller or imposing adverse loads on the propeller during a maneuver, i.e., to prevent operation in the brake state or the vortex ring state.

12.1.2.2 Control Surface Management



The *Dart T690/E550* is a new type of aircraft that mixes helicopter controls and standard aircraft controls. The closest similar control system is used on the V-22. However, that aircraft only mixes helicopter style controls with conventional aircraft controls during transition from hover to forward flight. In contrast, the *Dart* must seamlessly and progressively blend the standard helicopter cyclic commands with the airplane control surfaces over a large range of airspeeds.

Based on conventional airplane and helicopter pilot inputs, a control mixing scheme was developed and tested for feasibility on the X-Plane flight simulator. In addition to extensive testing in X-Plane, a trim method was developed that determined the stick inputs needed to keep the aircraft in steady level flight as a function of airspeed. The following control mixing schemes performed well during testing and were implemented in the *Dart*.

Yaw Control: To achieve maximum forward acceleration, and also maintain yaw control of the aircraft, a rudder was added. It is important to minimize the use of differential propeller blade pitch for yaw control at high airspeeds so that the full range of propeller collective can be used to provide thrust. However, testing with X-Plane and the trim method that was developed in-house showed that it would not be efficient to completely eliminate differential pitch from the control scheme at high airspeeds. Instead, rudder control is linearly phased into the control system starting at 50 kts until 70 kts.

Pitch and Roll Control: To improve agility and maneuverability at high speeds, the elevator is scheduled to phase into the control system at a speed of 50 kts and become fully active by 70 kts. The elevator acts together with the longitudinal cyclic inputs to control the aircraft in pitch. Following this same philosophy, the ailerons phase into the roll control system at 50 kts and become fully effective at 70 kts. Control mixing is performed by incorporating a washout scheduling scheme, with the flight controls phased into the control system by using linear washout. By adding ailerons and elevators to the control system, the maneuverability in forward flight was increased dramatically.

Elevator Control for Tail Download Mitigation: To reduce the effects of the main rotor wake on the tail during low-speed flight, the elevator automatically deflects downwards at an angle of, 65° in hover and deflect upwards with airspeed until reaching 15° at 45 kts. After this airspeed, the elevator follows the pitch control mixing scheme. More detailed information on tail download is given in Section 13.2.

Using the trim method, the pilot inputs to maintain steady level flight were determined. The trim approach uses the control mixing scheme as implemented on the aircraft. Figure 12.3 shows what stick, collective, and pedal commands the pilot needs to provide to maintain steady level flight. It is clear that the pilot can maintain trim with only 25% of the available control authority, leaving 75% of the the possible control input available to perform maneuvers. Also, it is clear that the control deflections required do not change much as airspeed increases. This outcome shows that a pilot can easily keep the aircraft trimmed as airspeed changes.

12.1.3 Control Coupling

Additional flight control couplings are included to reduce the pilot workload. The following control couplings are incorporated:

Main rotor collective stick to yaw control: A change in main rotor collective requires a corresponding change in the anti-torque. To this end, differential propeller blade pitch and the rudder are used to generate this anti-torque.

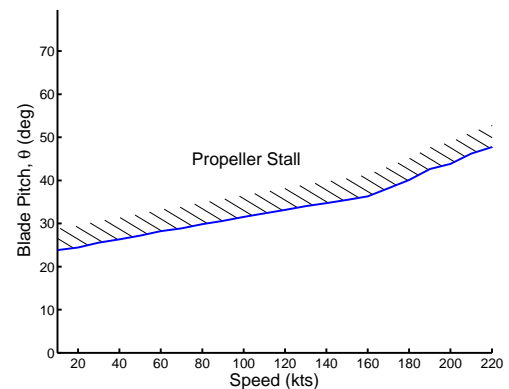


FIGURE 12.2: Maximum propeller pitch versus forward speed (kts).



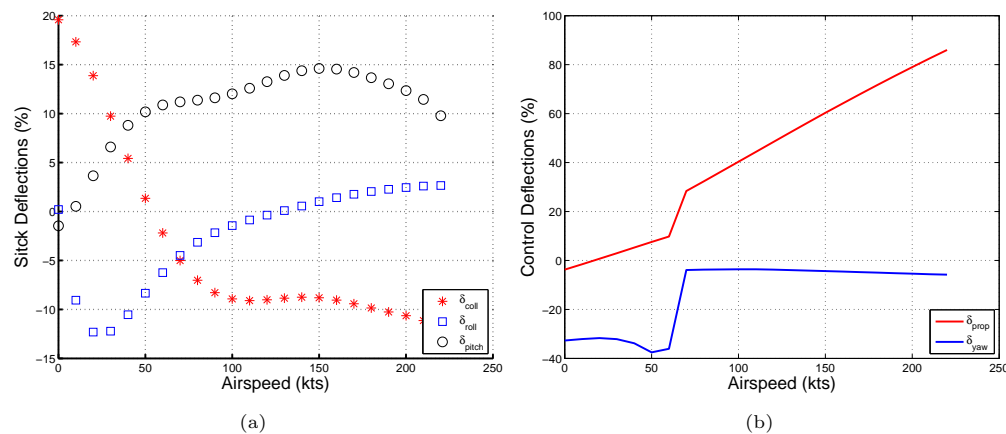


FIGURE 12.3: (a) Stick inputs for steady level flight (b) Propeller inputs for steady level flight.

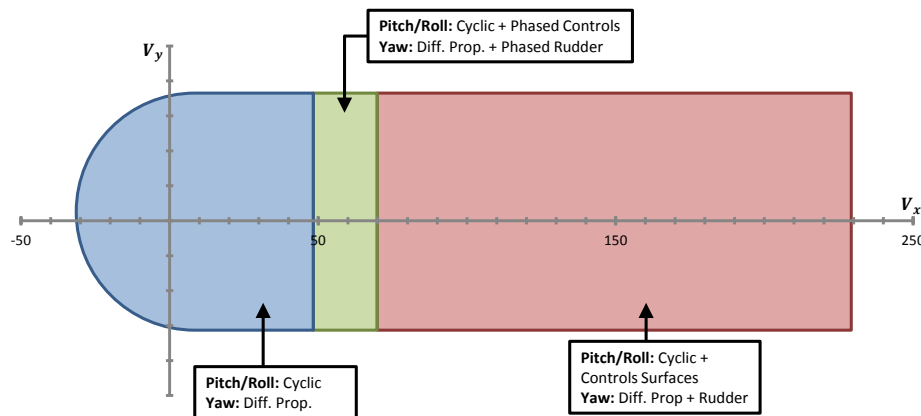


FIGURE 12.4: Control mixing scheme versus airspeed.

Main rotor collective stick to pitch control: At high airspeeds, increasing the main rotor collective leads to an increase in the angle of attack on the advancing blade. The consequence is that the rotor tip-path-plane tilts back, which generates a nose-up pitching on the aircraft. To compensate, a nose-down sidestick is automatically input to the aircraft control system when the pilot increases the rotor collective.

Main rotor collective stick to roll control: An increase in main rotor collective pitch increases blade coning. This response results in a lateral tilt of the tip-path-plane. To alleviate the corresponding rolling moment, a roll left input is applied when main rotor collective is added.

12.1.4 Digital Fly-by-Wire Architecture

A diagram of the flight control system architecture is shown in Fig. 12.5. Each subsystem within the flight control system was designed with redundancy and safety in mind. Three Flight Control Computers (FCCs) form the backbone of the system, which are responsible for all critical flight operations and calculations. To ensure accuracy, a voting scheme is implemented so that two FCCs must be in agreement before sending any control outputs. The *Dart* uses a triplex fly-by-wire system, with three separate channels to send data from the sensors to the FCS. An Air Data Computer (ADC) receives all sensor data, as well as aircraft



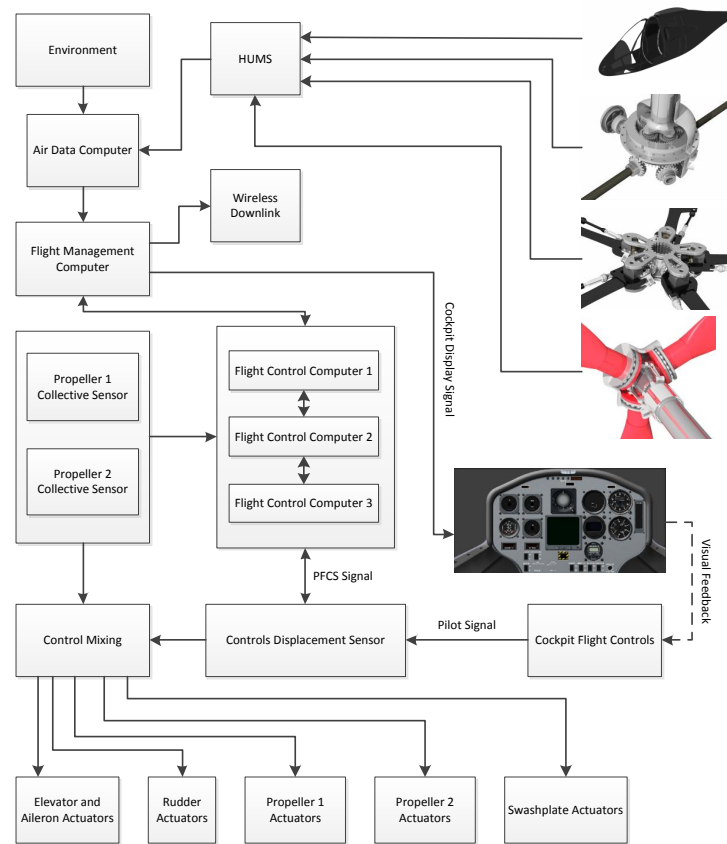


FIGURE 12.5: Flight Control System Architecture.

status data from the HUMS system. It then sends this data to the Flight Management Computer (FMC). The FMC processes all aircraft maintenance and HUMS information. It also forwards all of the sensor data to the cockpit and to the FCC. The FCC processes all of the sensor data, pilot control inputs, and HUMS data to generate the appropriate control output. Because the FCC is also coupled to the HUMS system, it is possible to apply violation constraints to prevent the pilot from performing maneuvers that could structurally damage the vehicle.

Given the high performance maneuver envelope of the aircraft, each portion of the flight control system is designed to be adjustable. An operator can modify the control mixing levels, the control scheduling, the force feedback to the stick, and the stick sensitivity. This methodology follows similar practices used in Formula-1 racing, where each vehicle is uniquely tuned to an individual driver and race course. The control settings can also be saved and transferred to another aircraft.

12.2 Dynamics and Stability

An in-depth analysis of the dynamic stability of the *Dart* was conducted. All control surfaces were modeled and the same control mixing strategy as the one used in X-Plane was implemented. Trim was performed across the range of operating airspeeds. A dynamic uniform inflow formulation was used for the rotor and both propellers, and other aerodynamic effects, such as propeller slipstream effects on the wing and tail, were accounted for. Because the *Dart* is such a unique hybrid aircraft with attributes of both a helicopter and an



airplane, it is difficult to identify each mode because they result from a combination of interactions between the rotor, the propellers, the wing, the horizontal and vertical stabilizers, and the fuselage. Figure 12.6(b) shows the frequency of the different modes as a function of airspeed. The No. 1 mode is a short period mode with heave damping; its frequency is much higher compared to the other body modes and its damping increases with increasing wing lift. It can be seen that at low speeds it is unstable. This mode is a trade off between the rotor reaction to the disturbance at high advance ratio and the fixed-wing short period stability, which nearly cancel and leads to low damping.

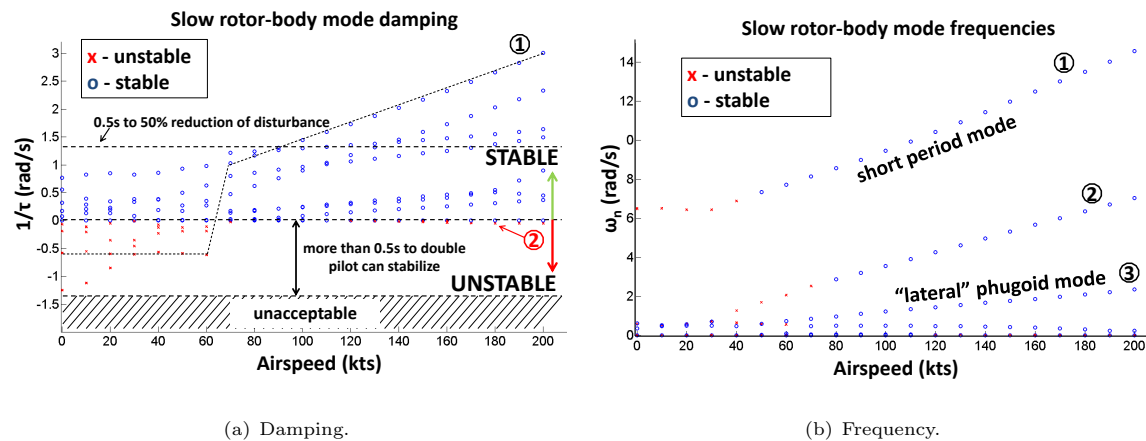


FIGURE 12.6: Damping and frequency of the different modes as a function of airspeed.

The No. 2 mode has a fairly high frequency at higher airspeeds. It arises when a gust hits the aircraft from the side. The rotor moves away from it as it flaps to the other side. No side force is generated because there is no tail rotor, and the vertical tail and the rudders do not create any force in hover, so the aircraft starts rolling and sideslipping. However, with increasing airspeed, the vertical tail becomes effective and helps return the vehicle back into the wind. This mode is a trade off between the destabilizing rotor reactions and the stabilization from the vertical tail; this gives marginal stability with small positive damping. The No. 3 mode is similar to a lateral phugoid mode with heave; it makes the aircraft want to sideslip and roll.

Figure 12.6(a) shows the real part of the different modes as a function of airspeed, a negative value meaning that the mode is unstable. Although it can be seen that some modes are unstable at low airspeeds, these instabilities are mild and give the pilot more than 0.5 seconds to stabilize the aircraft.

The No. 1 mode shows a jump from unstable to stable around 60 kts. This effect arises because of the starboard propeller that starts thrusting forward around this speed and gives positive stability to the aircraft. In hover, the starboard propeller, which is thrusting forward, enters into a climb condition and its thrust level decreases whereas the port propeller, which is thrusting backwards, enters into a descent condition and its thrust level increases. Because the starboard propeller has a negative twist and the port propeller a positive effective twist because its collective angle is negative, the difference in thrust as the gust hits the aircraft is greater for the port propeller and a nose-left yawing moment appears. In addition, the main rotor will pitch nose-up. Therefore, the aircraft moves backwards and turns to the left.

13 Performance Analysis

The *Dart T690* was designed for completing a pylon race course in the fastest time possible, and its compound configuration is crucial for achieving this goal. Its wings provide high levels of maneuverability and agility for



TABLE 13.1: Parasitic drag buildup.

	Parasitic Drag Area (ft ²)	% of Total
Fuselage	0.851	24.0 %
Rotor Shaft and Hub	1.68	47.5 %
Wing	0.522	14.7 %
Propeller Nacelles	0.063	1.79 %
Horizontal Empennage	0.170	4.80 %
Vertical Empennage	0.132	3.73 %
Miscellaneous	0.12	3.39 %
Total:	3.54	
+ additional 20%:	4.25	

performing quick turns and navigating pylons. The propellers give the *Dart T690* superior dash capabilities with high, responsive translational acceleration. By offloading lift onto the wing and using the propellers for forward thrust, the *Dart T690* significantly decreases its power requirements in forward flight compared to a conventional helicopter, enabling it to reach a maximum airspeed of 225 kts. The *Dart T690* is the ideal rotorcraft for pylon racing.

13.1 Drag Estimation

The aircraft drag can be decomposed into two components: parasitic and profile drag, and wing induced drag. The parasitic drag was determined by considering each vehicle component separately and summing the drag of each component. Using a methodology outlined by Raymer [7], the drag area of each component was calculated as the product of its wetted area, skin friction coefficient, interference factor, and form factor. The wetted areas of the wing and tail surfaces were calculated according to equations discussed by Roskam [34]. Values for skin friction coefficients, which are themselves functions of Reynolds number and Mach number, were calculated at MSL ISA conditions and an airspeed of 150 kts. The hub drag was determined using historical data trends [35].

The resulting drag of each component is shown in Table 13.1. The fuselage, which is streamlined for high-speed flight, has relatively low drag. The rotor hub, which supports a rotor designed to pull high load factors, takes up a large percentage of the total parasitic drag. The miscellaneous drag accounts for vehicle components such as the antennas, pitot probe, camera, door handles, and hinges. As recommended by Prouty [36], a 20% increment was added to the calculated parasitic drag area to obtain a more practical estimate of total drag. This increment also accounts for the drag area of the retracted landing gear. The parasitic drag area of the *Dart T690* was estimated to be 4.25 ft².

13.2 Aerodynamic Download

The *Dart T690* has a large wing to help produce high load factors during maneuvers, but contributes to a download penalty in hover. The flow velocity in the rotor wake, which is a function of rotor disk area and aircraft weight, exerts a force on the wing that was estimated to be approximately 14.5% of aircraft weight. However, the rotor, which was sized to sustain a 3.5g load factor, can easily lift the weight of the aircraft plus this vertical download. Consideration was given to using flaperons on the wing instead of ailerons to reduce the download. However, calculations indicated that flaperons would only give small reductions in download and power required to hover, and were deemed to add too much cost and mechanical complexity.



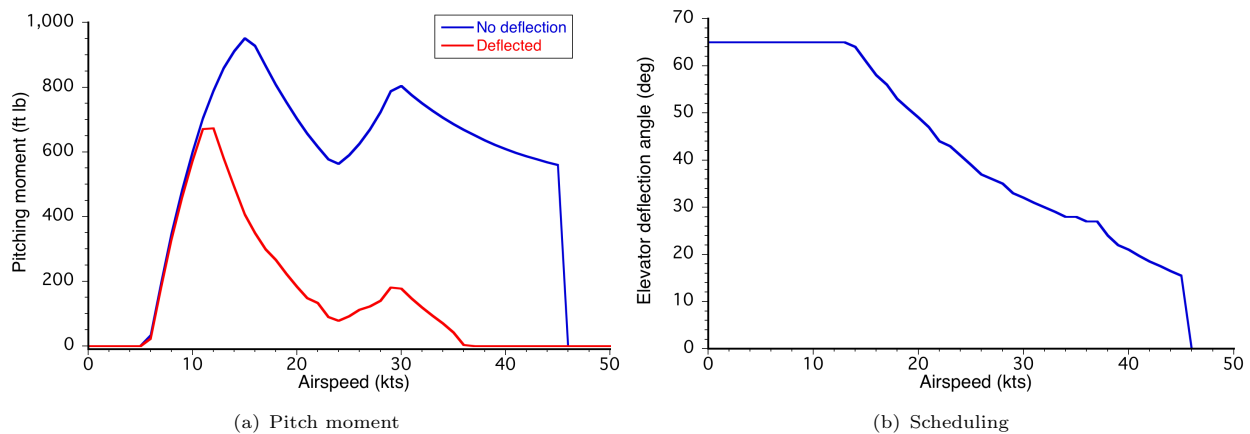


FIGURE 13.1: Elevator deflects to reduce download on the horizontal tail surface.

At low airspeeds, the rotor wake is skewed backwards and causes the horizontal tail to produce a download. The resulting nose-up pitching moment on the aircraft can create handling qualities issues for the pilot when transitioning from hover to forward speed or vice-versa. To alleviate this effect, the elevator is deflected to reduce the download on the tail at low airspeeds, as shown in Fig. 13.1(a). The tail download was calculated as a superposition of in-wake and out-of-wake tail areas; this method generally results in overpredictions of download, so a 0.75 reduction factor was applied. Figure 13.1(b) shows the scheduling for the elevator deflection that results in the largest download reductions; this scheduling is incorporated into the fly-by-wire control system.

13.3 Hover Performance

The *Dart T690*, which is designed for high-speed flight, requires only 41% of its interim rated power to hover at MSL ISA. This significant hover power margin, combined with the fact that the rotor is sized to sustain a 3.5g normal load factor, means that the *Dart T690* is capable of hovering at high density altitudes or while carrying heavy payloads. Figure 13.2(a) shows a maximum hover ceiling of 25,000 ft at ISA conditions; such a high ceiling is unprecedented for current helicopters. The ISA+25°C condition corresponds to 103°F at sea level, which is the condition given in the RFP at which the vehicle must demonstrate 60 kts sideward flight and 125 kts forward flight at 90% MCP. The engine power available was determined by calculating lapse rates from the data given in the RFP (see Chapter 8). Although the capability to hover at high altitudes does not apply to the *Dart T690's* intended usage for racing competitions, it highlights a potential second use of the aircraft, such as for operations at high-altitude in mountainous regions.

The maximum hover ceiling as a function of gross weight is shown in Fig. 13.2(b). The *Dart T690* is capable of operating at gross weights far higher than its design takeoff weight. The *Dart T690's* rotor, which is designed to provide 7,000 lbs of thrust without stalling during racing maneuvers, is fully capable of lifting the weight of the vehicle plus any wing download at maximum hover weight.



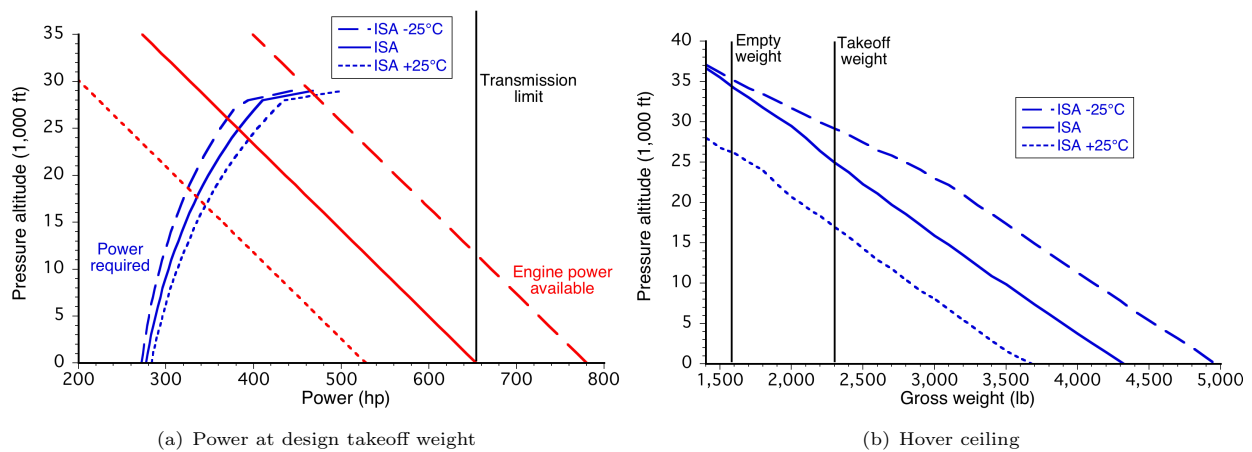


FIGURE 13.2: HOGE hover performance.

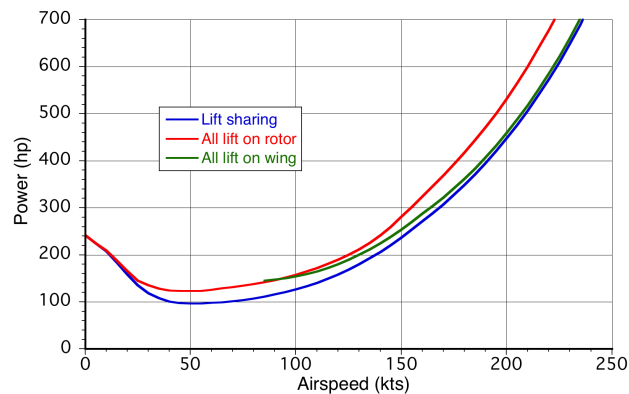


FIGURE 13.3: Load sharing reduces power compared to lifting with only the wing or rotor.

13.4 Rotor/Wing Load Sharing

The *Dart T690's* compound configuration allows it to offload lift onto the wing in forward flight and to decrease vehicle power requirements. The load sharing that results in the lowest power requirement was calculated across a range of airspeeds; Fig. 13.3 shows the reduced power benefits by offloading the rotor. Significant power reductions are apparent at 30 kts, and these reductions increase with further increases in airspeed. The aircraft is capable of carrying its entire weight on the wings without stalling at airspeeds greater than 83 kts. Having wings allows the *Dart T690* to combine the hover capability of a conventional helicopter with the lower power and better aerodynamic efficiency of an airplane.

The calculated optimum load sharing schedule is shown in Fig. 13.4(a). As airspeed increases, the best power reductions are realized by the wing providing a greater share of the lift. The *Dart T690* experiences only small increases in power for deviations from the optimum load sharing schedule, as shown in Fig. 13.4(b). This generous margin gives the pilot much latitude in the operation of the vehicle without experiencing changes in power requirements or other aircraft performance characteristics.



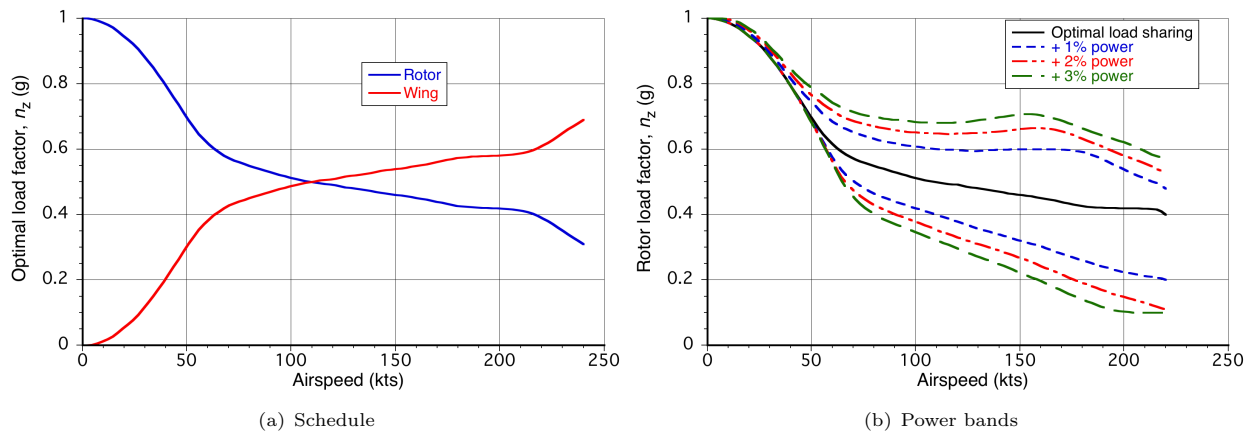


FIGURE 13.4: Rotor/wing load sharing: (a) load sharing schedule; (b) power bands.

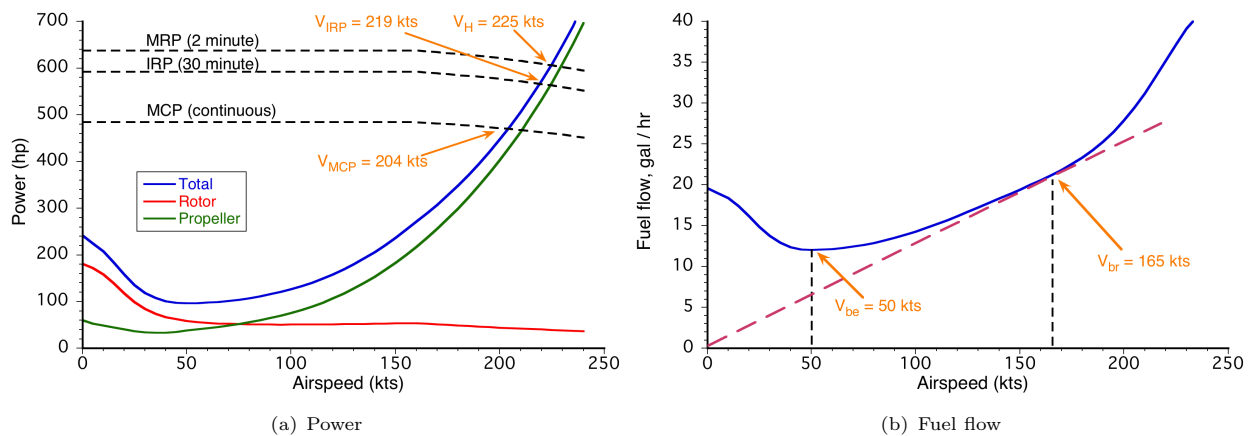


FIGURE 13.5: Power and fuel flow in forward flight. MSL 80°F.

13.5 Forward Flight Performance

Figure 13.5(a) shows the power required by the *Dart T690*, including the power consumed by the rotor and by the propellers, as a function of airspeed. At high airspeeds, the propellers require much more power than the rotor because the rotor is mostly offloaded by the wing and the propellers are overcoming all of the vehicle drag. Notice that the engine power available decreases at speeds higher than 160 kts; this is a consequence of the engine rpm being reduced to avoid advancing blade compressibility effects on the rotor. The *Dart T690* can reach a forward speed of 204 kts at MCP, which it reaches during the straight-away section of the course. At MRP, the vehicle can achieve an airspeed of 225 kts; although 225 kts is not reached during the course, the extra power margin improves the aircraft's dash capabilities. As shown by the results in Fig. 13.5(b), the best endurance is obtained at an airspeed of 50 kts and the best range is obtained at 165 kts. Using only its main fuel tanks, the *Dart T690* has a maximum endurance of 1.4 hours and a maximum range of 134 nm. With its auxiliary tanks included, it has a maximum endurance of 2.7 hours and a maximum range of 256 nm.



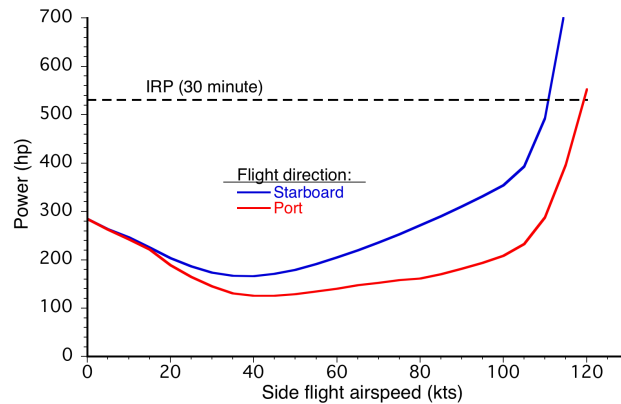


FIGURE 13.6: Power required in sideward flight at design takeoff weight. MSL 103°F.

13.6 Sideward Flight Performance

The RFP requires that the *Dart T690* be able to demonstrate a 60 kts sideward flight at MSL and 103°F. Figure 13.6 shows that a sideward flight speed of 60 kts is easily achievable, regardless of flight direction. Notice that more power is required when flying to starboard than when flying to port. This is because in sideward flight, the drag on the tail results in a net yawing moment that must be counteracted by anti-torque from the propellers. In starboard flight, this yawing moment is in the same direction as the moment caused by rotor torque, and so the propellers require more power. For the sideward flight calculations, a conservative estimate for the fuselage sectional drag coefficient of 1.0 was assumed.

13.7 Dash Capability

The *Dart T690* has excellent dash capabilities with high levels of translational acceleration/deceleration, allowing it to quickly complete the race course. The forward acceleration characteristics of the *Dart T690* based on engine MRP are shown in Fig. 13.7. At lower airspeeds, the maximum forward acceleration is limited by propeller stall and is roughly constant at a 0.7g translational load factor. At airspeeds higher than 70 kts, the maximum acceleration is limited by engine power and linearly decreases to 0 at $V_H=125$ kts. The maximum deceleration increases to over 1g at higher airspeeds because parasitic drag is larger at higher airspeeds.

14 Acoustics

14.1 Noise Requirements

There are two noise certification procedures: The FAR (Federal Air Regulation) Part 36 and The ICAO (International Civil Aviation Organization) Annex 16. Both require noise emission testing for three different flight conditions: takeoff, flyover, and approach. However, for smaller aircraft under 7,000 pounds, which is the case for the *Dart T690*, only the flyover testing is required (FAR 36 Appendix J / ICAO 16 Chapter 11). Measurements are to be made for level steady flight at an altitude of 150m (492ft) above the ground microphones and at 90% of the speed at maximum continuous power. The Effective Perceived Noise Level



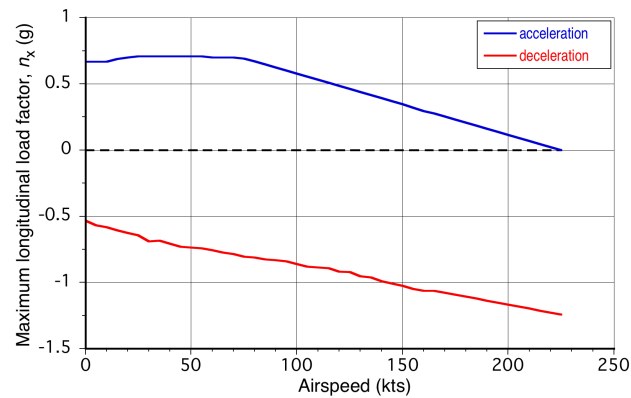


FIGURE 13.7: Dash capability versus airspeed. MSL 80°F.

(EPNL), in decibels, is typically the scale used, which gives a good measure of annoyance. Using Stage 3 of FAR 36, the EPNL of the *Dart T690* must not exceed 88 dB for the flyover test.

14.2 Rotor Noise

The *Dart T690* features a 5-bladed rotor with low disk loading and relatively modest rotational speed, which gives it relatively low loading noise levels and harmonics of higher frequency compared to rotorcraft with fewer numbers of blades. High Speed Impulsive noise (HSI) is avoided by keeping the blade tip Mach number under 0.85 for all flight conditions. In addition, having blade taper and sweep reduces shock delocalizations on the advancing side, delaying the onset of HSI noise. The relatively low blade thickness also helps to keep the in-plane acoustic signature to a minimum. Blade Vortex Interaction noise (BVI), which appears during descending or maneuvering flight, can be greatly reduced by modifying the effective tip-path-plane angle of attack; it is done for the *Dart T690* by using the two propellers as a mean of accelerating/decelerating the aircraft, and gives higher miss distances between the blade and the vortices. Furthermore, the low disk loading and higher number of blades leads to weaker vortices and lower BVI noise levels, which helps reduce the out-of plane noise signature.

14.3 Propeller Noise

The propellers operate at higher tip speeds and disk loadings, and they have a lower aspect ratio than the rotor. This design results in higher noise levels from the propellers than from the rotor. The propeller noise mainly radiates as in-plane noise, which means that the noise is greatest directly below the aircraft.

14.4 Other Sources of Noise

Because the *Dart T690* is a small aircraft, all other sources of noise are relatively low. In particular, the small engine and gear boxes lead to low noise levels. The streamlined fuselage with its low drag also helps to reduce flow noise.



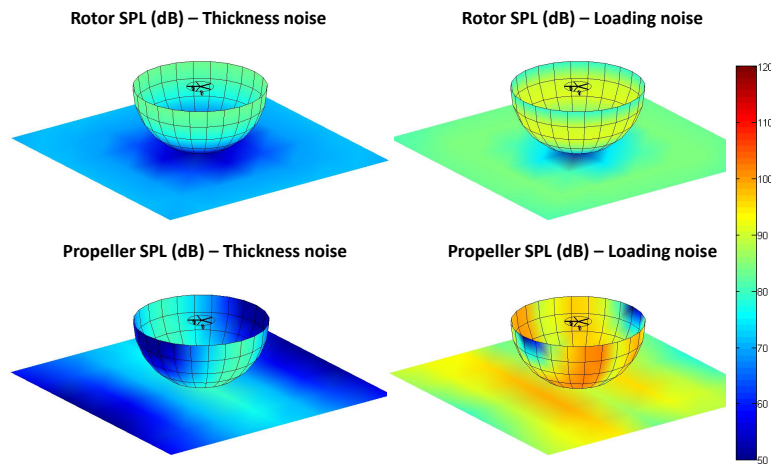


FIGURE 14.1: Comparison in hover of thickness and loading noise for one of the propellers and the rotor.

14.5 Numerical Simulation

Rotor noise estimations were obtained by using an acoustics code developed at the University of Maryland based on Formulation-1A of the Ffowcs Williams-Hawkings equation. Both thickness and loading noise were computed for the main rotor and the two propellers. Sound pressure levels (SPL) in decibels (dB) were calculated on a sphere surrounding the aircraft, as well as on a plane located five rotor radii below the main rotor; the radius of this sphere is also equal to five times the main rotor radius. To ensure that the noise levels do not exceed those mandated by the FAR/ICAO, sound pressure levels were calculated at a ground plane with the aircraft flying 150 m above it.

14.6 Results

Figure 14.1 shows thickness and loading noise in hover for the rotor and for one of the propellers. As expected, the thickness noise levels reach a maximum in the plane of the propellers and the rotor respectively, whereas the loading noise levels are maximum out of those planes. Thickness noise is lower than the loading noise both for the propeller and the rotor. The propeller gives the highest loading noise, which arises from its higher disk loading and higher tip speed.

Figure 14.2 shows the same sound pressure levels but in forward flight at 220 kts. The same trends are apparent here, but this high cruise speed leads to higher rotor tip speeds, which translates into higher noise levels in front of and below the aircraft.

Figure 14.3 shows the total SPLs of the entire aircraft at different airspeeds. In hover, the noise signature is symmetric. The higher levels shift towards the front of the rotor as airspeed is increased. At these higher airspeeds, the noise levels are closer to 120 dB and could be a problem in regard to the noise regulations discussed previously. Therefore, the sound levels for the *Dart T690* was computed for the flyover condition described by FAR 36. Figure 14.4 shows that the noise hotspot is located right under the rotor. Its noise level is 85.5 dB, which is below the maximum level prescribed by the regulation (88 dB). Therefore, the *Dart T690* can be easily certified to fly at any race location where noise standards apply.



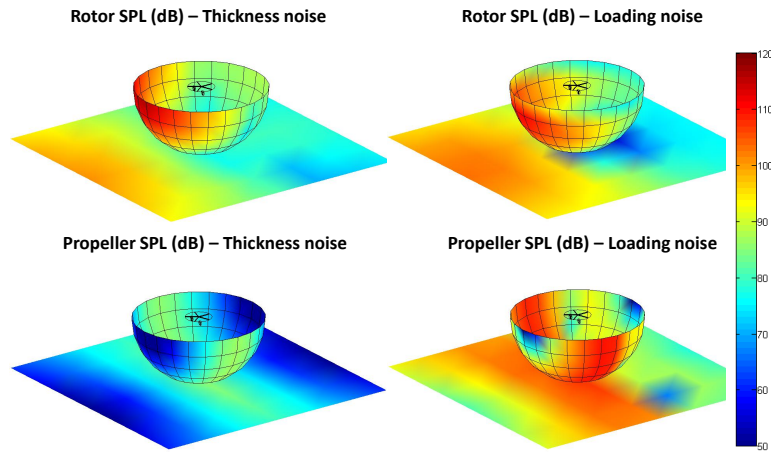


FIGURE 14.2: Comparison at 220 kts of thickness and loading noise for one of the propellers and the rotor.

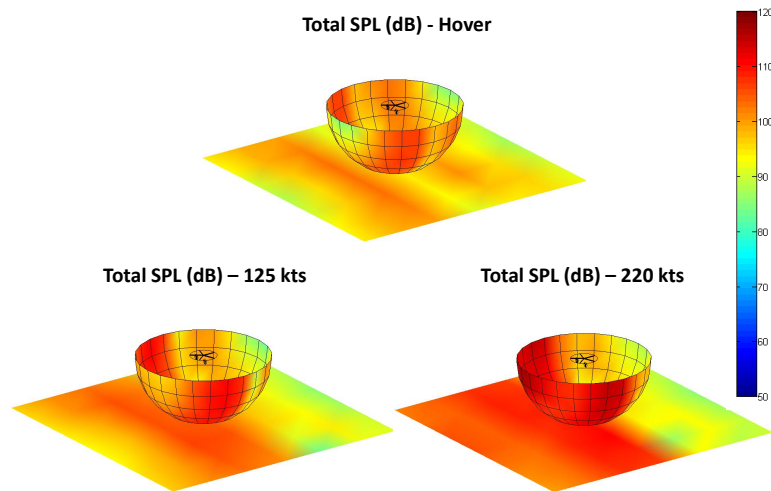


FIGURE 14.3: Comparison of total SPL at different airspeeds.



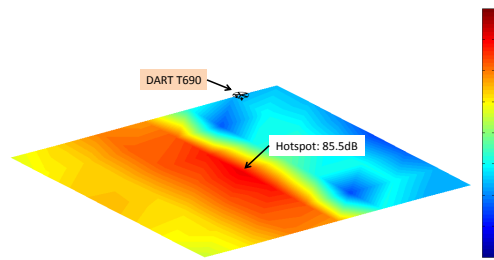


FIGURE 14.4: FAR36 flyover test (150m above ground microphones, 220kts).

15 Safety and Survivability

With any racing vehicle, safety must be a primary consideration, both for the pilot and the spectators. A recent tragedy at the Reno Air Races, where several spectators died, has placed a dark cloud over the sport and highlights the critical nature of safety. Several near accidents during the most recent Red Bull Air Races have put that sport on hold pending safety reviews [37]. It is, therefore, important that the pilot be able to maintain control of the vehicle in the event of any failure of the aircraft systems. The *Dart T690/E550* is designed so that in the event of any failure, the pilot can safely land the aircraft.

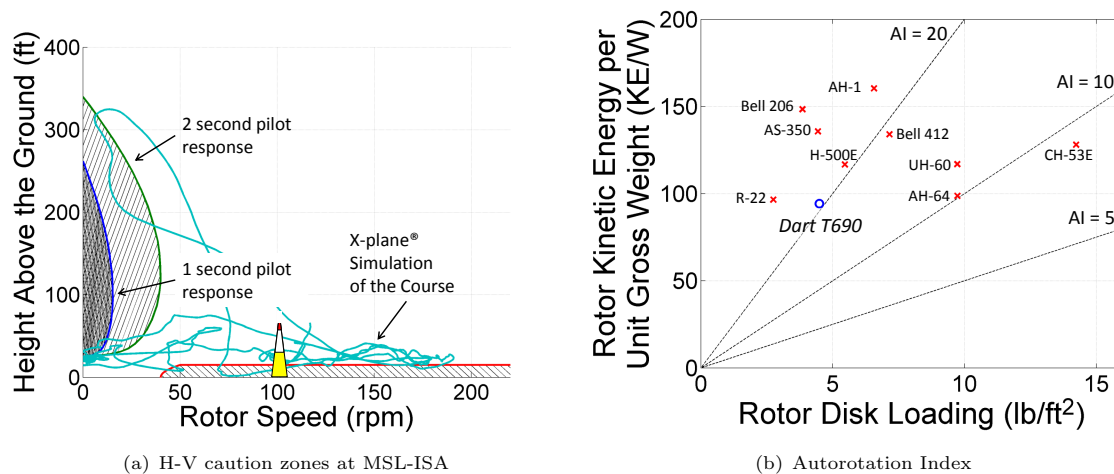
15.1 Electric System

The use of all power-by-wire controls means that the reliability of the electric system is critical. To reduce the likelihood of failure, a triple redundant electric generation and distribution system is used. Two generators are used to provide current, as well as to maintain the charge in the two batteries. In the event one generator fails, the other is completely capable of powering all of the electric systems. If both generators should fail, battery backup is capable of independently powering all of the flight control actuators. Flight critical systems, such as the rotor and propeller controls, are operated by double redundant electro-hydrostatic actuators (EHA), whereas the non-critical systems (ailerons, elevator, rudders) have single motor EHAs. As discussed earlier, the landing gear are designed to automatically deploy in the event of a power failure.

15.2 Lightning Strike

It is necessary to ensure electrical continuity of all parts of the airframe for protection against electrostatic build up and lightning strikes. This is a prime consideration in an aircraft with a non-conducting composite skin. Along the surface of the skin is a layer of expanded copper mesh on top of an isolation layer of glass fibers to resist lightning strikes. The wings, tail, nose cone, propeller blades, and rotor blades, utilize a 141.6 g/m^2 (0.0290 lb/ft^2) mesh capable of withstanding the direct effects of powerful Zone 1-A lightning strikes. The remainder of the fuselage, which is less likely to suffer a strike, uses a lighter 73 g/m^2 (0.0149 lb/ft^2) expanded copper mesh [38]. Utilizing a hybrid airframe with an aluminum structure within a composite shell also helps mitigate the indirect magnetic effects of a lightning strike that could affect electronic systems[39].



FIGURE 15.1: Engine out performance for the *Dart*

15.3 Engine Failure

In the unlikely event of an engine or electric power system failure in the *Dart T690* or *Dart E550*, respectively, an unpowered emergency landing will be necessary. Safe, unpowered emergency landings mean an autorotative landing will be required.

15.3.1 H-V Diagram

For the pilot, formal guidance on these issues is provided by the “avoid” regions on a Height-Velocity (H-V) diagram. This diagram must be established experimentally for every new helicopter by skilled pilots attempting autorotations from a variety of flight conditions until they identify the regions where an average pilot would be unlikely to have the skills to perform a successful autorotation. Historical trends can provide a first estimation of the H-V diagram; see Prouty [40]. The lower point of the H-V diagram is set by the strength of the landing gear, which for the *Dart T690/E550* is critical for the pirouette maneuver and the slung load pickup.

Predictions of the H-V diagram for the *Dart T690/E550* using both a 2-second pilot response delay (required by the military) and a 1-second delay (required by the FAA) are shown in Fig. 15.1, along with the actual flight path flown in X-Plane[®] (see Chapter 17). The shaded regions are cautionary zones, not absolute avoid regions. The pilot will also train to fly above the caution zone of the pylons, reducing the time spent in the higher speed caution zone. Any pylon racing pilot will be of the highest caliber and have high levels of attentiveness, and as such small avoid regions pose no impediment to racing.

15.3.2 Autorotational Index

Autorotative performance, especially the flare maneuver at the end, is affected by a number of factors, including the lift-to-drag ratio of the aircraft, the energy stored in the rotor system, and the control authority. With compound rotorcraft, autorotational performance is affected by the addition of wings, which improve the vehicle glide performance. A variety of autorotational indices (*AI*) exist to quantitatively compare the ability to perform the autorotational maneuver. The Sikorsky autorotative index (*AI*), $AI = I_R \Omega^2 / 2WDL$ [41], is a ratio between the kinetic energy ($I_R \Omega^2$) stored in the rotor, the weight of the helicopter (W),



and the disk loading (DL). Single engine helicopters with an AI above 20 have proven to have acceptable autorotational characteristics. The *Dart T690/E550* has an AI of 21, as shown in Fig. 15.1(b).

15.3.3 Zoom-Climb Performance

The final critical safety consideration is the performance at low altitude and high airspeeds. Civilian helicopters do not spend long periods of time in that region, but it is a critical aspect of the flight envelope of a racing helicopter. The *Dart T690/E550*'s zoom-climb capability is significantly improved by the wing, and for this reason the low altitude caution zone is lower than the 29 ft caution height of the pylons.

15.4 Impact Survivability

Provisions have been made for the pilot's safety in the event that the helicopter cannot be brought to a safe landing. The aircraft nose is shaped to prevent tipping or plowing in the event of a crash. The tail boom is designed to break away from the remainder of the fuselage upon impact. The landing gear, which automatically deploys in case of failure, will deflect and crumple upon striking the ground, reducing the energy to be absorbed by the fuselage. Reinforced door frames reduce the likelihood that the doors will jam shut in a mishap. In addition to the main door on the left side of the fuselage, the pilot is provided with an emergency exit on the right to help in escape if needed. Finally, the pilot seat is mounted on an inversion tube assembly. This seat starts stroking at a load of 14.5g, causing the tubes to collapse, absorbing energy and slowing the deceleration of the pilot as the seat strokes downward up to 12 inches. The pilot seat features a five point harness for restraint during an accident. It is also recommended that the pilot wears a Head and Neck Support Device (HANS). A requirement in most professional automobile racing circuits, the HANS device is a collar which ensures the head moves forward with the chest and is therefore arrested by the five point harness during impact, preventing whiplash. Though some pilots may dislike the loss of visibility from the restraint, the slung load camera will still allow the entire course to be performed easily.

15.5 Water Recovery

The *Dart T690* and *Dart E550* also feature emergency landing floats, as shown in Fig. 15.2. Mounted at four locations around the fuselage, two towards the nose and two aft of the center of gravity, the floats are capable of being deployed by the pilot in case it is necessary to ditch the helicopter in the water. The floats are sized to allow the helicopter to float for longer than 15 minutes, giving ample time for rescue crews to perform a recovery operation. The bottom skin panels of the fuselage have also been designed with extra thick honeycomb sandwich sections, allowing the skin to absorb energy upon a water impact. The pilot also is equipped with an inflatable life preserver and a 1.7 ft³ Spare Air[®] emergency air supply, good for about 30 breaths in the case that the pilot is submerged in the aircraft.

16 Project Development Timeline

16.1 Technology Development Program

The *Dart T690/E550* incorporates cutting-edge advances in rotorcraft technology, as shown in Table 16.1 along with their corresponding TRL levels. Several of these technologies have been tested and used on demonstrator aircraft, such as the Li-ion batteries and the PEM fuel cells. However, the *Dart* uses versions





FIGURE 15.2: *Dart T690* with emergency flotation deployed, four floats are placed symmetrically around the c.g. for stability.

of these technologies currently in development that have a TRL of 5. Table 16.1 also shows the dates when these technologies are projected to be ready.

TABLE 16.1: Current TRL and projected year ready for advanced technologies on the *Dart T690/E550*.

Component	Estimated TRL	Projected year ready
PEM fuel cell	5	2017
Li-ion batteries	5	2018
Composite hydrogen storage tank	5	2015
Retractable landing gear	5	2017
Halbach array motors	6	2016

16.2 Project Development

The *Dart T690* uses the ISO9001/AS9100 quality management system to guarantee that the needs of the customer are met throughout the design, development, construction, and testing of the vehicle. This approach includes continually reexamining the vehicle design to ensure that its cost is minimized and the production schedule is met. All design decisions will be made in accordance with the customer requirements in the RFP, and will be validated using engineering analysis, computer simulation, and wind tunnel/flight testing data. The design will be continually improved to meet or exceed the customer requirements. Progress reports will be provided to the customer at regular intervals, with a detailed description of the current design including extensive CAD drawings. Figure 16.1 shows the program schedule for the development, design, production, testing, and certification of the *Dart T690*.

16.3 Life-Cycle Cost Analysis

16.3.1 Acquisition Cost

Typically, the cost of the rotorcraft can be divided into three categories: the development cost, the production cost, and the operational cost. The sum of these three elements is often referred to as the life-cycle cost of the aircraft. In the case of the *Dart T690*, although it is a unique racing aircraft not designed for mass



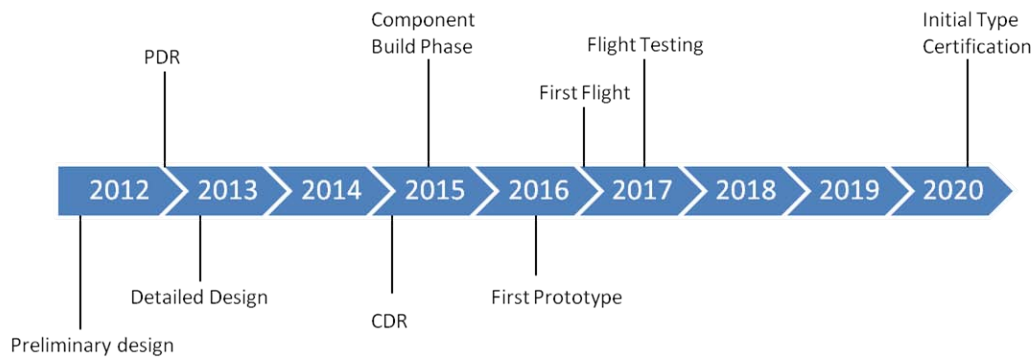
FIGURE 16.1: Milestones chart for development of the *Dart T690*

TABLE 16.2: Acquisition cost comparison in 2012 U.S. dollars.

Aircraft	Gross Weight (lb)	Acquisition Cost (\$)
<i>Dart T690</i>	2,300	\$1.6M
MD-500C	2,250	\$1.2M
Bell-206B	3,200	\$1.4M

production, keeping its acquisition cost relatively low was an important factor to make it an affordable option for racing. An estimate of the *Dart T690*'s acquisition cost was obtained, based on historical data using Harris and Scully's empirical model [42]. Annual inflation was taken into account to update the predicted prices from 2008 U.S. dollars to their 2012 value. Although this method has been widely used for conventional helicopters cost estimations, it had to be modified for the *Dart T690* and its compound configuration.

The *Dart T690*'s base price was estimated to be \$1.6 million. This price is slightly above that of helicopters in the same weight range, as shown in Table 16.2. Recall that the *Dart T690* is a very unique aircraft featuring an advanced composite structure and a retractable landing gear, which both drive the cost up.

The operating cost of the *Dart T690* was obtained through the direct and indirect operating cost model developed by Conklin and de Decker ([43]). This model is also based on historical data including more than 310 fixed- and rotary-wing aircraft designs.

16.3.2 Direct Operating Cost (DOC)

An operating cost that varies proportionally to the number of flight hours is called a direct operating cost (DOC). DOC's include the cost of fuel, additives, lubricants, maintenance, inspections, and the cost of parts. Figure 16.2(a) shows the relative percentage of each for the *Dart T690*. It can be seen that fuel and maintenance are the two highest costs.

To compare the *Dart T690* with helicopters in the same weight class, the DOC of the MD-500E and of the Bell-206B are shown on Fig 16.3(a). The different costs are very close for all three aircraft, although the *Dart T690* has a lower fuel budget, thanks to its "advanced" engine with low SFC.



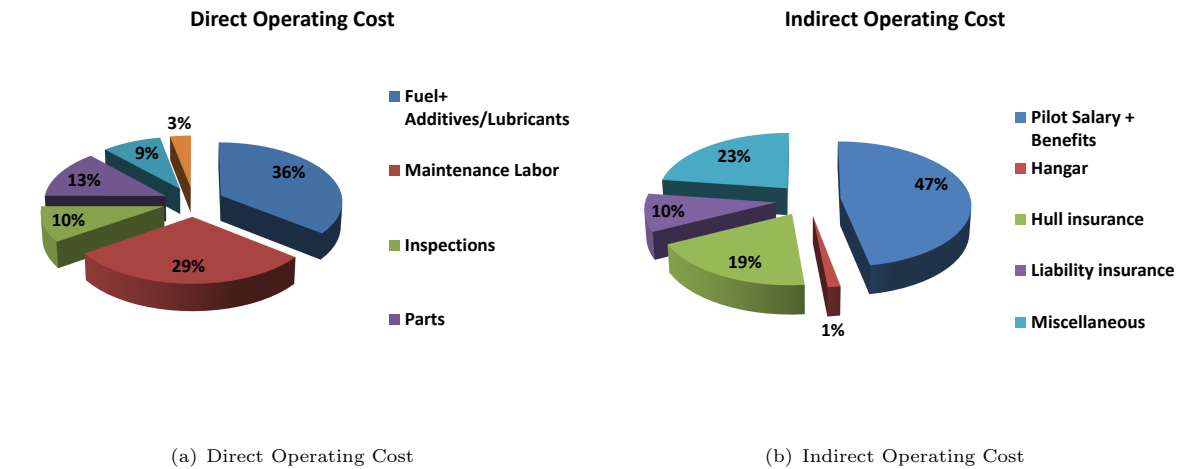


FIGURE 16.2: Operating costs of the *Dart T690*.

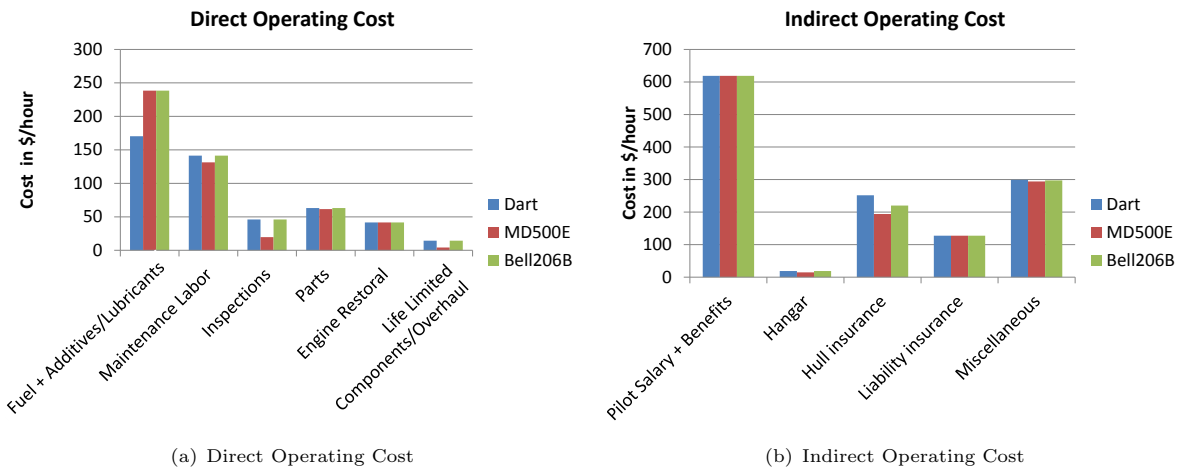


FIGURE 16.3: Comparison of the operating costs of the *Dart T690*, the MD-500E, and the Bell-206B.

16.3.3 Indirect Operating Cost (IOC)

The indirect operating cost (IOC) differs from the DOC in that it does not vary with the number of flight hours; it groups the pilot’s salary and benefits, hangarage, the insurance cost (hull and liability), and other fixed costs. Figure 16.2(b) shows the IOC of the *Dart T690*. The pilot’s salary represents the largest part (47%), although insurance also accounts for a large fraction of this cost (23% and 19%).

The indirect operating cost of two other aircraft are compared to that of the *Dart T690* in Fig 16.3(b); it can be seen that the different values are close for all three aircraft. Although the *Dart T690* is a racing aircraft that flies in potentially dangerous situations where the likelihood of accidents is high, its great survivability characteristics, like autorotation and spring-loaded retractable landing gear, make it a safe aircraft to fly. This is why the cost of insurance of the *Dart T690* remains close to the two other aircraft. The liability insurance also remains low because no passengers are carried.



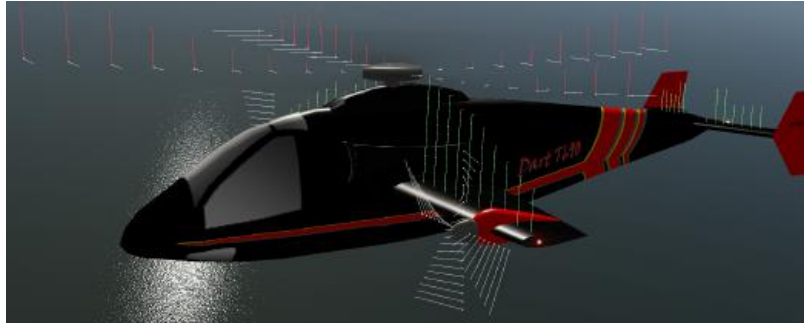


FIGURE 17.1: Graphical representation of the X-Plane flight dynamics model.

17 X-Plane Flight Simulator

An important outcome of this design project is that the X-Plane simulator became a key element in evaluating engineering design choices. The simulator provided a way to quickly model proposed designs, and then test the performance of the different design choices. Another significant benefit of X-Plane is that all aircraft states can be output in real-time so that performance metrics such as power, wing lift, rotor thrust, drag, etc., can be compared with other engineering data. To this end, X-Plane was used within the design loop, and helped validate several design decisions. This approach proved to be a significant benefit during the design, and flight tests in the simulator significantly influenced several critical engineering design decisions.

17.1 X-Plane Flight Dynamics Model

In contrast to all other current flight simulator programs that use estimated stability derivatives to calculate aircraft dynamics, X-Plane uses rotor blade element theory and wing strip theory for the calculation of the relative forces and moments acting on the aircraft. A graphical version of the flight dynamics model used by X-Plane is shown in Fig. 17.1. The coefficients of lift, drag, and moment for each aerodynamic section of the aircraft are created using the other two pieces of software namely, Planemaker and Airfoilmaker, which come bundled with X-Plane [44–46]. Planemaker is used to create the aircraft geometry used in X-Plane and define the aircraft specifications. For any airfoil that is included in an aircraft model, it is necessary to generate its lift, drag, and moment curves in Airfoilmaker.

17.2 Aircraft Development

Planemaker, Airfoilmaker, and X-Plane were used in conjunction with the design process to provide real-time feedback of the design decisions. The numerous models created for X-Plane provided qualitative observations that allowed the design team to gain a preliminary feel of the aircraft's handling qualities and flight performance.

17.2.1 Configuration Selection

During the configuration selection phase of the design process, numerous X-Plane models were created. Two early prototypes are shown in Fig. 17.2; both prototypes are modified versions of a Bell 206 because when creating a proof of concept model, it is much simpler to modify existing aircraft than to design a new





FIGURE 17.2: (a) Bell 206 with dual thrusters (b) Bell 206 with pusher propeller.

prototype. After testing each model, it was found that the dual thruster configuration had better forward acceleration and had a smaller rolling moment caused by propeller torque across a range of airspeeds. The flight behavior observed using X-Plane was one key factor in selecting a dual thruster configuration over other possible choices.

17.2.2 Rolling Moment Analysis

After the initial configuration was selected, a prototype model of the *Dart T690* was created. In the initial designs, the dual propellers were placed close to the fuselage so that wing weight could be reduced. However, after flying prototypes in X-Plane, a previously unidentified rolling moment was observed that had to be corrected with lateral cyclic; this rolling moment was traced to a differential propeller torque. The propeller position to minimize rolling moments was then determined (see Section 7.1.3).

17.2.3 Control Surfaces

After designing the propeller, additional test flights were made in X-Plane and it became apparent that the rotor provided enough roll authority in steady level flight. However, the optimization showed that an increase in roll and pitch authority would result in a faster course completion time (see Section 2.2). Therefore, ailerons and elevators were added to the aircraft design and tested in X-Plane. The required yaw rate was also examined. It was determined that rudders would be highly desirable as a means of yaw control at higher speeds; the use of rudders minimized the amount of differential thrust from the propellers. The addition of rudders also increased the overall translational acceleration of the vehicle.

To manage all of the control inputs on the vehicle, a control strategy was modeled in X-Plane. The qualitative feedback from test flights determined the control input phasing. These conclusions were then verified with a trim method that was developed. Further details about the control mixing analysis is given in Section 12.1.2.

17.2.4 Cockpit Design

Another benefit of X-Plane was its usefulness as a cockpit design tool. Planemaker has a cockpit creation module that contains a library of hundreds of cockpit gauges. By creating a cockpit in X-Plane it was possible to test the layout while flying the vehicle. It quickly became apparent that dial gauges were superior to a glass cockpit in a racing aircraft. The use of dial gauges allowed important airplane information such as airspeed, engine rpm, and altitude to be placed within the pilot's peripheral vision. The pilot was able to fly the course and monitor crucial flight status information without looking down directly at the instrument panel.



FIGURE 17.3: X-Plane model of *Dart T690/E550*.

17.2.5 Final Design

Upon the completion of preliminary sizing a final X-Plane model was created and is shown in Fig. 17.3. This model was based upon the detailed Computer Aided Design (CAD) drawings made of the aircraft. A rendering of the fuselage was imported into Planemaker and used to generate the exact vehicle shape. Unlike other flight simulation software, X-Plane uses aircraft shape to calculate the drag on the vehicle so it was extremely important to use a geometrically precise aircraft model. To ensure that the vehicle aerodynamics would be modeled correctly, each airfoil used in the vehicle was generated in Airfoilmaker. Other additional information, such as the engine specifications, wing geometry, center of gravity, weight, and fuel location were also input to the model. The detailed interface in Planemaker ensured that every aspect of the vehicle design could be incorporated into the X-Plane model.

17.3 Course Development

X-Plane has a large user base and a vibrant “modding” community. It is possible to download developer sanctioned scenery editing tools to add objects to the X-Plane environment. Google Sketch-Up was used to model the race pylons and then each pylon was converted into the unique “.obj” file format that X-Plane associates with scenery objects; an image of a race gate in X-Plane is given in Fig. 17.4. A helipad to hold the slung load and a reference point used to perform the pirouette maneuver were also created. After each scenery model was built, a user-developed program called Overlay Editor was used to create the race course in the X-Plane environment [47, 48]. Each race pylon was placed at the latitude and longitude corresponding to the picture of the course provided within the RFP. The complete course is given in Fig. 17.4.

17.4 Racing the Course

The X-Plane flight simulation proved that the *Dart* is an excellent VTOL aircraft for pylon racing. The *Dart* was flown in the flight simulator by a trained pilot and performed admirably. A video of the flight is provided along with this report. It is important to note that in this video the slung load object that hangs below the aircraft does not appear. This is due to an error in X-Plane 10 that occurs when recording movie files. The current version of X-Plane 10 only displays the rope hanging below the aircraft in the movie. A picture of the *Dart* flying the course is also provided to show that a slung load was developed and used to complete the course. Time-histories of the aircraft when flying the course are given in X-Plane Data foldout.



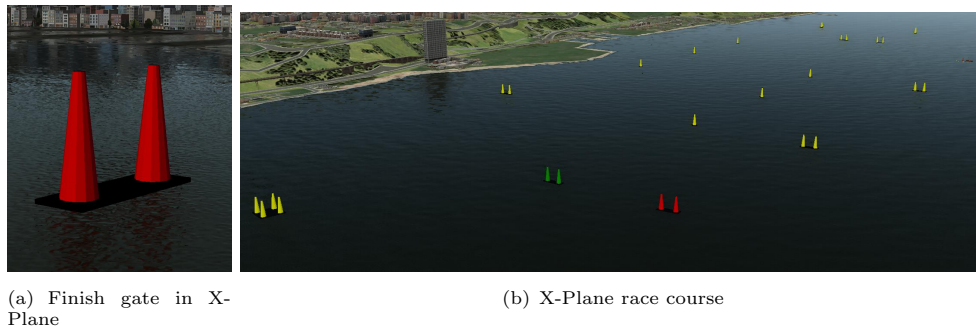


FIGURE 17.4: Race course model in X-Plane

TABLE 17.1: *Dart T690* race segment times.

Race Segment	Flight Path Optimizer (sec.)	X-Plane Results(sec.)
Slalom	19	20
Short Stop	5	16
Straight Away	20	19
Quad Pylon	11	14
Small Turn	9	7
Slalom 2	21	15
Coordinated Turn	13	16
Hover (including approach)	36	38
Pirouette	25	28
Sideward Flight	45	17
Last Leg	15	7
Total	219	222

TABLE 17.2: *Dart T690* race statistics.

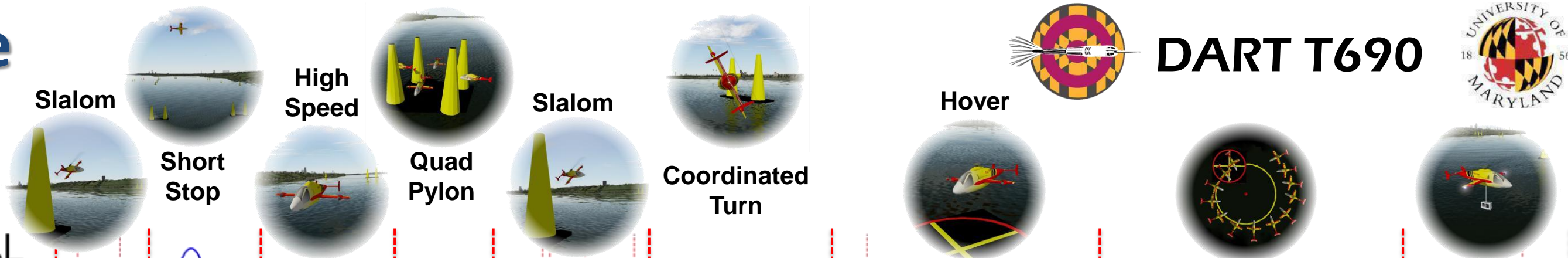
	Flight Path Optimizer	X-Plane Results
Max. Speed (kts)	208	191
Max. Acccel. (g's)	0.5	.85
Max. Deccel. (g's)	0.8	.86
Max. Load factor (g's)	5.0	5.0
Max. Alt. (ft.)	135	326
Max. Bank angle ($^{\circ}$)	85 $^{\circ}$	83 $^{\circ}$
Max. Pitch angle ($^{\circ}$)	15 $^{\circ}$	58 $^{\circ}$

In addition, some important information about the aircraft's performance such as its maximum airspeed, maximum acceleration, and maximum load factor, are given in Table 17.1.

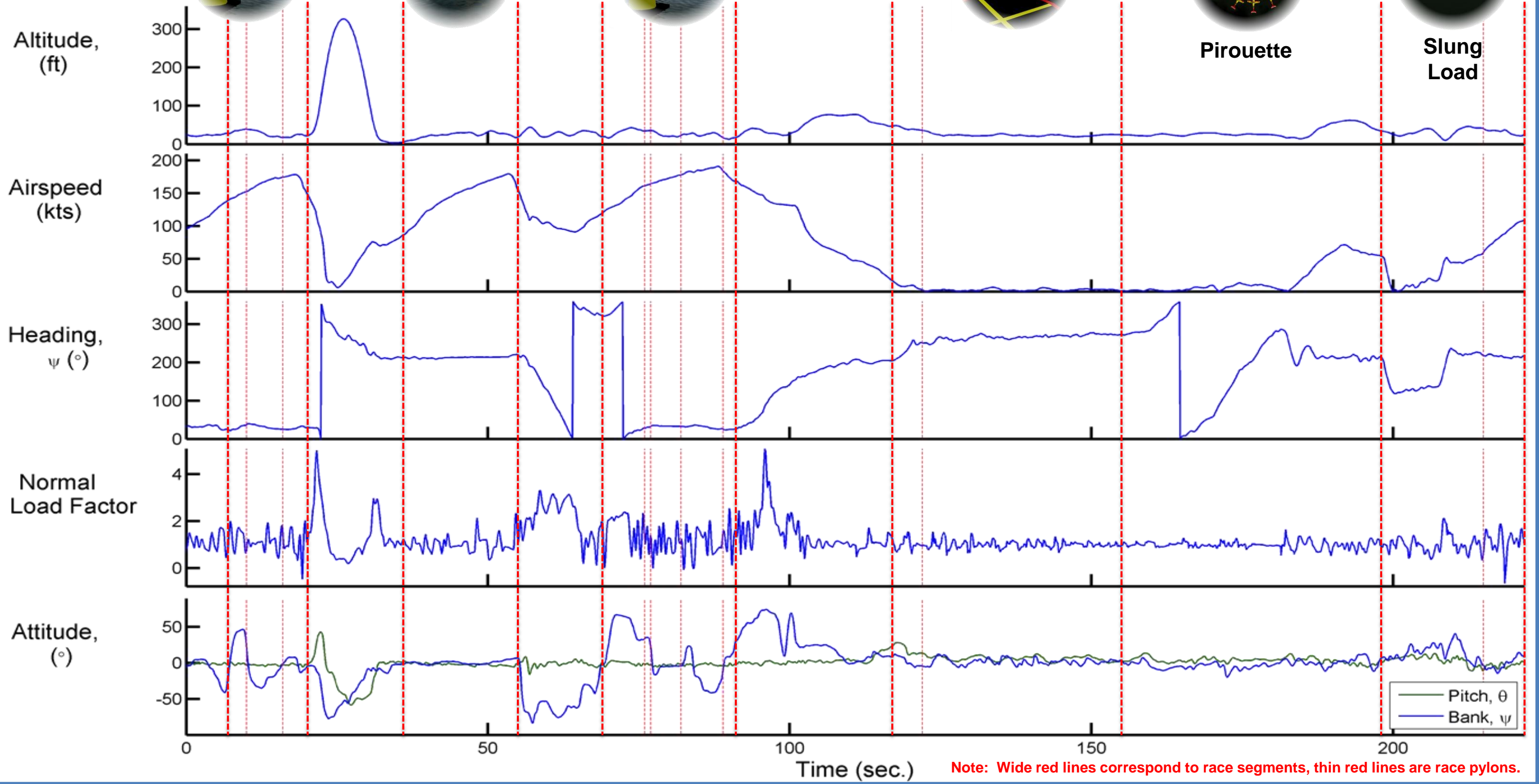
Foldout 8 show the exemplary performance of the *Dart*. The aircraft enters the race at exactly 100 kts. and reaches the hover segment of the race in only 125 seconds. Before reaching the hover stage, the aircraft experiences a 5g load factor during the Short Stop and Coordinated Turn portion of the race. In addition to encountering high load factors, the aircraft nearly reaches its maximum speed during three segments of the course. These results match the aircraft states that were given by the flight path optimizer (Section 2.2). The flight path optimizer was used to set the design requirements and it is significant to note that an actual



X-Plane Data



DART T690



pilot flying the course closely follows the optimized flight path. The flight path optimizer predicted a total race time of 219 sec and the course was completed in 222 sec.

18 Summary

Ultimately, the *Dart T690/E550* is designed to satisfy two distinct groups, the race organizers and the racers themselves. The race organizers are concerned primarily in presenting an exciting race that will attract large crowds, while also ensuring high levels of safety for the pilots. The racers are interested in a relatively low cost aircraft that will allow them to win the race, both to gain prestige and further sponsorships to cover operating costs.

The *Dart T690/E550* satisfies the race organizers by pushing the boundaries of maneuverability beyond that possible by a helicopter. It is capable of flying at 225 kts, 120 kts in sideward flight, sustaining a 5g load factor in pull-ups and coordinated turns, and performing dynamic yaw maneuvers. These flight capabilities will excite audiences and make rotorcraft races as popular as airplane races of today. The *Dart T690/E550* achieves these capabilities with a high level of safety, a triple redundant power-by-wire flight control system, advanced HUMS monitored by a dedicated ground crew, exceptional autorotative performance, emergency floats for a water landing, and a crash survivable airframe. The synergism of these systems ensures that the pilot will be able to react to a wide variety of failure modes and always be able to fly the aircraft to a safe landing on land or water.

The cost of the *Dart T690* is \$1.6 million, which is comparable to helicopters of this weight class even though this is a special high performance aircraft. The high maneuverability and top speed of the *Dart T690* allow the pilot to finish the defined race course in a competitive 219 seconds. The flight control system mixing schedule is customizable, allowing every pilot to tune the flight characteristics of the aircraft to their own personal preferences. A direct downlink from the vehicle HUMS allows the ground crew to monitor the aircraft condition in real-time, improving pilot safety and optimizing maintenance routines. The *Dart T690/E550* is optimized for short flights and has been designed to fit inside a customized trailer with the wings and rotor blades removed, making it easy to transport worldwide.

The 2012 Student Design Competition Request for Proposals, issued by the American Helicopter Society and Sikorsky Aircraft Corp., desired the development of a pylon racing rotorcraft. This proposal has defined the design of the *Dart T690/E550*, an innovative VTOL aircraft capable of competing effectively in pylon races. Using the flight path optimization along with the X-plane simulation, it was determined that the fastest flight time of the *Dart T690* is **183** seconds. With the flight time and a max rated power of 740 lb, it was determined that the fuel consumption during the course is 19.6 lb. This gives the *Dart T690* an efficiency rating, η , of **1204**.

The *Dart T690/E550* is optimized to have superior maneuverability, agility, dash capability, and speed than any other VTOL aircraft or rotorcraft in its class. The *Dart T690/E550* truly hits the bullseye in VTOL air racing.



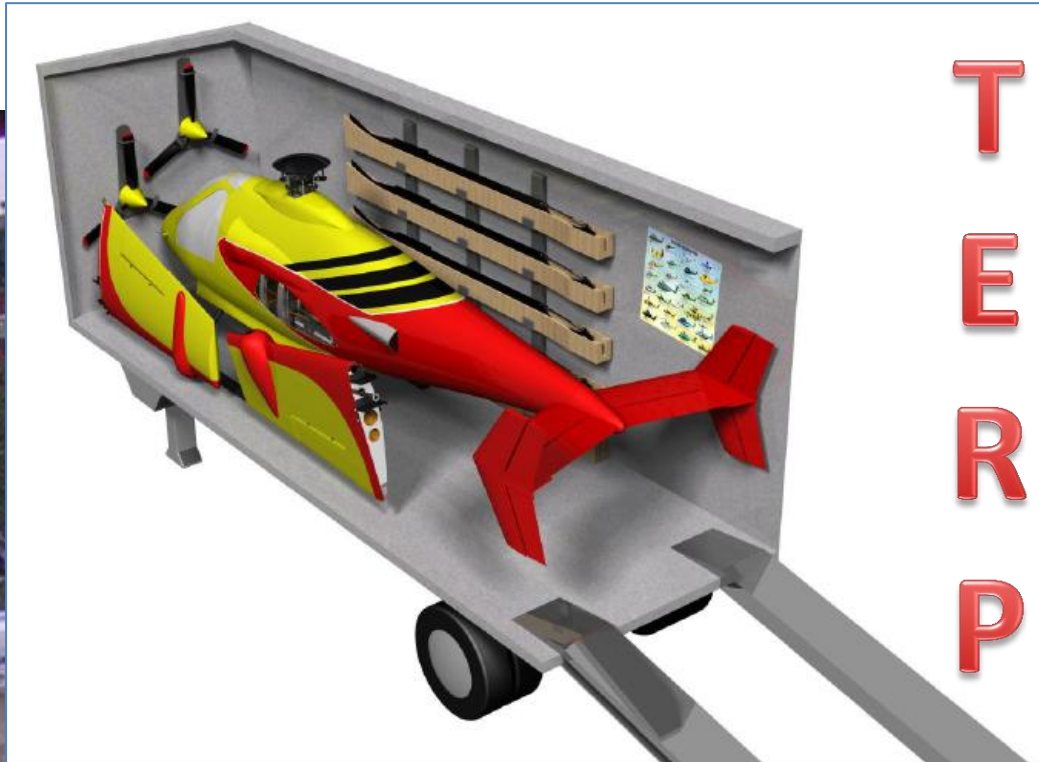
Staging and Transportation



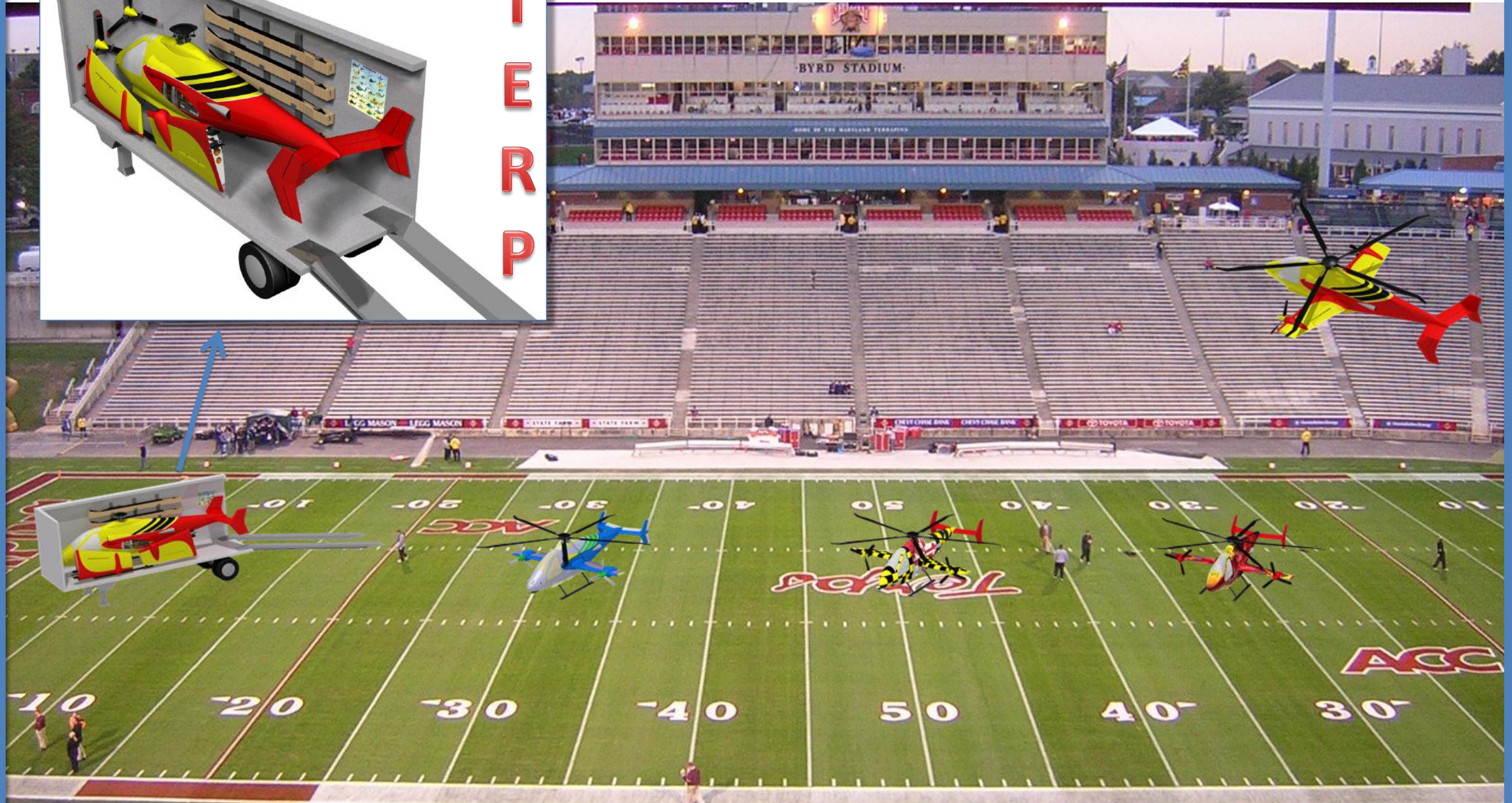
DART T690



Trailer for Enhanced Range & Payload



T
E
R
R
P



Bibliography

- [1] Launchpoint Technologies, “Launchpoint Technologies 6” Diameter Halbach Air-Core Motor,” Motor Datasheet, 2010.
- [2] Benson, D. A., *A Gauss Pseudospectral Transcription for Optimal Control*, Ph.D. thesis, Massachusetts Institute of Technology, November 2004.
- [3] Moore, M. D., “NASA Puffin Electric Tailsitter VTOL Concept,” NASA NF1676L-11227, Sept 2010.
- [4] Tishchenko, M. N. and Nagaraj, V. T., ENAE 634 Helicopter Design Lecture Notes, University of Maryland, College Park, 2008.
- [5] Schoen, A. H., Rosenstein, H., Stanzione, K., and Wisniewski, J. S., *User’s Manual for VASCOMP II, The V/STOL Aircraft Sizing and Performance Computer Program*, Boeing Company, Vertol Division, Report D8-0375, Volume VI.
- [6] Roskam, J., *Airplane Design — Part V: Component Weight Estimation*, Design, Analysis and Research Corporation, Lawrence, KS, 2004.
- [7] Raymer, D. P., *Aircraft Design: A Conceptual Approach* (3rd ed.), American Institute of Aeronautics and Astronautics, Inc., Reston, VA, 1999.
- [8] Leishman, J. G., *Principles of Helicopter Aerodynamics* (2nd ed.), Cambridge University Press, New York, NY, 2006.
- [9] Gay, D. and Hoa, S. V., *Composite Materials: Design and Applications*, CRC Press, Boca Raton, FL, 2007.
- [10] Lord Aerospace Products, “Lastoflex Bearing: Design Guide,” Pb-6500d, 1968.
- [11] MTK Bearings, “Full Complement Cylindrical Roller Bearings,” Catalogue fcs09/011, 2012.
- [12] Johnson, W., *Helicopter Theory*, Dover Publications, Mineola, NY, 1980.
- [13] Stahlhut, C. and Leishman, J. G., “Aerodynamic Design Optimization of Convertible-Rotor Concepts,” *American Helicopter Society 68th Annual Forum Proceedings*, Fort Worth, TX, May 1–3 2012.
- [14] Tester, J. W., “Sustainable Energy,” University Lecture, Massachusetts Institute of Technology, 2005.
- [15] Broussely, M. and Archdale, G., “Li-ion Batteries and Portable Power Source Prospects for the Next 5-10 Years,” *Journal of Power Sources*, Vol. 136, 2004, pp. 386–394.
- [16] United States Department of Energy, “Fuel Cell Technologies Program Multi-Year Research, Development and Demonstration Plan,” Research Plan, 2011.
- [17] M. Winter and Brodd, R. J., “What are Batteries, Fuel Cells, and Supercapacitors,” *Chemical Review*, Vol. 104, 2004, pp. 4245–4269.
- [18] Barbir, F., *PEM Fuel Cells: Theory and Practice*, Academic Press, 2005.
- [19] Ricci, M., “High Efficiency, High Power Density Electric Motors,” Product Presentation, 2010.
- [20] Merritt, B. T., Post, R. F., Dreifuerst, G. R., and Bender, D. A., “Halbach Array Motor/Generators - A Novel Generalized Electric Machine,” *Halbach Festschrift Symposium*, 1995.
- [21] White, G., “A Lightweight Split-Torque Transmission for a 330 kW Helicopter,” *Proceedings of the Institution of Mechanical Engineers*, Vol. 196, June 1982, pp. 11–22.



- [22] Botten, S. L., Whitley, C. R., and King, A. D., “Flight Control Actuation Technology for Next-Generation All-Electric Aircraft,” *Technology Review Journal - Millennium Issue*, Fall/Winter 2000, pp. 73–74.
- [23] Engleder, A. and Görlich, S., “Skid-type Landing Gear for a Helicopter,” European Patent EP 2371710A1, 2011.
- [24] United States of America, Department of Defense, “Weight and Balance Data Reporting Forms for Aircraft (Including Rotorcraft),” Mil-std-1374a, 1977.
- [25] Federal Aviation Administration, “§91.205 - Powered Civil Aircraft with Standard Category U.S. Airworthiness Certificates: Instruments and Equipment Requirements,” FAR 91.205, May 2012.
- [26] Bose, “A20 Aviation Headset,” Tech. rep., 2012.
- [27] Repperger, D. W., Green, R. H., LaFleur, T., and Haas, M. W., “Effects of Haptic Feedback and Turbulence on Landing Performance Using an Immersive Cave Automatic Virtual Environment (CAVE),” *Perceptual & Motor Skills*, , No. 97, 2003, pp. 820–832.
- [28] Hoh, R. H., “Helicopter Force-Feel and Stability Augmentation System with Parallel Servo-Actuator,” U.S. Patent 758,215, 2005.
- [29] Wright, J., “Emerging Results Using IMD-HUMS in a Black Hawk Assault Battalion,” *Proceedings of the American Helicopter Society 61st Annual Forum*, AHS, Grapevine, TX, 2005.
- [30] Delgado, I. R., Dempsey, P. J., and Simon, D. L., “A Survey of Current Rotorcraft Propulsion Health Monitoring Techniques,” NASA TM-2012-217420, Jan 2012.
- [31] Zakrajsek, J. J. and Dempsey, P. J., “Rotorcraft Health Management Issues and Challenges,” NASA/TM-2006-214022, Feb 2006.
- [32] Landis, K., Aiken, E., Hilbert, K., and Dunford, P., “A Piloted Simulator Investigation of Side-Stick Controller/Stability and Control Augmentation System Requirements for Helicopter Visual Flight Tasks,” *Proceedings of the American Helicopter Society 39th Annual Forum*, AHS, St. Louis, MO, 1983.
- [33] DeBellis, W., “Anthropometric Considerations for a Four-axis Side-arm Flight Controller,” N86-32993, U.S. Army Human Engineering Laboratory Aberdeen Proving Ground, MD, Feb 1986.
- [34] Roskam, J., *Airplane Design — Part II: Preliminary Configuration Design and Integration of the Propulsion System*, Design, Analysis and Research Corporation, Lawrence, KS, 2004.
- [35] Keys, C. N., “Rotary-Wing Aerodynamics: Volume II — Performance Predictions of Helicopters,” NASA CR 3083, 1979.
- [36] Prouty, R. W., *Helicopter Performance, Stability, and Control*, Kreiger Publishing Company, Malabar, FL, 1995.
- [37] Marsh, A. K., “Red Bull Air Race grounds 2011 Series,” <http://www.aopa.org/aircraft/articles/2010/100804redbull.html> [retrieved 29 MMay 2011].
- [38] Dexmet, “Lightning Strike Protection for Carbon Fiber Aircraft,” *Proceedings of the Society for the Advancement of Materials Process Engineering (SAMPE)*, Baltimore, MD, June 2007.
- [39] Poncon, M., Guillet, S., and Gosmain, A., “The Lightning Indirect Effect Protection of More Electrical and More Composite Modern Helicopters,” *Proceedings of the American Helicopter Society 68th Annual Forum*, Fort Worth, TX, May 1-3 2012.



-
- [40] Prouty, R. W., *Helicopter Performance, Stability, and Control*, Krieger Publishing Company, Malabar, FL, 1986.
- [41] Fradenburgh, E. A., “A Simple Autorotative Flare Index,” *Journal of the American Helicopter Society*, Vol. 29, July 1984, pp. 73–74.
- [42] Harris, F. and Scully, M., “Supplemental Appendix: Helicopter Cost Too Much,” *Proceedings of the American Helicopter Society 53rd Annual Forum*, April 1997.
- [43] Conklin and Associates, D. D., *The AircraftComparator: Helicopter Life Cycle Cost*, Computer Software, 2008.
- [44] Laminar Research, “X-Plane 10 Desktop Manual,” Tech. rep., May 2012.
- [45] Thong, C. W. S., “Modeling Aircraft Performance and Stability on X-Plane,” 2010.
- [46] Laminar Research, “Appendix A: How X-Plane Works,” Tech. rep., 2012.
- [47] Harris, J., “X-Plane Scenery Tools,” Tech. rep., Mar 2012.
- [48] Harris, J., “Overlay Editor Manual,” Tech. rep., Mar 2012.

